Nonlinear Optomechanical Dynamics of a Quantum Particle in a Single-Mode Cavity

Masterarbeit

zur Erlangung des akademischen Grades
Master of Science

eingereicht an der
Fakultät für Mathematik, Informatik und Physik
der Universität Innsbruck

von

Dominik Winterauer, BSc

Betreuung der Masterarbeit:

Univ.-Prof. Dr. Helmut Ritsch,
Institut für Theoretische Physik,
Universität Innsbruck

Innsbruck, Oktober 2014

Danksagung

Zuallererst möchte ich mich ganz herzlich bei Helmut Ritsch bedanken, mir die Möglichkeit gegeben zu haben, in seiner Gruppe meine Masterarbeit zu schreiben. Danke auch für die lockere und angenehme Arbeitsatmosphäre, die Du in Deiner Gruppe geschaffen hast und aufrecht erhältst!

Besonderers hervorheben möchte ich Wolfgang Niedenzu, der seine Aufgabe als „Taschen(post)doktorand“ sehr ernst genommen hat und am Ende auch in physischer Abwesenheit noch mit Rat und Tat zur Seite stand. Seine fachlichen wie auch persönlichen Beiträge haben nicht unwesentlich zum Gelingen dieser Arbeit beigetragen. Danke Wolfgang!

Bei Sebastian Krämer und Raimar Sandner bedanke ich mich für ihre Unterstützung bei C++QED und Hilfestellungen bei numerischen Fragen aller Art.

Matthias Sonnleitner danke ich für seine Hilfsbreitschaft bei sämtlichen GnuPlot Fragen.

Meinen Master-Mitstudenten Stefan Ostermann und Thomas Maier, sowie unserem „Gruppengastmitglied“ Michael Schuler, danke ich für die fortwährende moralische Unterstützung.

Ich möchte mich noch bei allen Mitgliedern der Ritsch-Gruppe für die tolle Zeit und den familiären Umgang, der gepflegt wird, bedanken.

Abschließend richtet sich mein Dank auch noch an meine Familie und meine Freunde, die mich in dieser Zeit unterstützt haben.

Danke!

Introduction

The simplest example of a bistable system is a sphere at rest at the top of a hill with two adjacent valleys. In an ideal world the sphere will rest there forever. The equilibrium experienced by the sphere is *unstable*, i.e. even the tiniest perturbation will cause the sphere to roll down the hill. Our real world, however, is full of perturbations, thus a real sphere on earth will always roll down the hill due to wind, moon's gravity or other perturbing forces[1]. Eventually the sphere ends up in one or the other valley, but it is unpredictable in which because perturbing forces are usually unknown. The electronic pendant of such a static bistable system is the *RS flip-flop*[2] first implemented by Jordan and Eccles in 1918 [1].

That bistability, multistability and chaotic behavior are a result of non-linearity of differential equations became apparent in the late 19^{th} century at the emergence of chaos theory. Investigating the three-body problem Poincaré summed up his findings about integrability of differential equations in [2]. Duffing first characterized non-linear response curves of mechanical systems subject to external vibrations exhibiting bistable behavior [3]. In the 1920s van der Pol studied the response of electric triodes to forced vibrations [4] and found that in a certain regime the system oscillates at either of two possible frequencies, but *never at both simultaneously*, due to the non-linearity of the problem [5]. Lamb found double-frequency solutions in his theory of the optical maser [6] that may, however, occur simultaneously, even in the steady state. The observation of bistable behavior in non-linear *absorptive* [7] and *dispersive* media [8] in Fabry-Perot-Interferometers triggered the field of quantum electronics. The book of Gibbs [9] provides a thorough introduction to the topic. At the same period of time Drummond and Walls introduced a quantum theory of non-linear media in a cavity [10], while first experiments were not conducted until the early 1990s [11].

Optical bistability effects as discussed in quantum electronics are connected to *hysteresis*, so the selection of a stable solution in the bistable regime depends on the history of the system. With the advent of optical lattices as effective quantum simulators [12] a new type of bi- and multistability was accessible: *spontaneous symmetry breaking* at quantum critical points. In contrast to hysteresis the actual state of the system does *not* depend on its history.

Approaching Feynman's vision of a universal quantum simulator [13] optical lattices realized by standing waves in optical resonators seem to be a promising setup. At current stage almost arbitrary physical models can be implemented on optical lattices, including Abelian [14] and non-Abelian [15] gauge theories.

[1] unless it is subject to strong friction

[2] The perturbing forces are thermal fluctuations and electromagnetic noise.

In 2002 Ritsch and Domokos found that atoms in a transversely pumped cavity align along one of two possible self-organized checkerboard patterns [16]. The symmetry is spontaneously broken at the transition to a super-radiant phase at critical pump. The atoms' alignment maximizes scattering of the transverse field into the cavity which causes *self-trapping* of particles in a runaway process. The atomic motion in the optical potential wells is cooled via the cavity [17, 18]. A more detailed analysis of the self-organization process is found in [19]. A complete and thorough summary of state-of-the-art theory and experiment of ultracold atoms in high-finesse optical resonators is found in [20].

By the replacement of non-linear media as of quantum electronics by single atoms or a cloud of cold atoms the quantum nature of both photon field *and* atomic motion became accessible. Optical resonators allow for strong coupling of atoms/polarizable particles and photon field, so we expect rich dynamics and steady states even at low photon number and small particle numbers.

As the title suggests this thesis is about *Nonlinear Optomechanical Dynamics of a Quantum Particle in a Single-Mode Cavity*. But what does that imply? The *non-linearity* stems from the non-linear optics that will be encountered. We will find refractive indices that change with varying light intensity. The term *optomechanical*, however, calls for a clarification. An optomechanical system is usually understood as a cavity with one or more moveable mirrors that oscillate, but the system considered here is a cavity with two fixed mirrors. Where is the *mechanical* part? It is in the quantum particle. The quantum particle moves inside the cavity and shifts the resonance frequency via interaction with the light field, just like a moving mirror does by changing the length of the cavity. The quantum particle may be an atom or any other type of polarizable particle. The terms *particle* and *atom* will therefore be used synonymously.

We will derive the quantum optical master equation from first principles and model an effective Hamiltonian for a quantum particle in a single-mode cavity. The properties of the system will be examined in a semi-classical and a fully quantum mechanical manner and their results will be compared to each other.

Except for section 1.2 all calculations will be given in natural units, i.e. $\hbar = c = k_B = 1$. Italic letters like m are numbers, roman letters like p are operators, bold italic letters like $\boldsymbol{k}$ are vectors and bold roman letters like $\mathbf{E}$ are vector operators.

Contents

1 Master Equation for Generic Quantum Optical Systems with Vacuum Inputs

The master equation is the equation of motion for the density operator of a finite part of the Hilbert space of a very large composite system. The finite part under consideration is generally termed the *system*, the part traced out is called the *bath* and often contains infinitely many degrees of freedom. In quantum optics the bath Hilbert space is modeled as an infinite set of harmonic oscillators with angular frequencies ranging continuously over all positive real numbers. The density of oscillators $\kappa(\omega)$ in the interval $[\omega, \omega + d\omega]$ is given by the mode density of the electromagnetic field and thus depends on the spatial dimensionality of the bath. For the derivation of the master equation given below the bath is the electromagnetic field in three dimensions. We will briefly discuss the approximations that enter [21, 22, 23]. Tracing over the bath of harmonic oscillators will eventually yield a non-unitary, though trace preserving, time evolution.

1.1 Derivation of the Master Equation

The Hilbert space of the bath is assumed to have much more degrees of freedom than that of the system. The concept of system and bath is modeled on its thermodynamic counterpart. The bath is considered large enough such that the effects of the system on it are negligible. On the opposite, the system dynamics is significantly affected by the bath properties. Mathematically this is expressed by

$$\rho(t) = \rho_{sys}(t) \otimes \rho_{bath}(t_0) \ \forall t, \tag{1.1}$$

i.e. the system and bath density operators factorize at all times and the bath remains in its initial state[1]. Eq. (1.1) is called the *weak coupling assumption.*[2]

[1] A driven bath may show some *explicit* time-dependence that is, however, independent from the systems dynamics.

[2] Our derivation follows mainly chapter 5.1 of [21], since they provide the most relevant physical and mathematical grounds of the master equation. They also consider thermal excitations of the bath. The most general results are given in chapter 6.1 of [22], who considers arbitrary bath inputs. We will also provide these results below, however, without any rigorous derivation.

1.1.1 Thermal States

In many cases ρ_{bath} is a *thermal* state,

$$\rho_{bath}(T) = Z^{-1} \sum_i \exp\left(-\frac{E_i}{T}\right) |E_i\rangle\langle E_i| \tag{1.2}$$

or

$$\rho_{bath}(T) = \mathcal{Z}^{-1} \int \nu(E) \exp\left(-\frac{E}{T}\right) |E\rangle\langle E|\, dE \tag{1.3}$$

for a discrete and continuous Hilbert space, respectively. Z and $\mathcal{Z}$ are normalization constants known as (canonical) partition functions. $\nu(E)$ is the *density of states* (DOS) and depends on the system Hamiltonian, the spatial dimensionality of the system and, for many-body systems, on the (anti-)commutation relations of the particle species involved. For our purposes it is advantageous to reformulate eq. (1.3) in terms of harmonic oscillators with angular frequency ω

$$\rho_{bath}(T) = \mathcal{Z}^{-1} \int \kappa(\omega)\rho_{ho}(\omega, T)d\omega, \tag{1.4}$$

where $\rho_{ho}(\omega, T)$ is, up to a normalization constant, the density matrix of a harmonic oscillator of angular frequency ω and temperature T

$$\rho_{ho}(\omega, T) = \sum_{n_\omega=0}^{\infty} \exp\left(-\frac{\left(n_\omega + \frac{1}{2}\right)\omega}{T}\right) |n_\omega\rangle\langle n_\omega|\,. \tag{1.5}$$

As before, $\kappa(\omega)$ is the density of harmonic oscillators in $[\omega, \omega + d\omega]$ and $|n_\omega\rangle$ are harmonic oscillator eigenstates (see also eqs. (1.11)). That the electromagnetic field is a quantum field of bosons whose particle number is not conserved already enters the expression for ρ_{ho}. There is no chemical potential μ that controls the number of particles (for particle number conservation $\mathrm{H} \to \mathrm{H} - \mu\mathrm{N}$) and the oscillator quantum number n_ω may be greater than 1. In quantum optics, however, one usually considers the limit $T \to 0$ for which

$$\rho_{bath}(T = 0) = \mathcal{Z}^{-1} \int \kappa(\omega)\, |0_\omega\rangle\langle 0_\omega|\, d\omega, \tag{1.6}$$

i.e. ρ_{bath} becomes a *vacuum* bath.

1.1.2 The Master Equation for Vacuum Baths

We consider a system interacting with a bath of harmonic oscillators in *rotating wave approximation* (see section 2.1.4):

$$\mathrm{H}_{bath} = \int \omega \mathrm{b}_\omega^\dagger \mathrm{b}_\omega d\omega \tag{1.7}$$

$$\mathrm{H}_{int} = i \int \kappa(\omega) \left(\mathrm{b}_\omega^\dagger \mathrm{c} - \mathrm{c}^\dagger \mathrm{b}_\omega\right) d\omega \tag{1.8}$$

where

$$\left[\mathrm{c},\, \mathrm{c}^\dagger\right] = 1 \tag{1.9}$$

$$\left[\mathrm{b}_\omega,\, \mathrm{b}^\dagger_{\omega'}\right] = \delta\left(\omega - \omega'\right) \tag{1.10}$$

and all other commutators equal zero.

$\mathrm{c}^{(\dagger)}$ and $\mathrm{b}^{(\dagger)}$ destroy (create) excitations in the system and bath, respectively. The nature of these excitations is irrelevant in our formalism. In quantum optics they are usually identified as photons, but they could as well be other bosonic particles or quasi-particles. At that point it seems reasonable to introduce the Fock states of the bath which also form the energy eigenstates. For $n^{(\prime)}_{\omega^{(\prime)}} \in \mathbb{N}$ the Fock states are defined as

$$|n_\omega\rangle \equiv \frac{\left(\mathrm{b}^\dagger_\omega\right)^{n_\omega}}{\sqrt{n_\omega!}}\,|0\rangle \tag{1.11a}$$

$$\mathrm{b}_\omega\,|0\rangle \equiv 0 \tag{1.11b}$$

$$\langle n_\omega | n'_{\omega'}\rangle = \delta_{nn'}\delta(\omega - \omega') \tag{1.11c}$$

and $|0\rangle$ is called the *vacuum state* of the bath. Fock states are eigenstates to the number operator N_ω

$$\mathrm{N}_\omega \equiv \mathrm{b}^\dagger_\omega \mathrm{b}_\omega \tag{1.12}$$

$$\mathrm{N}_\omega\,|n_{omega}\rangle = n_\omega\,|n_\omega\rangle \tag{1.13}$$

The system Hamiltonian H_{sys} remains unspecified. All we demand is that

$$\begin{aligned}\mathrm{c_I}(t) &= e^{-i\mathrm{H}_{sys}t}\mathrm{c}e^{i\mathrm{H}_{sys}t}\\ &= \mathrm{c}e^{-i\omega_0 t},\end{aligned} \tag{1.14}$$

where ω_0 is the system's resonance frequency. We transform to an interaction picture to arrive at

$$\mathrm{H}_{int,\,I} = i\int \kappa(\omega)\left(\mathrm{b}^\dagger_\omega e^{i(\omega-\omega_0)t}\mathrm{c} - \mathrm{c}^\dagger \mathrm{b}_\omega e^{-i(\omega-\omega_0)t}\right)d\omega. \tag{1.15}$$

The integrand in eq. (1.15) is rapidly oscillating. Main contributions to the integral will come from a region where $\omega \approx \omega_0$. Therefore we introduce a finite cutoff $\theta \ll \omega_{sys}$ in the bath integral

$$\mathrm{H}_{int,\,I} = i\int_{\omega_0-\theta}^{\omega_0+\theta} \kappa(\omega)\left(\mathrm{b}^\dagger_\omega e^{i(\omega-\omega_0)t}\mathrm{c} - \mathrm{c}^\dagger \mathrm{b}_\omega e^{-i(\omega-\omega_0)t}\right)d\omega \tag{1.16}$$

and assume that within this finite range $\kappa(\omega) \approx \sqrt{\frac{\gamma}{2\pi}} = const.$ In atomic physics the decay rate of a state, γ, is usually determined by measurement, in cavity QED, where $\gamma \to 2\kappa$, it may be tuned by changing cavity properties or selecting a different mode.

Therefore γ just enters as a parameter in our calculation, for a detailed derivation and analytic expression of γ based on microscopic properties we refer to the original work of Weisskopf and Wigner [24]. We define

$$\mathrm{b}(t) = \sqrt{\frac{1}{2\pi}} \int_{\omega_0-\theta}^{\omega_0+\theta} \mathrm{b}_\omega e^{-i\omega t} d\omega \tag{1.17a}$$

$$\begin{aligned}\left[\mathrm{b}(t),\, \mathrm{b}^\dagger(t')\right] &= \frac{1}{2\pi} \int_{\omega_0-\theta}^{\omega_0+\theta} e^{-i(\omega-\omega_0)(t-t')} d\omega \\ &\equiv \delta_s(t-t'),\end{aligned} \tag{1.17b}$$

where $\delta_s(t-t')$ is a slowly varying delta function, which acts like a delta function at timescales $\tau \gg \frac{1}{\theta}$. We plug in the weak coupling assumption eq. (1.1) and vacuum inputs to define

$$\rho_{bath}(t) = |0\rangle\langle 0| \;\; \forall t. \tag{1.18}$$

The time evolution of ρ_I is given by

$$\dot{\rho}_I(t) = -i \left[\mathrm{H}_{int,\,I}(t),\, \rho_I(t)\right] \tag{1.19}$$

which can be integrated and expanded in a power series in $\mathrm{H}_{int,\,I}$ [21]

$$\begin{aligned}\rho_I(t) &= \rho_I(t_0) - i \int_{t_0}^{t} \left[\mathrm{H}_{int,\,I}(t'),\, \rho_I(t')\right]\, dt' \\ &= \rho_I(t_0) - i \int_{t_0}^{t} \left[\mathrm{H}_{int,\,I}(t'),\, \rho_I(t_0)\right]\, dt' \\ &\qquad - \int_{t_0}^{t}\int_{t_0}^{t} \Big[\mathrm{H}_{int,\,I}(t'),\, \left[\mathrm{H}_{int,\,I}(t''),\, \rho_I(t'')\right]\Big]\, dt''dt' \\ &= \text{etc.}\end{aligned} \tag{1.20}$$

The series could be expanded to include arbitrarily many terms, which, however, is not very useful for any practical calculations. We continue with the second order expression of eq. (1.20) and differentiate with respect to t to arrive at the integro-differential equation

$$\dot{\rho}_I(t) = -i \left[\mathrm{H}_{int,\,I}(t),\, \rho_I(t_0)\right] - \int_{t_0}^{t} \Big[\mathrm{H}_{int,\,I}(t),\, \left[\mathrm{H}_{int,\,I}(t'),\, \rho_I(t')\right]\Big]\, dt'. \tag{1.21}$$

Employing the weak coupling assumption $\rho_I(t')$ becomes

$$\begin{aligned}\rho_I(t') &= \rho_{sys,\,I}(t') \otimes \rho_{bath,\,I} \\ &= \rho_{sys,\,I}(t') \otimes |0\rangle\langle 0|\,.\end{aligned} \tag{1.22}$$

When we insert the explicit form of $\mathrm{H}_{int,\,I}$ we use

$$\begin{aligned}\mathrm{b}(t)\mathrm{b}^\dagger(t')\,|0\rangle &= \left[\mathrm{b}(t),\, \mathrm{b}^\dagger(t')\right]|0\rangle \\ &= \delta_s(t-t')\,|0\rangle\end{aligned} \tag{1.23}$$

and employ the cyclic property of the trace

$$\begin{aligned}\mathrm{Tr}\{\mathrm{ABC}\} &= \mathrm{Tr}\{\mathrm{BCA}\} \\ &= \mathrm{Tr}\{\mathrm{CAB}\}\end{aligned} \tag{1.24}$$

when tracing over the bath. Noting that

$$\mathrm{Tr}_{bath}\{\mathrm{b}_\omega |0\rangle\langle 0|\} = 0 \tag{1.25a}$$

$$\mathrm{Tr}_{bath}\left\{\mathrm{b}_\omega^\dagger |0\rangle\langle 0|\right\} = 0 \tag{1.25b}$$

we find

$$\mathrm{Tr}_{bath}\{[\mathrm{H}_{int,\,I}(t),\, \rho_I(t_0)]\} = 0. \tag{1.26}$$

Using

$$\mathrm{Tr}_{bath}\{\mathrm{b}_\omega \mathrm{b}_\omega |0\rangle\langle 0|\} = 0 \tag{1.27a}$$

$$\mathrm{Tr}_{bath}\left\{\mathrm{b}_\omega^\dagger \mathrm{b}_\omega^\dagger |0\rangle\langle 0|\right\} = 0 \tag{1.27b}$$

eventually yields

$$\begin{aligned}\dot{\rho}_{sys,\,I}(t) = \gamma \int_{t_0}^{t} \Big(&\mathrm{c}\rho_{sys,\,I}(t')\mathrm{c}^\dagger + \mathrm{c}\rho_{sys,\,I}(t')\mathrm{c}^\dagger \\ &- \mathrm{c}^\dagger\mathrm{c}\rho_{sys,\,I}(t') - \rho_{sys,\,I}(t')\mathrm{c}^\dagger\mathrm{c}\Big)\delta_s(t-t')\,dt'.\end{aligned} \tag{1.28}$$

Keeping in mind that $\rho_{sys,\,I}(t')$ evolves on longer timescales than the bath operators, the slowly varying δ-function $\delta_s(t-t')$ behaves like a real δ-function. By virtue of

$$\int_{t_0}^{t} \delta_s(t-t')\,dt' = \frac{1}{2} \tag{1.29}$$

we evaluate the time integral in eq. (1.28) and obtain

$$\dot{\rho}_{sys,\,I}(t) = \frac{\gamma}{2}\Big(2\mathrm{c}\rho_{sys,\,I}(t)\mathrm{c}^\dagger - \mathrm{c}^\dagger\mathrm{c}\rho_{sys,\,I}(t) - \rho_{sys,\,I}(t)\mathrm{c}^\dagger\mathrm{c}\Big). \tag{1.30}$$

Undoing the system interaction picture and suppressing the functional time dependence of the operators involved, we arrive at the *master equation* for vacuum inputs

$$\dot{\rho}_{sys} = -i\,[\mathrm{H}_{sys},\, \rho_{sys}] + \frac{\gamma}{2}\Big(2\mathrm{c}\rho_{sys}\mathrm{c}^\dagger - \mathrm{c}^\dagger\mathrm{c}\rho_{sys} - \rho_{sys}\mathrm{c}^\dagger\mathrm{c}\Big). \tag{1.31}$$

The general form of the master equation can be derived in a similar manner. We follow chapter 6.1 of [22] and define

$$\mathrm{Tr}\left\{\rho_{bath}\mathrm{b}(\omega)\mathrm{b}^\dagger(\omega')\right\} = \Big(N(\omega)+1\Big)\delta(\omega-\omega') \tag{1.32a}$$

$$\mathrm{Tr}\left\{\rho_{bath}\mathrm{b}^\dagger(\omega)\mathrm{b}(\omega')\right\} = N(\omega)\delta(\omega-\omega') \tag{1.32b}$$

$$\mathrm{Tr}\{\rho_{bath}\mathrm{b}(\omega)\mathrm{b}(\omega')\} = M(\omega)\delta(2\omega_0-\omega-\omega') \tag{1.32c}$$

$$\mathrm{Tr}\left\{\rho_{bath}\mathrm{b}^\dagger(\omega)\mathrm{b}^\dagger(\omega')\right\} = M^*(\omega)\delta(2\omega_0-\omega-\omega'). \tag{1.32d}$$

Redoing the time evolution integrals with this definitions eq. (1.32) yields the *master equation for general inputs* [21]

$$\begin{aligned}\dot{\rho}_{sys} = -i\left[\mathrm{H}_{sys},\, \rho_{sys}\right] &+ \frac{\gamma}{2}\Big(N(\omega_0)+1\Big)\cdot\Big(2\mathrm{c}\rho_{sys}\mathrm{c}^\dagger - \mathrm{c}^\dagger\mathrm{c}\rho_{sys} - \rho_{sys}\mathrm{c}^\dagger\mathrm{c}\Big)\\ &+ \frac{\gamma}{2}N(\omega_0)\cdot\Big(2\mathrm{c}^\dagger\rho_{sys}\mathrm{c} - \mathrm{c}\mathrm{c}^\dagger\rho_{sys} - \rho_{sys}\mathrm{c}\mathrm{c}^\dagger\Big)\\ &- \frac{\gamma}{2}M(\omega_0)\cdot\Big(2\mathrm{c}^\dagger\rho_{sys}\mathrm{c}^\dagger - \mathrm{c}^\dagger\mathrm{c}^\dagger\rho_{sys} - \rho_{sys}\mathrm{c}^\dagger\mathrm{c}^\dagger\Big)\\ &- \frac{\gamma}{2}M^*(\omega_0)\cdot\Big(2\mathrm{c}\rho_{sys}\mathrm{c} - \mathrm{c}\mathrm{c}\rho_{sys} - \rho_{sys}\mathrm{c}\mathrm{c}\Big). \end{aligned} \tag{1.33}$$

The terms in the first two lines of eq. (1.33) correspond to a system in a thermal bath with occupation number $N(\omega_0) = \langle \mathrm{N}(\omega_0)\rangle$ (see eq. (1.45)). The terms in the other two lines stem from phase dependent correlations which are non-vanishing if the bath is e.g. in a squeezed state. A shorthand notation for the master equation is

$$\dot{\rho} = \mathcal{L}\rho, \tag{1.34}$$

where $\mathcal{L}$ is the *Liouville (super-)operator*, or *Liouvillian*. The Liouvillian needs to be of the so-called *Lindblad form* [25] as in eq. (1.30), which has a rather simple representation and is, most importantly, trace preserving:

$$\begin{aligned}\partial_t \operatorname{Tr}\{\rho\} &= \frac{\gamma}{2}\operatorname{Tr}\Big\{2\mathrm{c}\rho\mathrm{c}^\dagger - \mathrm{c}^\dagger\mathrm{c}\rho - \rho\mathrm{c}^\dagger\mathrm{c}\Big\}\\ &= \frac{\gamma}{2}\operatorname{Tr}\Big\{\mathrm{c}^\dagger\mathrm{c}\rho - \mathrm{c}^\dagger\mathrm{c}\rho - \mathrm{c}^\dagger\mathrm{c}\rho\Big\}\\ &= 0. \end{aligned} \tag{1.35}$$

The time evolution from the master equation differs significantly from the time evolution generated by the Schrödinger equation: It is non-unitary. This may sound like a mathematical detail, but that is what allows to describe effects like decay and spontaneous emission, which cannot be accounted for in the original Schrödinger equation. Non-unitary dynamics can be simulated by adding stochastic terms to the Schrödinger equation to give the *Quantum Stochastic Schrödinger Equation* (QSSE) [21]. The QSSE can be solved by means of the *Quantum Monte Carlo Wavefunction Method* (QMWF), which will be discussed in greater detail in section 4.3. The operator pendant of the QSSE are the *Heisenberg-Langevin equations*, which play a big part in the *input-output formalism*, an electronics-alike scheme that is concerned with the response of a system (e.g. resonators) to a given input field.[3]

1.2 Why Vacuum Inputs?

In section 1.1.1 we already encountered thermal states. The average number of bosonic excitations, such as photons, in a thermal state is given by the Bose-Einstein

[3] Rigorous derivations of the Heisenberg-Langevin equations can be found in [26] or chapter 3 of [21]. A neat application of the input-output formalism is shown in [27]

distribution

$$\langle \mathrm{N}_\omega \rangle = \frac{1}{e^{\frac{\omega}{T}} - 1}, \tag{1.36}$$

where the temperature T is in units of $\frac{\hbar}{k_B}$. Eq. (1.36) gives the mean number of excitations created by thermal fluctuations. Due to the exponential in the denominator, eq. (1.36) decreases rapidly with increasing ω for $\omega \approx T$. This expectation value, however, is for each mode with given excitation energy ω. To find the total number of excitations for a given temperature we also need to know the number of modes involved. To get some definitive numbers we will plug in $\hbar$, k_B and c explicitly:

$$\begin{aligned} \langle \mathrm{N} \rangle &= \sum_{\boldsymbol{p}} \langle \mathrm{N}_{\boldsymbol{p}} \rangle \\ &= \sum_{\boldsymbol{p}} \frac{1}{e^{\frac{\hbar\omega_{\boldsymbol{p}}}{k_B T}} - 1} && (1.37) \\ &\to \frac{V}{(2\pi\hbar)^3} \int \frac{1}{e^{\frac{\hbar\omega_{\boldsymbol{p}}}{k_B T}} - 1} \, d^3p. && (1.38) \end{aligned}$$

Photons obey

$$\begin{aligned} \boldsymbol{p} &= \hbar \boldsymbol{k} && (1.39) \\ \omega_p &= c\frac{|\boldsymbol{p}|}{\hbar} \\ &= c|\boldsymbol{k}|. && (1.40) \end{aligned}$$

Therefore we can perform the integration of the angular parts of eq. (1.38) and replace dp by $\frac{\hbar}{c} d\omega$ to arrive at

$$\langle \mathrm{N} \rangle = \frac{V}{2\pi^2} \int \frac{1}{e^{\frac{\hbar\omega}{k_B T}} - 1} \frac{\omega^2}{c^3} \, d\omega. \tag{1.41}$$

Multiplying the integrand of eq. (1.41) by $\hbar\omega$ yields the well-known *Planck's radiation law*. We are, however, not interested in the full spectrum but rather in the part that might potentially affect our system under consideration. Only a small interval around the resonance frequency ω_0 will contribute, thus we approximate eq. (1.41) to

$$\langle \mathrm{N}(\omega_0) \rangle \approx \frac{V}{2\pi^2} \frac{1}{e^{\frac{\hbar\omega_0}{k_B T}} - 1} \frac{\omega_0^2}{c^3} \Delta\omega. \tag{1.42}$$

$\Delta\omega$ is the bandwidth of the bath, which is typically much larger than κ, but smaller than the typical system energy ω_0,

$$\kappa \ll \Delta\omega \ll \omega_0. \tag{1.43}$$

We take $\Delta\omega \approx \theta^{-1}$, where θ is the same as in eq. (1.17). The volume V in eq. (1.42) is still undefined, but we can give a rough estimate for it. Assuming the cavity has a surface area A_C, then approximately half of the photons in the volume

$$V = A_C \cdot c \cdot \Delta t \tag{1.44}$$

will reach the cavity. Now the relevant time scale Δt in eq. (1.44) for our bath correlation functions is nothing but the inverse of the bandwidth $\Delta\omega$. Putting that into eq. (1.42) yields

$$\langle \mathrm{N}(\omega_0)\rangle \approx \frac{A_C}{4\pi^2} \frac{1}{e^{\frac{\hbar\omega_0}{k_B T}} - 1} \frac{\omega_0^2}{c^2}, \tag{1.45}$$

so $\Delta\omega$ cancels out. For arbitrary processes that have $\Delta\omega \ll \omega_0$ eq. (1.45) gives the number of bath particles (photons) that have to be considered, usually termed *bath occupation number*. The bath occupation number is very insensitive to the details of the processes involved as long as eq. (1.43) holds. Therefore eq. (1.43), called the *separation of time/frequency scales*, is one of the main pillars upon which the validity of the quantum optical master equation rests.

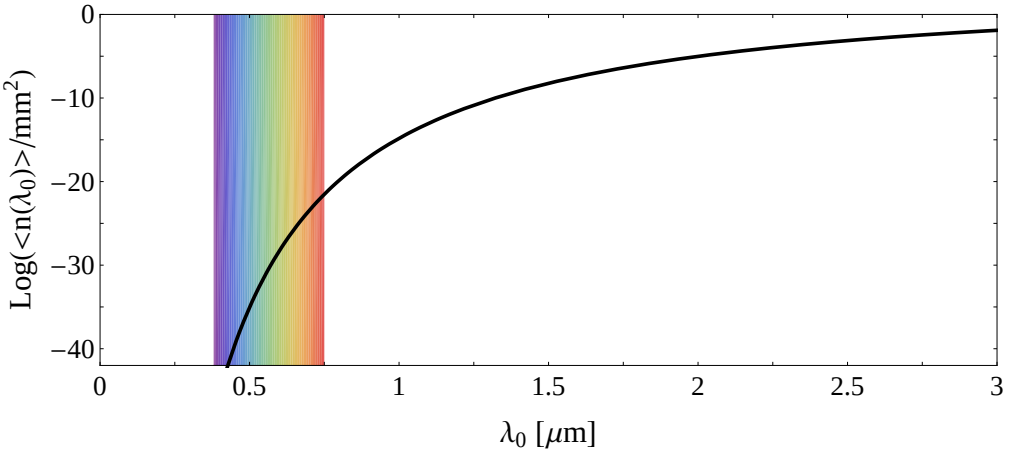

Figure 1.1 Logarithm of the bath occupation number $\langle \mathrm{N}(\lambda_0)\rangle$ given by eq. (1.46) at $T = 300K$ for various wavelengths λ_0. The colored region highlights the visible range.

For better comparison with experimental setups we rewrite eq. (1.45) in terms of wavelengths, using $\omega_0 = \frac{2\pi c}{\lambda_0}$:

$$\frac{\langle \mathrm{N}(\lambda_0)\rangle}{A_C} \approx \frac{1}{\lambda_0^2} \frac{1}{e^{\frac{2\pi\hbar c}{\lambda_0 k_B T}} - 1}. \tag{1.46}$$

Fig. (1.1) shows a logarithmic plot of eq. (1.46) in units of mm^{-2}. We see that in the visible range $A_C^{-1} \langle \mathrm{N}(\lambda_{vis})\rangle \ll 10^{-20}\mathrm{mm}^{-2}$ and even in the near infrared we have

$A_C^{-1} \langle \mathrm{N}(\lambda_{nir}) \rangle \ll 1\mathrm{mm}^{-2}$. It is therefore perfectly valid to assume the heat bath of a quantum optical system is in the vacuum state eq. (1.18).[4]

[4]Optical microcavities have $A_C < 1\mathrm{mm}^2$, so the numerical values shown in fig(1.1) represent upper bounds for the bath occupation number.

2 The Model Hamiltonian for an Atom in a High Finesse Cavity

The physical system under consideration is an atom trapped by the light field of a high-finesse cavity. The atomic center of mass motion, the internal excitations and the cavity light field as well as their mutual interaction will be treated in a fully quantum-mechanical manner. The quantum theory of light and its fundamental interactions with matter will provide the solid ground upon which we shall construct our model.

2.1 Discussion of the Model Hamiltonian

In this section we will discuss the different contributions to the Hamiltonian separately. The motivation and derivation will be rather coarse, so the interested reader is referred to the standard literature on this topic where necessary.

2.1.1 The Free Electric Field

The three-dimensional quantized vector potential $\mathbf{A}$ for an empty resonator is found to be [1]

$$\mathbf{A}(\mathbf{r}) = \sum_{\lambda} \int \sqrt{\frac{1}{2\omega_k \varepsilon_0 V}} \left(\boldsymbol{\epsilon}^*_{\boldsymbol{k},\lambda} \mathrm{a}^\dagger_{\boldsymbol{k},\lambda} v^*_k(\mathbf{r}) + v_k(\mathbf{r}) \mathrm{a}_{\boldsymbol{k},\lambda} \boldsymbol{\epsilon}_{\boldsymbol{k},\lambda} \right) d^3k, \tag{2.1}$$

with

$$\left[\mathrm{a}^\dagger_{\boldsymbol{k},\lambda}, \mathrm{a}_{\boldsymbol{k}',\lambda'} \right] = \delta_{\lambda\lambda'} \delta(\boldsymbol{k} - \boldsymbol{k}'), \tag{2.2}$$

$$\omega_k = |\boldsymbol{k}|, \tag{2.3}$$

where V is the quantization volume, ε_0 the permittivity of free space, $\boldsymbol{\epsilon}_{\boldsymbol{k},\lambda}$ the (possibly complex) polarization unit vector and the mode function $v_k(\boldsymbol{x})$ is a solution to the three-dimensional Helmholtz equation [22]

$$\left(\nabla^2 + k^2 \right) v_k(\mathbf{x}) = 0. \tag{2.4}$$

[1] The representation of the quantized electromagnetic field operators in the Coulomb gauge will mainly follow chapter III of [28].

The mode functions $v_k(\mathbf{x})$ are normalized according to

$$\int v_k^*(\boldsymbol{x}) v_k(\boldsymbol{x})\, d^n x = \int d^n x \equiv V \tag{2.5}$$

for $n = 1, 2, 3$.

The quantized electric and magnetic field operators are defined analogously to their classical electrodynamic counterparts:

$$\mathbf{E}_{\mathrm{H}}(\mathbf{r}, t) = -\partial_t \mathbf{A}(\mathbf{r}, t) \tag{2.6}$$

$$\mathbf{B}_{\mathrm{H}}(\mathbf{r}, t) = \nabla \times \mathbf{A}(\mathbf{r}, t). \tag{2.7}$$

These definitions apply for the corresponding Heisenberg operators only, labeled by the subscript H, but we would like to continue our discussion in the Schrödinger picture. Eq. (2.7) does not trouble us at all, since it holds in the Schrödinger picture as well. For eq. (2.6) we need a little workaround. We transform $\mathbf{A}(\mathbf{r})$ to the Heisenberg picture, apply eq. (2.6) and then return back to the Schrödinger picture. This yields the Schrödinger electric field operator

$$\mathbf{E}(\mathbf{r}) = i \sum_\lambda \int \sqrt{\frac{\omega_k}{2\varepsilon_0 V}} \left(\boldsymbol{\epsilon}^*_{\boldsymbol{k},\lambda} \mathrm{a}^\dagger_{\boldsymbol{k},\lambda} v^*_k(\mathbf{r}) - v_k(\mathbf{r}) \mathrm{a}_{\boldsymbol{k},\lambda} \boldsymbol{\epsilon}_{\boldsymbol{k},\lambda} \right) d^3k. \tag{2.8}$$

The electric field will be the main generator of particle-light interactions as will be derived below. The Hamiltonian of the free electromagnetic field is written as

$$\begin{aligned} \mathrm{H}_{em} &= \frac{\varepsilon_0}{2} \int \left(\mathbf{E}^2(\mathbf{r}) + \mathbf{B}^2(\mathbf{r}) \right) d^3r \\ &= \sum_\lambda \int \omega_k \left(\mathrm{a}^\dagger_{\boldsymbol{k},\lambda} \mathrm{a}_{\boldsymbol{k},\lambda} + \frac{1}{2} \right) d^3k. \end{aligned} \tag{2.9}$$

The ground state energy term $\frac{\omega_{\boldsymbol{k}}}{2}$ in the integrand yields an infinite contribution called the *vacuum energy*. Since it is a number and not an operator it affects all states equally and does not generate any dynamics. Its manifestation is topic of ongoing discussions in high-energy physics and cosmology which we shall not be concerned with [29]. It is formally removed by *normal ordering*[2], a reordering of subsequent applications of creation and annihilation operators that puts all creation operators to the left and all annihilation operators to the right. The expression to be normally ordered is enclosed by colons, e.g.

$$: \mathrm{a}\mathrm{a}^\dagger \mathrm{a}\mathrm{a}^\dagger := \mathrm{a}^\dagger \mathrm{a}^\dagger \mathrm{a}\mathrm{a}. \tag{2.10}$$

Removing the infinite constant we arrive at

$$\mathrm{H}_{em} = \sum_\lambda \int \omega_k \mathrm{a}^\dagger_{\boldsymbol{k},\lambda} \mathrm{a}_{\boldsymbol{k},\lambda}\, d^3k. \tag{2.11}$$

[2]Normal ordering originates from quantum field theory. Normally ordered strings of operators with at least one annihilation operator have zero vacuum expectation value. Wick's theorem [30] allows for the expression of arbitrary strings of creation and annihilation operators as a combination of normally ordered strings of operators, so one has to consider normally ordered operators only. The interested reader is referred to the thorough introductory book of Peskin and Schröder [31] for more details.

2.1.2 Atom-Light Interaction

The Hamiltonian for charged particles (e.g. electrons) interacting with electromagnetic fields via *minimal coupling* reads[3]

$$\mathrm{H} = \sum_{\alpha} \frac{1}{2m_\alpha} \left[\mathbf{p}_\alpha - q_\alpha \mathbf{A}(\mathbf{r}_\alpha)\right]^2 + \mathrm{V}_{Coul}. \tag{2.12}$$

In principle, we are done, but eq. (2.12) is not very handy for any practical calculations. In the case of atoms interacting with light at optical frequencies, i.e. $\lambda_{opt} \approx 10^{-7} - 10^{-6}$m, we may simplify this expression. Since the extend of an atom, i.e. the radius of the electron orbitals, is much smaller than the wavelength of the incident light, $r_{e^-} \approx 10^{-10}\mathrm{m} \ll \lambda_{opt}$, we can perform the *long wavelength approximation*

$$\mathrm{H} \approx \sum_{\alpha} \frac{1}{2m_\alpha} \left[\mathbf{p}_\alpha - q_\alpha \mathbf{A}(\mathbf{R}_a)\right]^2 + \mathrm{V}_{Coul}, \tag{2.13}$$

where we assume that the field each electron experiences is approximately the same as at the atom's center of mass position $\boldsymbol{R}_a$.[4] Defining the *dipole moment operator*

$$\mathbf{d} = \sum_{\alpha} q_\alpha \mathbf{r}_\alpha \tag{2.14}$$

we apply the unitary transformation

$$\mathrm{U} = \exp\left[-i\mathbf{d}\cdot\mathbf{A}(\mathbf{R}_a)\right] \tag{2.15}$$

$$\begin{aligned}\mathrm{H}' &= \mathrm{U}\mathrm{H}\mathrm{U}^\dagger \\ &= \sum_{\alpha} \frac{\mathbf{p}_\alpha^2}{2m_\alpha} + \mathrm{V}_{Coul} + \varepsilon_{dip} + \sum_{\lambda} \int \omega_k a^\dagger_{\boldsymbol{k},\lambda} a_{\boldsymbol{k},\lambda}\, d^3k - \frac{1}{\varepsilon_0}\mathbf{d}\cdot\mathbf{D}'(\mathbf{R}_a).\end{aligned} \tag{2.16}$$

$\mathbf{D}'(\mathbf{R}_a)$ is the transformed *displacement operator*

$$\begin{aligned}\mathbf{D}'(\mathbf{R}_a) &= i\varepsilon_0 \sum_{\lambda} \int \sqrt{\frac{\omega_k}{2\varepsilon_0 V}} \left(\boldsymbol{\epsilon}^*_{\boldsymbol{k},\lambda} a^\dagger_{\boldsymbol{k},\lambda} v^*_k(\mathbf{R}_a) - v_k(\mathbf{R}_a) a_{\boldsymbol{k},\lambda} \boldsymbol{\epsilon}_{\boldsymbol{k},\lambda}\right) d^3k \\ &= \varepsilon_0 \mathbf{E}(\mathbf{R}_a).\end{aligned} \tag{2.17}$$

So the transformed displacement operator is of the same form as the untransformed electric field operator. The form of the particle-light interaction part is thus often termed as *d times E*, as opposed to the initial *p times A*. The long wavelength approximation became a *dipole approximation*. V_{Coul} is the Coulomb potential acting among the charged particles. The dipole self-energy ε_{dip} represents another infinite, but constant, contribution to the Hamiltonian. It will not be considered because it does not alter the system dynamics, just like the vacuum energy before. The fourth term on the right hand side of eq. (2.16) is the already normally ordered Hamiltonian

[3] Here we follow Complement $\mathrm{A_{IV}}$ of [28].

[4] Whenever we talk about an atom's position we are referring to the location of its center of mass.

of the free electromagnetic field eq. (2.11). By virtue of eq. (2.17) we get the resulting particle-field Hamiltonian

$$\mathrm{H}_{pf} = \sum_{\alpha} \frac{\mathbf{p}_{\alpha}^2}{2m_{\alpha}} + \mathrm{V}_{Coul} + \sum_{\lambda} \int \omega_k a^{\dagger}_{\boldsymbol{k},\lambda} a_{\boldsymbol{k},\lambda}\, d^3k - \mathbf{d}\cdot\mathbf{E}(\mathbf{R}_a). \tag{2.18}$$

2.1.3 The Cavity

In cavity quantum electrodynamics (C-QED) the quantization volume V from eqs. (2.8) and (2.5) is taken as the volume enclosed by the cavity. However, one can approximate the mode functions inside the cavity, simplifying calculations without noticeably changing the physics. A first step is to solve the paraxially approximated form of eq. (2.4), which would give us the well known *Gaussian beams* [32]. In the vicinity of the beam waist, however, we may even go further and treat the electromagnetic field as one-dimensional standing wave and the quantization volume becomes a quantization length. Equivalently, we could have approximated the cavity by two infinite mirrors a distance L apart. So we eventually arrive at

$$\mathbf{E}(x) = i\sum_{\lambda} \int \sqrt{\frac{\omega_k}{2\varepsilon_0 L}} \left(\boldsymbol{\epsilon}^*_{k,\lambda} \mathrm{a}^{\dagger}_{k,\lambda} u^*_k(x) - u_k(x) \mathrm{a}_{k,\lambda} \boldsymbol{\epsilon}_{k,\lambda} \right) dk, \tag{2.19}$$

where $u_k(x)$ is now a solution to the 1D Helmholtz equation

$$\left(\frac{d^2}{dx^2} + k^2 \right) u_k(x) = 0, \tag{2.20}$$

which is solved by

$$u_k(x) = \sqrt{2}\cos(kx + \phi). \tag{2.21}$$

The factor $\sqrt{2}$ stems from our normalization condition eq. (2.5). Since we are free to choose ϕ on our behalf, we opt for $\phi \equiv 0$. For $m \in \mathbb{N}$

$$\begin{aligned} \omega_C &= k_C \\ &= 2\pi m \frac{1}{L}, \end{aligned} \tag{2.22}$$

where

$$\frac{1}{L} = \nu_{FSR} \tag{2.23}$$

is the *free spectral range* of the cavity. ω_C is the frequency of a specific mode, an integer multiple of ν_{FSR}, eq. (2.22). The cavity wave-number k_C is usually termed *recoil wave-number* k_{rec} since it is proportional to the recoil momentum transferred to the atom or particle by absorption of a single photon,

$$k_C \equiv k_{rec}. \tag{2.24}$$

For a high-finesse cavity with a narrow transmission window, which means that κ from eq. (2.44) is much smaller than ν_{FSR}, we may consider a single mode only. For our purpose we choose $m \gg 1$.

Omitting the index k the mode function takes the form

$$u(x) = \sqrt{2}\cos(k_{rec}x). \tag{2.25}$$

and the electric field operator inside the cavity then reads

$$\mathbf{E}(x) = i\sqrt{\frac{\omega_C}{\varepsilon_0 L}}\cos(k_{rec}x)\left(\boldsymbol{\epsilon}^*_{k_{rec},\lambda_C}\mathrm{a}^\dagger_{k_{rec},\lambda_C} - \mathrm{a}_{k_{rec},\lambda_C}\boldsymbol{\epsilon}_{k_{rec},\lambda_C}\right). \tag{2.26}$$

The Hamiltonian eq. (2.18) then reduces to

$$\mathrm{H}_{pf} = \sum_\alpha \frac{\mathbf{p}_\alpha^2}{2m_\alpha} + \mathrm{V}_{Coul} + \omega_{k_C} a^\dagger_{\boldsymbol{k}_C,\lambda_C} a_{\boldsymbol{k}_C,\lambda_C} - \frac{1}{\varepsilon_0}\mathbf{d}\cdot\mathbf{E}(\mathrm{X}_a). \tag{2.27}$$

with X_a the atom's center of mass position along the cavity axis. Since there will be no other modes involved but the single cavity mode, we will drop the subscripts $\boldsymbol{k}_C$, λ_C of the cavity mode operators for practical convenience

$$\mathrm{a}^{(\dagger)}_{\boldsymbol{k}_C,\lambda_C} \to \mathrm{a}^{(\dagger)}. \tag{2.28}$$

2.1.4 The Atom

The atom, as we know it, is a complex structure of electron orbits. We may obtain analytical expressions for the orbital structure for its simplest form only, the hydrogen atom. And yet the single-mode cavity permits for a fully quantum mechanical treatment of any kind of atoms, with certain sound approximations being made. Since there is only one mode in our cavity, we may drive a very specific transition that involves two orbitals only. This means that we neglect contributions from other orbitals and treat the atom effectively as a two-level system. However, some criteria must be met. The transition under consideration must be a *dipole transition*, i.e. $\Delta l = 1$.[5] For large detuning between cavity mode and the transition frequency of choice one has to ensure that no other transition is close to the mode frequency, *independent* of their multipole moment. Quadrupole or higher order transitions at resonance may contribute as much as far off-resonant dipole transitions. We reduce the atom's internal state space to a two-level system with states $|g\rangle$ and $|e\rangle$, denoting the *ground* state and *excited* state, respectively. Speaking about two-level systems it seems inevitable to introduce the *Pauli operators*

$$\sigma_+ = |e\rangle\langle g| \tag{2.29}$$

$$\sigma_- = |g\rangle\langle e| \tag{2.30}$$

$$\sigma_z = |e\rangle\langle e| - |g\rangle\langle g| \tag{2.31}$$

[5] For a standard electronic orbital labeling scheme see e.g. chapter 7 of [33]. For a brief introduction to multipole operators, selection rules etc. see chapter 10.8 of [33].

and their well-known commutation relations

$$[\sigma_+,\, \sigma_-] = \sigma_z \tag{2.32}$$

$$[\sigma_\pm,\, \sigma_z] = \mp 2\sigma_\pm. \tag{2.33}$$

With that at hand we are now able to tie contributions from both kinetic and Coulomb energy of the ground and excited state to a single parameter: the total energy difference, denoted ω_a.[6] Separating relative and center of mass motion of electrons and nucleus we may replace

$$\sum_\alpha \frac{\mathbf{p}_\alpha^2}{2m_\alpha} + \mathrm{V}_{Coul} \to \omega_a \sigma_+ \sigma_- + \frac{\mathbf{p}_a^2}{2m_a}. \tag{2.34}$$

where $\mathbf{p}_a$ is the atom's center of mass momentum. In the 1D case we replace the momentum operator by its projection along the cavity axis, $\mathbf{p}_a \to \mathrm{p}_a$.

The kinetic energy of the electrons' relative motion as well as the total Coulomb energy is absorbed into ω_a. We proceed similarly for the interaction part. Since we can arbitrarily choose the phase of a wave-function we may define the matrix element

$$\boldsymbol{d} \equiv \langle e|\, \mathbf{d}\, |g\rangle \tag{2.35}$$

to be real-valued. Assuming real polarization vectors and mode functions, i.e. $\boldsymbol{\epsilon}^*_{\boldsymbol{k}_C,\,\lambda_C} = \boldsymbol{\epsilon}_{\boldsymbol{k}_C,\,\lambda_C}$ and $u(x) = u^*(x)$, respectively, we define

$$\begin{aligned} g(x) &= \sqrt{\frac{\omega_C}{2\varepsilon_0 L_m}}\boldsymbol{d}\cdot\boldsymbol{\epsilon}_{\boldsymbol{k}_C,\,\lambda_C} u(x) \\ &= \sqrt{\frac{\omega_C}{\varepsilon_0 L}}\boldsymbol{d}\cdot\boldsymbol{\epsilon}_{\boldsymbol{k}_C,\,\lambda_C} \cos(k_{rec}x) \\ &\equiv g_0 \cos(k_{rec}x). \end{aligned} \tag{2.36}$$

Adopted to the two-level description, the dipole interaction term becomes

$$-\mathbf{d}\cdot\mathbf{E}(\mathrm{X}_a) \to -ig(\mathrm{X}_a)\left(\mathrm{a}^\dagger - \mathrm{a}\right)(\sigma_+ + \sigma_-)\,. \tag{2.37}$$

Summarizing, we find the Hamiltonian for a two-level system interacting with a single-mode electromagnetic field

$$\mathrm{H}' = \frac{\mathrm{p}_a^2}{2m_a} + \omega_a\sigma_+\sigma_- - ig(\mathrm{X}_a)(\sigma_+ + \sigma_-)\left(\mathrm{a}^\dagger - \mathrm{a}\right) + \omega_{k_C}\mathrm{a}^\dagger\mathrm{a}. \tag{2.38}$$

The first term on the right hand side of eq. (2.38) is the kinetic energy of the atom's center of mass motion, which is basically the kinetic energy of its nucleus. The last term on the right hand side of eq. (2.38) gives the energy of the intracavity photons. Taking a closer look on the interaction part, we observe four processes being formally considered:

[6] Though not stated explicitly, ω_a may also account for Stark shifts arising from couplings to non-resonant energy levels.

(i) $\sigma_+ \mathrm{a}$ - excitation of the atom via absorption of a photon,

(ii) $\sigma_- \mathrm{a}^\dagger$ - emission of a photon via de-excitation of the atom,

(iii) $\sigma_+ \mathrm{a}^\dagger$ - emission of a photon and excitation of the atom,

(iv) $\sigma_- \mathrm{a}$ - de-excitation of the atom and absorption of a photon,

two of which are energy conserving and two which are not. Discarding the non-energy conserving terms is part of the *rotating wave approximation*. The subject is clearer if one transforms eq. (2.38) to an interaction picture:

$$\mathrm{H}_I' = \frac{\mathrm{p}_a^2}{2m_a} - ig(\mathrm{X}_a)\Big(\sigma_- \mathrm{a}^\dagger e^{i(\omega_C-\omega_a)t} - \sigma_+ \mathrm{a} e^{-i(\omega_C-\omega_a)t} + \sigma_+ \mathrm{a}^\dagger e^{i(\omega_C+\omega_a)t} - \sigma_- \mathrm{a} e^{-i(\omega_C+\omega_a)t}\Big). \tag{2.39}$$

The first two, energy conserving, terms on the right hand side of eq. (2.39) oscillate with $\pm(\omega_C - \omega_a)$, while the other two, so-called *counter-rotating*, terms oscillate with $\pm(\omega_C + \omega_a)$. In the case where

$$\omega_C + \omega_a \gg |\omega_C - \omega_a|\,, \tag{2.40}$$

a typical situation for quantum optical systems, one argues that the counter-rotating terms average to zero quite rapidly [21, 23]. More rigorously, if we calculate the time evolution operator $U_I(t_0, t_0 + \Delta t)$ for $(\omega_C + \omega_a)^{-1} \ll \Delta t \ll |\omega_C - \omega_a|^{-1}$, we find that the contributions from co- and counter-rotating terms scale with $|\omega_C - \omega_a|^{-1}$ and $(\omega_C + \omega_a)^{-1}$, respectively. By virtue of eq. (2.40) we find

$$\frac{|\omega_C - \omega_a|}{\omega_C + \omega_a} \ll 1. \tag{2.41}$$

Plugging in some typical values, ω_C, $\omega_a \approx 10^{15}\,\mathrm{Hz}$, $|\omega_C - \omega_a| \approx 10^{7}\,\mathrm{Hz}$, we get

$$\frac{|\omega_C - \omega_a|}{\omega_C + \omega_a} \approx 10^{-8} \ll 1, \tag{2.42}$$

so eq. (2.41) is well satisfied. Returning to the Schrödinger picture and dropping the counter-rotating terms we arrive at what is known as the *Jaynes-Cummings Hamiltonian* [34]

$$\mathrm{H_{JC}} = \frac{\mathrm{p}_a^2}{2m_a} + \omega_a \sigma_+ \sigma_- - ig(\mathrm{X}_a)\left(\sigma_- \mathrm{a}^\dagger - \sigma_+ \mathrm{a}\right) + \omega_C \mathrm{a}^\dagger \mathrm{a} \tag{2.43}$$

including atomic motion and a position-dependent coupling constant $g(\mathrm{X}_a)$.

2.1.5 External Cavity Pumping and Spontaneous Emission

The effective equation of motion for a system immersed in a heat bath, the *master equation* has been discussed in chapter 1. There are two parts in our model that couple to a bath:

- the atom via spontaneous emission with decay rate γ
- the cavity via leakage with leakage rate 2κ.

After the general discussion in chapter 1 all we have to do is find the corresponding system operators earlier denoted as $\mathrm{c}^{(\dagger)}$. Spontaneous emission implies the de-excitation of the atom. The operator that de-excites the atom is σ_-. Analogously, the loss of a photon is obtained by application of a. The resulting contributions to the Liouvillian read (see eq. (1.30))

$$\mathcal{J}_C\rho = \kappa\left(2\mathrm{a}\rho\mathrm{a}^\dagger - \mathrm{a}^\dagger\mathrm{a}\rho - \rho\mathrm{a}^\dagger\mathrm{a}\right) \tag{2.44}$$

$$\mathcal{J}_a\rho = \frac{\gamma}{2}\left(2\sigma_-\rho\sigma_+ - \sigma_+\sigma_-\rho - \rho\sigma_+\sigma_-\right) \tag{2.45}$$

and

$$\mathcal{J} = \mathcal{J}_C + \mathcal{J}_a. \tag{2.46}$$

The resulting master equation is

$$\begin{aligned}\partial_t\rho &= -i\left[\mathrm{H},\,\rho\right] + \mathcal{J}\rho \\ &\equiv \mathcal{L}\rho.\end{aligned} \tag{2.47}$$

Rather than just observe the cavity's decays we would like to drive it with an external laser pump field. The laser field pumping the cavity is a time-dependent coherent state in the bath modes

$$\begin{aligned}\left|\beta_{\omega_p}e^{-i\omega_p t}\right\rangle &\equiv \mathrm{D}(\beta_{\omega_p}e^{-i\omega_p t})\left|0\right\rangle \\ &\equiv \exp\left[\beta_{\omega_p}e^{-i\omega_p t}\mathrm{b}^\dagger_{\omega_p} - \beta^*_{\omega_p}e^{i\omega_p t}\mathrm{b}_{\omega_p}\right]\left|0\right\rangle,\end{aligned} \tag{2.48}$$

where $\mathrm{D}(\alpha)$ is also called the *displacement operator*.[7] Filling the bath with a coherent state might shatter our vacuum assumption from section 1.2. Therefore we rewrite the interaction Hamiltonian to give

$$\begin{aligned}\mathrm{H}_{int} = i\sqrt{\frac{\kappa}{\pi}}\int_{\omega_0-\theta}^{\omega_0+\theta}\Big(&\left(\mathrm{b}^\dagger_\omega\mathrm{a} - \mathrm{a}^\dagger\mathrm{b}_\omega\right) - \left(\beta^*_\omega e^{i\omega_p t}\mathrm{a} - \mathrm{a}^\dagger\beta_\omega e^{-i\omega_p t}\right)\delta(\omega-\omega_p) \\ &+ \left(\beta^*_\omega e^{i\omega_p t}\mathrm{a} - \mathrm{a}^\dagger\beta_\omega e^{-i\omega_p t}\right)\delta(\omega-\omega_p)\,d\omega\Big).\end{aligned} \tag{2.49}$$

[7] Unfortunately the operators defined in eq. (2.17) and eq. (2.48) are named alike although their mathematical form and physical interpretation are quite different.

The terms in the first line in eq. (2.49) mutually cancel when they act on the coherent state eq. (2.48) while the second line is an operator that acts on the system Hilbert space only. Thus we can absorb the second line of eq. (2.49) into the system Hamiltonian H_{sys}, which gives rise to the coherent *pump term*[8]

$$\mathrm{H}_p(t) = -i\eta \left(\mathrm{a}^\dagger e^{-i\omega_p t} - \mathrm{a} e^{i\omega_p t}\right) \tag{2.50}$$

with

$$\eta = \sqrt{\frac{\kappa}{\pi}}\beta_{\omega_p}. \tag{2.51}$$

2.2 Adiabatic Elimination of the Internal Atomic States

At the current stage the system Hamiltonian reads (eqs. (2.43) and (2.50))

$$\begin{aligned}\mathrm{H}_{sys} &= \mathrm{H}_{\mathrm{JC}} + \mathrm{H}_p \\ &= \frac{\mathrm{p}_a^2}{2m_a} + \omega_a \sigma_+\sigma_- - ig(\mathrm{X}_a)\left(\sigma_-\mathrm{a}^\dagger - \sigma_+\mathrm{a}\right) + \omega_C \mathrm{a}^\dagger\mathrm{a} - i\eta\left(\mathrm{a}^\dagger e^{-i\omega_p t} - \mathrm{a}e^{i\omega_p t}\right).\end{aligned} \tag{2.52}$$

The explicit time dependence from eq. (2.50) can be eliminated by a transformation to a rotating frame

$$\mathrm{U}(t) = \exp[-i\omega_p\left(\mathrm{a}^\dagger\mathrm{a} + \frac{\sigma_z}{2}\right)t] \tag{2.53}$$

we transform

$$\begin{aligned}\mathrm{H}'_{sys} &= \mathrm{U}(t)\mathrm{H}_{sys}\mathrm{U}^\dagger(t) - i\mathrm{U}^\dagger(t)\partial_t\mathrm{U}(t) \\ &= \frac{\mathrm{p}_a^2}{2m_a} - \Delta_a\sigma_+\sigma_- - ig(\mathrm{X}_a)\left(\sigma_-\mathrm{a}^\dagger - \sigma_+\mathrm{a}\right) - \Delta_C\mathrm{a}^\dagger\mathrm{a} - i\eta\left(\mathrm{a}^\dagger - \mathrm{a}\right)\end{aligned} \tag{2.54}$$

with

$$\Delta_a = \omega_p - \omega_a \tag{2.55a}$$

$$\Delta_C = \omega_p - \omega_C. \tag{2.55b}$$

Time-independent operators in the Schrödinger picture obey

$$\begin{aligned}\partial_t \langle \cdot \rangle &= \mathrm{Tr}\{\cdot\,\partial_t\rho\} \\ &= \mathrm{Tr}\{\cdot\,\mathcal{L}\rho\}.\end{aligned} \tag{2.56}$$

Therefore we combine eqs. (2.45) and (2.54), and note that

$$\sigma_+\sigma_- = \frac{1}{2}\left(\sigma_z + 1\right), \tag{2.57}$$

[8] Here we assume $\beta^*_{\omega_p} = \beta_{\omega_p}$.

to obtain the equations of motion for the mean-values of the atomic variables[9]

$$\partial_t \langle \sigma_- \rangle_a = \left(i\Delta_a - \frac{\gamma}{2} \right) \langle \sigma_- \rangle_a + g(\mathrm{X}_a) \langle \sigma_z \rangle_a \mathrm{a} \tag{2.58a}$$

$$\partial_t \langle \sigma_+ \rangle_a = \left(-i\Delta_a - \frac{\gamma}{2} \right) \langle \sigma_+ \rangle_a + g(\mathrm{X}_a) \langle \sigma_z \rangle_a \mathrm{a}^\dagger. \tag{2.58b}$$

The subscript a denotes that the trace is only performed along the atomic degrees of freedom i.e.

$$\begin{aligned} \langle \cdot \rangle_a &= \mathrm{Tr} \{ \cdot \}_a \\ &= \langle e | \cdot \rho | e \rangle + \langle g | \cdot \rho | g \rangle . \end{aligned} \tag{2.59}$$

In case that κ from eq. (2.44), Δ_a from eq. (2.58) and γ of eq. (2.45) obey

$$\gamma, \Delta_a \gg \kappa \tag{2.60}$$

the atomic variables evolve on much faster timescales than the cavity. The internal states of the atom approach a steady-state under the constraints provided by the cavity. The cavity field is considered constant at the short time scales of the atomic variables and the atomic variables have to adapt. Therefore the atomic variables are *enslaved* by the cavity field, one of the many manifestations of *Haken's slaving principle*. This slaving principle provides the basis for *adiabatic elimination*.[10] The action of the atom on the cavity dynamics is then governed by the steady-state solutions of eqs. (2.58)

$$\langle \sigma_- \rangle_{a,\,ss} = \frac{g(\mathrm{X}_a) \langle \sigma_z \rangle_{a,\,ss} \mathrm{a}}{-i\Delta_a + \frac{\gamma}{2}} \tag{2.61a}$$

$$\langle \sigma_+ \rangle_{a,\,ss} = \frac{g(\mathrm{X}_a) \langle \sigma_z \rangle_{a,\,ss} \mathrm{a}^\dagger}{i\Delta_a + \frac{\gamma}{2}}. \tag{2.61b}$$

When we trace over the internal atomic states in their steady-state in eq. (2.54) using the results of eqs. (2.61) we are left with (by virtue of eq. (2.57))

$$\begin{aligned} \mathrm{Tr} \left\{ \mathrm{H}'_{sys} \right\}_a &= \frac{\mathrm{p}_a^2}{2m_a} - \Delta_a \langle \sigma_+ \sigma_- \rangle_{a,\,ss} - ig(\mathrm{X}_a) \left(\langle \sigma_- \rangle_{a,\,ss} \mathrm{a}^\dagger - \langle \sigma_+ \rangle_{a,\,ss} \mathrm{a} \right) \\ &\quad - \Delta_C \mathrm{a}^\dagger \mathrm{a} - i\eta \left(\mathrm{a}^\dagger - \mathrm{a} \right) \\ &= \frac{\mathrm{p}_a^2}{2m_a} - \frac{\Delta_a}{2} \left(\langle \sigma_z \rangle_{a,\,ss} + 1 \right) + \langle \sigma_z \rangle_{a,\,ss} \frac{2|g(\mathrm{X}_a)|^2 \Delta_a}{\frac{\gamma^2}{4} + \Delta_a^2} \mathrm{a}^\dagger \mathrm{a} \\ &\quad - \Delta_C \mathrm{a}^\dagger \mathrm{a} - i\eta \left(\mathrm{a}^\dagger - \mathrm{a} \right). \end{aligned} \tag{2.62}$$

[9] Here $\sigma_{\pm,\,z}$ are extended to the full Hilbert space $\sigma_{\pm,\,z} \to \sigma_{\pm,\,z} \otimes 1 \equiv \sigma_{\pm,\,z}$. The notation is often ambiguous, but whether or not the extended version of $\sigma_{\pm,\,z}$ is in charge should be clear from context.

[10] See [35], [36] and [37] for general introduction to synergetics. See [38] for adiabatic elimination in stochastic differential equations and [21] for specific application in quantum optics.

The resulting effective Hamiltonian depends on $\langle\sigma_z\rangle_{a,\,ss}$ which is found for vacuum baths as

$$\langle\sigma_z\rangle_{a,\,ss}(\mathrm{X}_a) = -\frac{\Delta_a^2 + \frac{1}{4}\gamma^2}{\Delta_a^2 + \frac{1}{4}\gamma^2 + \frac{1}{2}|g(\mathrm{X}_a)|^2\mathrm{a}^\dagger\mathrm{a}}. \tag{2.63}$$

If we define

$$\mathrm{U}_0 = -\langle\sigma_z\rangle_{a,\,ss}\frac{2g_0^2\Delta_a}{\frac{\gamma^2}{4} + \Delta_a^2}, \tag{2.64}$$

with g_0 from eq. (2.36), we may rewrite eq. (2.62) as

$$\mathrm{Tr}\left\{\mathrm{H}'_{sys}\right\}_a = \frac{\mathrm{p}_a^2}{2m_a} - \frac{\Delta_a}{2}\left(\langle\sigma_z\rangle_{a,\,ss} + 1\right) - \left(\Delta_C - U_0|u(\mathrm{X}_a)|^2\right)\mathrm{a}^\dagger\mathrm{a} - i\eta\left(\mathrm{a}^\dagger - \mathrm{a}\right). \tag{2.65}$$

With the steady-state expression for $\langle\sigma_z\rangle_{a,\,ss}$, eq. (2.63), U_0 is an operator on the photonic and momentum subspace. In the far detuned limit where

$$\Delta_a \gg \gamma \tag{2.66a}$$

$$\Delta_a \gg \frac{\eta}{\kappa} \tag{2.66b}$$

we find

$$\langle\sigma_z\rangle_{a,\,ss} \approx -1, \tag{2.67}$$

which is independent of X_a and $\mathrm{a}^\dagger\mathrm{a}$. The increase of Δ_a has to be within the constraints discussed in section 2.1.4, otherwise the validity of our two-level model would break down. Eq. (2.66a) permits for neglecting the effects of spontaneous emission from the atom. Looking at the internal states $|g\rangle$ and $|e\rangle$ only, this may sound a bit unnecessary at first. However, if we include the atom's motion along the cavity, we should become aware that the Liouvillian eq. (2.45) is incomplete. Spontaneous emission of a photon goes along with a recoil on the atom[11], which is not considered in eq. (2.45). The corresponding system operator reads

$$\mathrm{c} = \sigma_- \int_{-1}^{1} \Phi(u)\exp\left[-ik_{rec}\mathrm{X}_a u\right]\,du, \tag{2.68}$$

where u is the projection of the unit photon momentum vector onto the cavity axis and $\Phi(u)$ the corresponding distribution of projected values. Going to the far detuned limit allows retaining the form of eq. (2.45) a posteriori.

With eq. (2.67) the nature of U_0 changes from operator to number. This enables us to use it as a parameter in our Hamiltonian rather than worrying about its operator structure

$$\mathrm{U}_0 \to \frac{2g_0^2\Delta_a}{\frac{\gamma^2}{4} + \Delta_a^2} = U_0. \tag{2.69}$$

[11] This is the basic mechanism for laser cooling.

Eq. (2.67) also removes the second term on the right hand side of eq. (2.62).

Collecting the above results and approximations we arrive at the effective Hamiltonian

$$\begin{aligned} \mathrm{H}'_{1p1m} &\equiv \mathrm{Tr}\left\{\mathrm{H}'_{sys}\right\}_a \\ &= \frac{\mathrm{p}_a^2}{2m_a} - \left(\Delta_C - U_0 u(\mathrm{X}_a)^2\right)\mathrm{a}^\dagger\mathrm{a} - i\eta\left(\mathrm{a}^\dagger - \mathrm{a}\right). \end{aligned} \tag{2.70}$$

We apply a unitary transformation

$$\mathrm{U} = \exp\left[-i\frac{\pi}{2}\mathrm{a}^\dagger\mathrm{a}\right] \tag{2.71}$$

and plug in the explicit form of the mode function eq. (2.25) to get

$$\mathrm{H}_{1p1m} = \frac{\mathrm{p}_a^2}{2m_a} - \left(\Delta_C - U_0\cos^2(k_{rec}\mathrm{X}_a)\right)\mathrm{a}^\dagger\mathrm{a} + \eta\left(\mathrm{a}^\dagger + \mathrm{a}\right). \tag{2.72}$$

The two forms eqs. (2.70) and (2.72) are physically equivalent. However, as becomes apparent in section 4.4.1, the mathematical form of eq. (2.72) turns out to be advantageous for our purposes. Eq. (2.72) is the Hamiltonian for a two-level atom moving along the axis of a one-dimensional single mode cavity. This sounds like a special case, but there are many quantum particles and objects that can be prescribed or approximated as two-level atoms. The form of the Hamiltonian eq. (2.72) is therefore capable of handling a much wider class of physically realized quantum particles than just two-level atoms. It may also account for a Bose-Einstein condensate (BEC) with very weak interparticle interaction (low scattering length) [39]. In the following chapters we will analyze the one particle - one mode system evolving under eqs. (2.72) and (2.44) and try to characterize its properties for different parameters U_0, η, Δ_C and κ. We will not be concerned, however, with the true nature of the quantum particle inside the cavity.

3 General Discussion of the Hamiltonian and Semi-Classical Treatment of the One Particle-One Mode System

The Hamiltonian eq. (2.72) looks very innocent, but the effective interaction term derived in section 2.2

$$\mathrm{H}_{int,\,eff} = \left(\Delta_C - U_0 \cos^2(k_{rec}\mathrm{X}_a)\right) \mathrm{a}^\dagger \mathrm{a} \tag{3.1}$$

is obviously *non-linear*. Including dissipation the system's equation of motion obeys a *master equation*, which explicitly reads

$$\begin{aligned} \dot{\rho} &= -i[\mathrm{H}_{1p1m},\, \rho] + \kappa(2\mathrm{a}\rho\mathrm{a}^\dagger - \mathrm{a}^\dagger\mathrm{a}\rho - \rho\mathrm{a}^\dagger\mathrm{a}) \\ &\equiv \mathcal{L}_{1p1m}\rho. \end{aligned} \tag{3.2}$$

A first approach to characterize the system is to look at the Heisenberg equations of motion for mean values, which are directly obtained from eq. (3.2) via

$$\begin{aligned} \partial_t \langle \mathrm{A} \rangle &= \partial_t \,\mathrm{Tr}\,\{\mathrm{A}\rho\} \\ &= \mathrm{Tr}\,\{\mathrm{A}\partial_t\rho\} \\ &= \mathrm{Tr}\,\{\mathrm{A}\mathcal{L}_{1p1m}\rho\}\,, \end{aligned} \tag{3.3}$$

where A is a time-independent operator in the Schrödinger picture. Eq. (3.3) yields the equations of motion for the field amplitude $\alpha = \langle \mathrm{a} \rangle$ and mean photon number $n = \left\langle \mathrm{a}^\dagger\mathrm{a} \right\rangle$

$$\begin{aligned} \partial_t\alpha &= \mathrm{Tr}\,\{\mathrm{a}\dot{\rho}\} \\ &= \left[i\left(\Delta_C - U_0\left\langle \cos^2(k_{rec}\mathrm{X}_a)\right\rangle\right) - \kappa\right]\alpha + \eta \end{aligned} \tag{3.4}$$

$$\begin{aligned} \partial_t n &= \mathrm{Tr}\left\{\mathrm{a}^\dagger\mathrm{a}\dot{\rho}\right\} \\ &= \eta\,(\alpha^* + \alpha) - 2\kappa n. \end{aligned} \tag{3.5}$$

Without interaction, i.e. $U_0 = 0$, we can separate particle and field space and solve them independently.[1] The solution is a direct product of the initial momentum distribution and a coherent field state (see eq. (2.48))

$$|\alpha(t)\rangle = \mathrm{D}\,(\alpha(t))\,|0\rangle\,. \tag{3.6}$$

[1] The case $U_0 = 0$ is called the *empty cavity* because the presence of the atom does not alter the cavity dynamics. In a truly empty cavity, however, a particle momentum space would be superfluous.

If the cavity is initially in a vacuum state, the field amplitude α obeys

$$\alpha(t) = \frac{\eta}{\kappa - i\Delta_C}\Big(1 - e^{(\Delta_C - \kappa)t}\Big). \tag{3.7}$$

In this way the empty cavity is trivially solved. Hence we expect that for small U_0 a product ansatz can still be a good approximation. With increasing U_0, however, this ansatz may give less and less accurate results.

In the remainder of this chapter we are concerned with the system's steady-state properties. We set the left hand sides of eqs. (3.4) and (3.5) equal to zero and combine the results to formulate a *self-consistency equation*

$$n = \frac{\eta^2}{\kappa^2 + \left(\Delta_C - U_0 \left\langle \cos^2(k_{rec}\mathrm{X}_a)\right\rangle\right)^2}. \tag{3.8}$$

The second term in the denominator of eq. (3.8),

$$\left(\Delta_C - U_0 \left\langle \cos^2(k_{rec}\mathrm{X}_a)\right\rangle\right)^2 \equiv \Delta_{eff}^2(\mathrm{X}_a), \tag{3.9}$$

can be interpreted as an *effective detuning* $\Delta_{eff}(\mathrm{X}_a)$ that depends on the particle position X_a. Since $\Delta_{eff}^2 \geq 0$ we find

$$n \leq \frac{\eta^2}{\kappa^2} \tag{3.10}$$

in the steady-state. The $U_0 \cos^2$-interaction term that contributes to Δ_{eff} plays two roles. Evidently it shifts the cavity' resonance frequency via Δ_{eff}, eq. (3.9). Combining eqs. (2.55b) and (3.9) we get

$$\begin{aligned} \Delta_{eff} &= \Delta_C - U_0 \left\langle \cos^2(k_{rec}\mathrm{X}_a)\right\rangle \\ &= \omega_p - \omega_C - U_0 \left\langle \cos^2(k_{rec}\mathrm{X}_a)\right\rangle \\ &\equiv \omega_p - \omega_{eff}, \end{aligned} \tag{3.11}$$

where we defined the effective cavity frequency

$$\omega_{eff} = \omega_C + U_0 \left\langle \cos^2(k_{rec}\mathrm{X}_a)\right\rangle \tag{3.12}$$

Whether the interaction term increases or decreases the resonance frequency depends on the sign of U_0 because

$$\left\langle \cos^2(k_{rec}\mathrm{X}_a)\right\rangle \geq 0 \tag{3.13}$$

in any case. A shift of the resonance frequency at constant cavity length corresponds to a shift of the cavity's refractive index via internal medium. A positive shift marks a decreased refractive index and vice versa. Therefore a refractive index below 1 seems to be theoretically achievable [20].

If we return to the Hamiltonian eq. (2.72) the second role of the interaction term in the self-consistent mean-value equations becomes apparent. $U_0 \cos^2(k_{rec}\mathrm{X}_a)\mathrm{a}^\dagger\mathrm{a}$ serves as trapping potential for the particle, which becomes

$$\mathrm{V}(\mathrm{X}_a) = nU_0 \cos^2(k_{rec}\mathrm{X}_a) \tag{3.14}$$

in terms of mean intensity. From that point of view U_0 is the potential depth per photon. Its sign determines whether the atom is a *low-field seeker* or a *high-field seeker*, i.e. whether it is pushed towards the nodes or antinodes of the cavity light field, respectively.

Exploring the steady-state properties for different parameter values, we see that this double role of the interaction term makes the one particle - one mode problem a non-trivial one. A fluctuation in the photon number may change the depth of the potential and by that the refractive index via the shape of the particle wave-function and the changing refractive index acts back on the photon number.[2] Since the mean value equation eq. (3.8) is intrinsically non-linear, we expect to find multiple self-consistent solutions in some ranges of the parameter space and probably witness multistability.

To obtain self-consistent solutions to eq. (3.8) we proceed according to the following scheme:

(i) we assume a steady-state mean photon number n

(ii) we assume a potential $U_0 \cos^2(k_{rec}\mathrm{X}_a)n$ without taking care of the quantum nature of the photon field

(iii) we solve the corresponding Schrödinger equation for the particle (analytically or numerically, depending on the employed model)

(iv) we calculate the expectation value $\langle \cos^2(k_{rec}\mathrm{X}_a)\rangle$ for the various eigenfunctions

(v) we vary Δ_C and try to identify conditions when eq. (3.8) holds self-consistently for the photon number.

From this semi-classical treatment we expect a guideline to multistability regions in the parameter space. It does, however, by no means provide a steady-state solution to the master equation.

3.1 The Harmonic Oscillator Regime of Particle Motion

In a first approach, we may consider a deep trap limit. For large photon numbers and strong light-momentum coupling, i.e.

$$\sqrt{\frac{U_0}{\omega_{rec}}\langle a^\dagger a\rangle} \gg 1, \tag{3.15}$$

[2] An intensity-dependent index of refraction is a typical problem of non-linear optics.

we can treat the optical potential as harmonic oscillator potentials at each lattice site. Assuming the atom is strongly localized at a given side, we approximate

$$\cos^2(k_{rec}\mathrm{X}_a) \approx 1 - k_{rec}^2\mathrm{X}_a^2 \tag{3.16}$$

yielding a harmonic oscillator potential. Looking at the mean-value equations of motion eq. (3.3) we discover a nice property of the harmonic oscillator. The equations (see eqs. (3.4) and (3.5))

$$\partial_t\alpha^{(*)} = \left(i\Delta_C \pm iU_0\left(1 - k_{rec}^2\left\langle \mathrm{X}_a^2\right\rangle\right) - \frac{\kappa}{2}\right)\alpha^{(*)} + \eta^{(*)} \tag{3.17a}$$

$$\partial_t n = \eta\left(\alpha^* + \alpha\right) - \kappa n \tag{3.17b}$$

$$\partial_t\left\langle \mathrm{X}_a^2\right\rangle = \frac{1}{m}\left(\langle \mathrm{p}_a\mathrm{X}_a\rangle + \langle \mathrm{X}_a\mathrm{p}_a\rangle\right) \tag{3.17c}$$

$$\partial_t\left(\langle \mathrm{p}_a\mathrm{X}_a\rangle + \langle \mathrm{X}_a\mathrm{p}_a\rangle\right) = \frac{2}{m}\left\langle \mathrm{p}_a^2\right\rangle + 4U_0\left(k_{rec}^2\left\langle \mathrm{X}_a^2\right\rangle\right)n \tag{3.17d}$$

$$\partial_t\left\langle \mathrm{p}_a^2\right\rangle = 2U_0k_{rec}^2\left(\langle \mathrm{p}_a\mathrm{X}_a\rangle + \langle \mathrm{X}_a\mathrm{p}_a\rangle\right)n \tag{3.17e}$$

turn out to form a closed set [40]. Eqs. (3.17) describe a harmonic oscillator with time-dependent trap frequency, time-dependent solutions can be obtained numerically [40], [41]. A stationary analysis reveals a variety of steady-states [41].

We hope to find similar elegant solutions at higher orders as well. Extending eq. (3.16) to fourth order

$$\cos^2(k_{rec}\mathrm{X}_a) \approx 1 - k_{rec}^2\mathrm{X}_a^2 + \frac{1}{3}k_{rec}^4\mathrm{X}_a^4, \tag{3.18}$$

we repeat the previous calculation. Our expectations are declined, however, as the mean-value equations of motion do not turn out to form a closed set. Their explicit form is found in appendix A in eqs. (A.6). It appears that closure is reserved to the harmonic oscillator model.

The previous discussion has been purely classical. Returning to a semi-classical treatment we put the approximation eq. (3.16) in eq. (3.8) to find

$$n = \frac{\eta^2}{\left(\Delta_C - U_0\left(1 - k_{rec}^2\left\langle \mathrm{X}_a^2\right\rangle\right)\right)^2 + \kappa^2}. \tag{3.19}$$

We neglect the quantum nature of the photonic potential, i.e. only the mean value $\left\langle a^\dagger a\right\rangle = n$ enters our calculation. The quantum nature of particle motion, however, enters via the harmonic oscillator eigenstates. As given below, $\left\langle \mathrm{X}_a^2\right\rangle$ can be calculated analytically for each harmonic oscillator eigenstate. We then try to find self-consistent solutions of eq. (3.19) for various harmonic oscillator eigenstates. Our quantum particle is subject to the potential

$$V(x) = |U_0|nk_{rec}^2x^2. \tag{3.20}$$

Comparing the expressions

$$\frac{1}{2}m\omega_{ho}^2x^2 = V(x) = |U_0|nk_{rec}^2x^2 \tag{3.21}$$

we arrive at

$$\begin{aligned}\omega_{ho} &= 2\sqrt{\omega_{rec}|U_0|n} \\ \frac{\omega_{ho}}{\omega_{rec}} &= 2\sqrt{\frac{|U_0|}{\omega_{rec}}n} \gg 1\,.\end{aligned} \tag{3.22}$$

For the harmonic oscillator state

$$|n_{ho}\rangle = \frac{\left(a_{ho}^\dagger\right)^{n_{ho}}}{\sqrt{n_{ho}}}\,|0\rangle_{ho}\,, \tag{3.23}$$

where n_{ho} is the harmonic oscillator excitation number and $|0\rangle_{ho}$ denotes the harmonic oscillator ground state, the expectation value of x^2 is found to be

$$\begin{aligned}\left\langle \mathrm{x}^2\right\rangle_{n_{ho}} &= \langle n_{ho}|\,\mathrm{x}^2\,|n_{ho}\rangle \\ &= \frac{2n_{ho}+1}{2m\omega_{ho}}\,,\end{aligned} \tag{3.24}$$

which gets us to

$$\begin{aligned}k_{rec}^2\left\langle \mathrm{x}^2\right\rangle_{n_{ho}} &= (2n_{ho}+1)\,\frac{\omega_{rec}}{\omega_{ho}} \\ &= \frac{2n_{ho}+1}{2\sqrt{\frac{|U_0|}{\omega_{rec}}n}}\,.\end{aligned} \tag{3.25}$$

Eventually we are looking for self-consistent solutions of

$$n = \frac{\eta^2}{\kappa^2 + \left(\Delta_C - U_0\left(1 - \frac{2n_{ho}+1}{2\sqrt{\frac{|U_0|}{\omega_{rec}}n}}\right)\right)^2} \tag{3.26}$$

for different n_{ho}, where n enters on both sides of the equation. We solve eq. (3.26) graphically. Fig. (3.1) shows contours in the Δ_C-$n-$plane where eq. (3.26) holds for a chosen set of parameters.

The contours suggest that the effect of the interaction term increases with higher intensity (larger n), which can be seen in the shift of the resonance frequency.[3] With increasing photon number n, implying a higher pump rate η, the resonance frequency asymptotically approaches U_0, which corresponds to complete localization at the

[3]The resonance frequency is the value $\Delta_{C,\,max}$ for which the contour reaches its maximum photon number n_{max}.

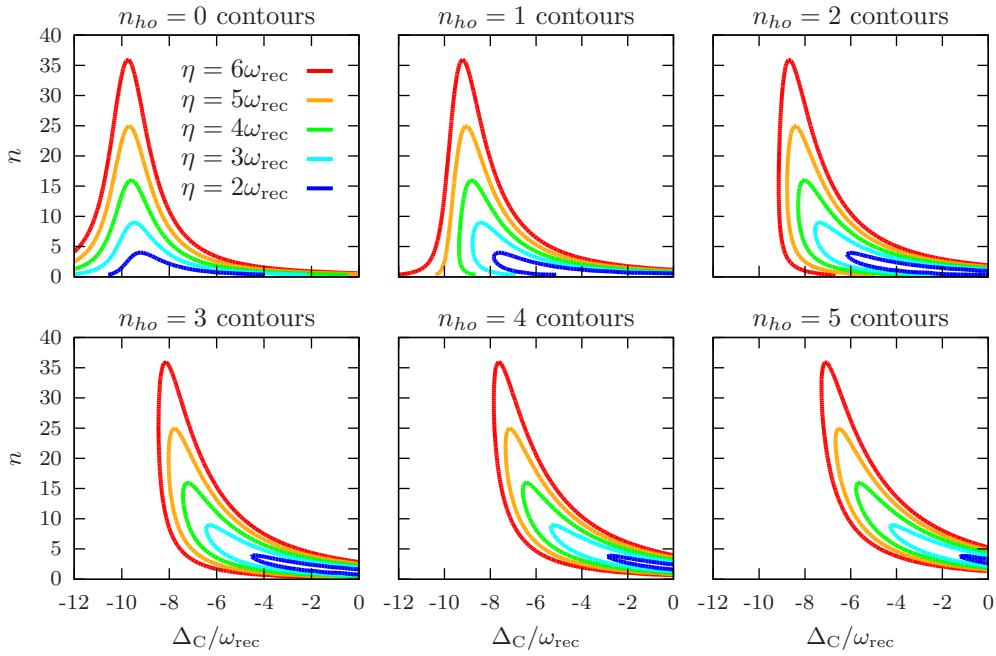

Figure 3.1 Contours of self-consistent photon numbers for eq. (3.26) and the lowest harmonic oscillator eigenstates: $\kappa = 1$, $U_0 = -10$. The quantities are given in units of ω_{rec}.

potential minimum. Since the expectation value $\langle \mathrm{x}^2 \rangle$ increases with n_{ho}, eq. (3.25), higher harmonic oscillator modes are less localized and therefore the corresponding resonance frequency is less shifted. For a given Δ_C the excited states $n_{ho} \neq 0$ show up to two different n which solve eq. (3.26). This may give rise to multistability in some regions of our parameter space.

3.2 Periodic Potential using Wannier Functions

While a harmonic oscillator potential is a valid approximation for large photon numbers (strong localization), it gets inaccurate for low photon numbers and high oscillator excitation numbers n_{ho} because the potential depth is not large enough to form many bound states. In that case we need to consider the full optical lattice. In order to relate the results to the harmonic oscillator for large n we make use of the *Wannier states*, which are localized states in a periodic potential. For simplicity we assume periodic boundary conditions at the edges of the cavity and hope that the error is small when the cavity length L is much larger than the wavelength of the desired cavity mode λ_C, $L \gg \lambda_C$.

The procedure carried out is analogous to the harmonic oscillator case, only that we need to numerically compute the Wannier states for each n, since there is no analytic expression available. We will briefly introduce Wannier functions and continue with

an interpretation of the obtained self-consistency contours.

3.2.1 Definition and Basic Properties of Bloch States

We still neglect the quantum nature of the optical lattice and solve the stationary Schrödinger equation in the periodic potential [42]

$$\begin{aligned} V(x) &= U_0 n \cos^2(k_{rec} x) \\ &= \frac{U_0 n}{2} \left(1 + \cos(2k_{rec} x)\right) \end{aligned} \tag{3.27}$$

This is done best in momentum space, where the potential couples the states $|q\rangle \leftrightarrow |q \pm 2k_{rec}\rangle$. We then look for eigenstates of the Hamiltonian

$$\mathrm{H} = \left(\mathrm{p} + q\right)^2 + \mathrm{V(x)} \tag{3.28}$$

for different q in the first Brillouin zone, $q \in [-k_{krec}, k_{rec}]$. The spacing between two different values of q, Δq, is given by the length of the lattice L or the number of lattice sites N_{ls} under consideration, respectively:

$$\begin{aligned} \Delta q &= \frac{\pi}{L} \\ &= \frac{k_{rec}}{N_{ls}} \,. \end{aligned} \tag{3.29}$$

For each q we get eigenfunctions $\Psi_{mq}(x)$, which are just the eigenfunctions to the m^{th} eigenvalue of the Hamiltonian for a given q represented in real space, $\Psi_{mq}(x) = \langle x|m,\, q\rangle$, the so-called *Bloch functions* [43]. From this set of functions we may construct a set of localized, orthonormal functions [44]

$$\begin{aligned} w_n(x - R) &= \frac{1}{\sqrt{N_{ls}}} \sum_q e^{-iqR} \Psi_{mq}(x) \\ &= \frac{1}{\sqrt{N_{ls}}} \sum_q e^{-iqR} \Psi_{mq}(x - R) e^{iqR} \\ &= \frac{1}{\sqrt{N_{ls}}} \sum_q \Psi_{mq}(x - R) \,, \end{aligned} \tag{3.30}$$

the so-called *Wannier functions* [4]. Each $w_m(x - R)$ is localized at R, where R is a lattice site position, an integer multiple of $\frac{\pi}{k_{rec}}$. The $w_m(x - R)$ obey

$$\int w_n^*(x - R_1)\, w_m(x - R_2)\, dx = \delta_{mn} \delta_{R_1 R_2} \,. \tag{3.31}$$

[4] In line 2 of eq. (3.30) we employ Bloch's periodicity property of eigenfunctions for periodic potentials: $\Psi_{mq}(x + R) = \Psi_{mq}(x) e^{iqR}$, where R is a lattice site position [43].

The phases of the individual Bloch functions in eq. (3.30) are still arbitrary. While a transformation like

$$\Psi_{mq}(x) \to \Psi'_{mq}(x) = e^{i\alpha_{mq}}\Psi_{mq}(x) \tag{3.32}$$

does not change the properties of the Bloch functions, the properties of the corresponding Wannier function may be very sensitive to the specific choice of the α_{mq} [45]. Though this is not relevant for our purposes, and hence we do not examine the varying behavior of Wannier functions for different choices of α_{mq}, it should be mentioned for the sake of completeness.

Fig. (3.2) shows the energy bands of the Bloch states $|\Psi_{mq}\rangle$ for the lowest m in dependence of the potential depth $|U_0 n|$. A band crossing the $E = 0$-line (dashed line in fig. (3.2)) indicates the transition from free to bound states.

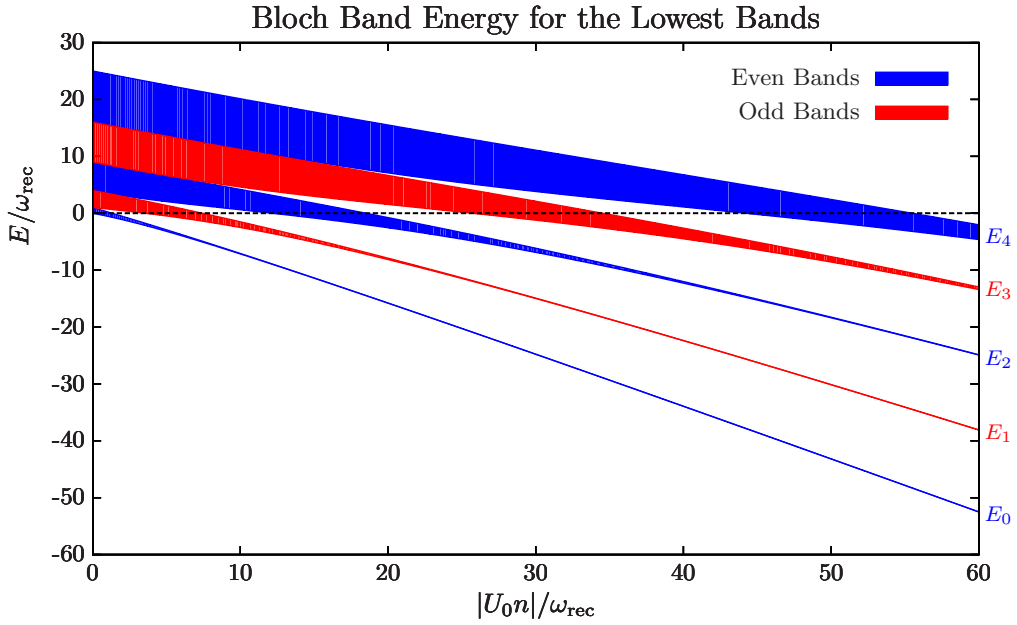

Figure 3.2 Energy for the lowest Bloch bands: For large potentials the dimensionless energy of the lowest band goes as $\sqrt{\frac{|U_0|}{\omega_{rec}}n} - \frac{|U_0|}{\omega_{rec}}n$, eq. (3.22). The lowest bands form an almost equidistant ladder for large potentials (harmonic oscillator regime).

For deep potentials the energy bands approach the harmonic oscillator ladder with equal spacing between the energy levels. The spacing between the levels is then given by eq. (3.22). Once we have numerical values for the $w_m(x - R)$ we again try to find self-consistent solutions to

$$n = \frac{\eta^2}{\left(\Delta_C - U_0 \left\langle \cos^2(k_{rec}x)\right\rangle_{n,m}\right)^2 + \kappa^2}\,, \tag{3.33}$$

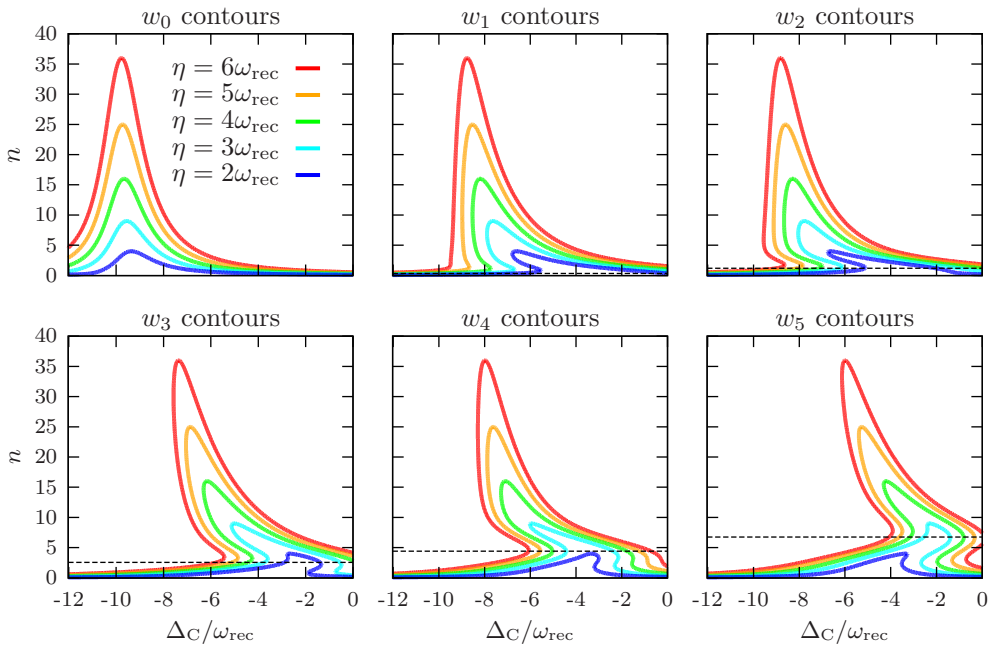

Figure 3.3 Contours of self-consistency of eq. (3.33) for the lowest Wannier states: $\kappa = \omega_{rec}$, $U_0 = -10\,\omega_{rec}$: The dashed lines indicate the transition from free to bound states.

where

$$\left\langle \cos^2(k_{rec}x) \right\rangle_{n,\,m} = \int w^*_{n,\,m}(x)\, \cos^2(k_{rec}x)\, w_{n,\,m}(x)\, dx \tag{3.34}$$

and $w_{n,\,m}(x)$ is the m^{th} Wannier function to the potential for mean photon number n given in eq. (3.27), localized at $R = 0$. Fig. (3.3) shows contours of self-consistency for eq. (3.33) in the Δ_C-$n-$plane, analogously to the harmonic oscillator case.

Once the Wannier states form bound states, above the dashed lines in fig. (3.3), the contours in fig. (3.3) become very much like those in fig. (3.1), below they show different behavior. The properties of unbound states cannot be accounted for in the harmonic oscillator model, hence the discrepancy. Following the contours $W_{n\neq 0}$ from left to right, we see that they take a sharp turn just when they enter the bound regime. The turn indicates that the effect of the atom on the index of refraction decreases just before it starts to increase again. The nature of this phenomenon becomes apparent when we look at the spatial distribution of the Bloch or Wannier states, fig. (3.4). Just before the states become bound, they tend to localize at the potential maxima $V_{max} = 0$. A classical point of view suggests that, just before being bound in a single potential well, a moving particle has its lowest velocity at the top of each potential hill and therefore it is most likely found there.

Due to the non-monotonous effect of the particle in the transition from free to bound states, the self-consistent contours in fig. (3.3) exhibit up to three different,

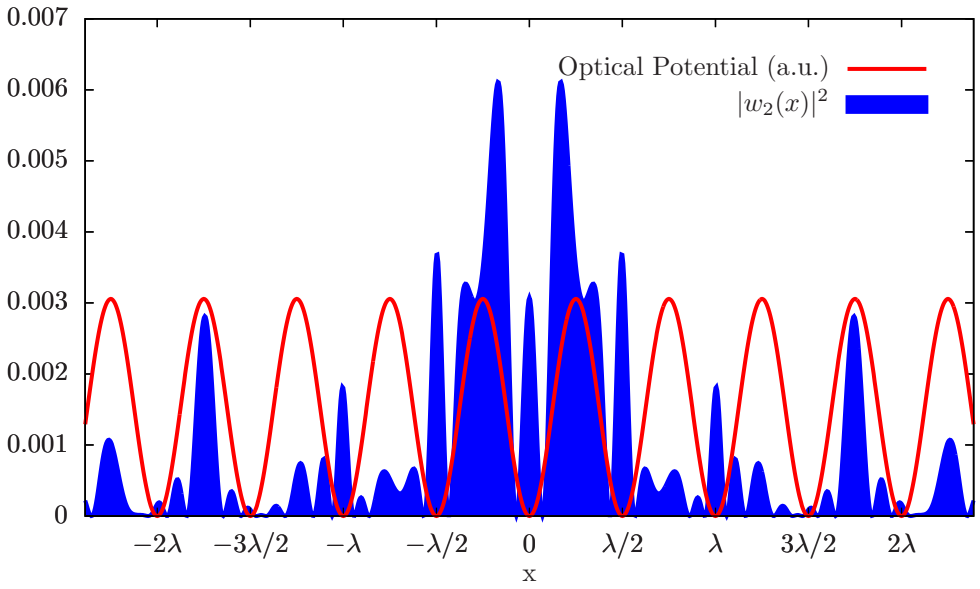

Figure 3.4 Spatial distribution of a quantum particle in a 2^{nd} Bloch band Wannier state. The blue filled curve shows the absolute square of $w_2(x)$ for an average photon number $n = 1.36$ and $U_0 = -10\,\omega_{rec}$. At these parameters some of the Bloch states forming the Wannier state are already bound, see fig. (3.2). The red line sketches the shape of the optical potential in arbitrary units.

self-consistent n for a given detuning Δ_C, pump rate η and band m. Thus it is not unlikely that fully quantum mechanical simulations yield multistabilities in the same range of parameters, too. Given that the spatial part of the density matrix may be a mixture/superposition of several bands, it seems more likely that the system might support multistable solutions.

3.2.2 Stability of Self-Consistent Solutions

Stability analysis is usually performed in a time-dependent context. Though we are looking at stationary cases only, we may still provide some physical arguments to classify self-consistent solutions of eq. (3.33) as *stable* or *unstable*. The following paragraph is just meant to illustrate the idea of stability analysis. Since we are considering a single Bloch band only, the outlined scheme is certainly not complete.

Fig. (3.5) shows a map of the *difference function*

$$f(\Delta_C,\, n) = \frac{\eta^2}{\left(\Delta_C - U_0 \left\langle \cos^2(k_{rec}x)\right\rangle_{n,\,m}\right)^2 + \kappa^2} - n. \tag{3.35}$$

with $m = 2$, $\kappa = \omega_{rec}$, $\eta = 4\omega_{rec}$ and $U_0 = -10\omega_{rec}$. $f(\Delta_C,\, n) > 0$ means that the photon number appearing from the resonance condition (rhs. of eq. (3.33)) is larger than the actual photon number. What does that imply? The momentum wave

function in that regime permits for a larger photon number, the photon number increases through pumping. The larger photon number acts back on the momentum space and changes the resonance condition. This process continues until a (possibly) steady-state is reached at

$$f(\Delta_C, n) = 0. \tag{3.36}$$

The opposite process takes place for $f(\Delta_C, n) < 0$. How does this affect the stability of our self-consistent solutions of eq. (3.33) at $f(\Delta_C, n) = 0$? According to the previous passage a self-consistent solution can be regarded stable if

$$\partial_n f(\Delta_C, n) \mid_{f(\Delta_C, n)=0} < 0. \tag{3.37}$$

The black line in fig. (3.5) indicates the points where $f(\Delta_C, n) = 0$ and is one of the contours found in fig. (3.3). The solid part corresponds to stable self-consistent solutions while the dotted part shows unstable ones. Two stable self-consistent solutions exist for a certain range of Δ_C. We expect that traces of that bistable behavior might be found in a fully quantum-mechanical simulation as well.

In [46] a self-consistency equation for the steady-state photon number expectation value is formulated for the same model Hamiltonian eq. (2.72) employing a Wigner-function approach. The stability of the obtained solutions is classified according to the response to small time-dependent perturbations. In [39] the dynamic properties of eq. (2.72) are characterized via spectral analysis of the photon field amplitude and contour shapes of phase space orbits. Though our analysis was conducted naively, the contour in fig. (3.5), along with our stability consideration, is remarkably similar to the results found in both [46] and [39].

3.3 Limits of Self-Consistent Mean Value Equations

The shape of the self-consistency contours are very sensitive to the model of the spatial/momentum distributions. The resemblance discovered between figs. (3.1) and (3.3) appears by construction, since Wannier states approach harmonic oscillator states in a tight binding limit. The choices made seemed natural, but one may as well follow a different ansatz, plugging in mixtures or superpositions of different states for the spatial/momentum wave function, or supposing a coherent photonic state instead of just dealing with a classical potential, an infinite variety of possibilities. The contours will look different each time and there is little hope to find a steady-state solution. The contour plots, however, can be used as guidelines[5] to interesting parameter ranges. Solving the mean value equations only may be insufficient, but it provides for parameter values that seem interesting enough to be investigated in greater detail. Consequently we will turn to numerical methods that contain the full quantum properties of the system.

[5] literally

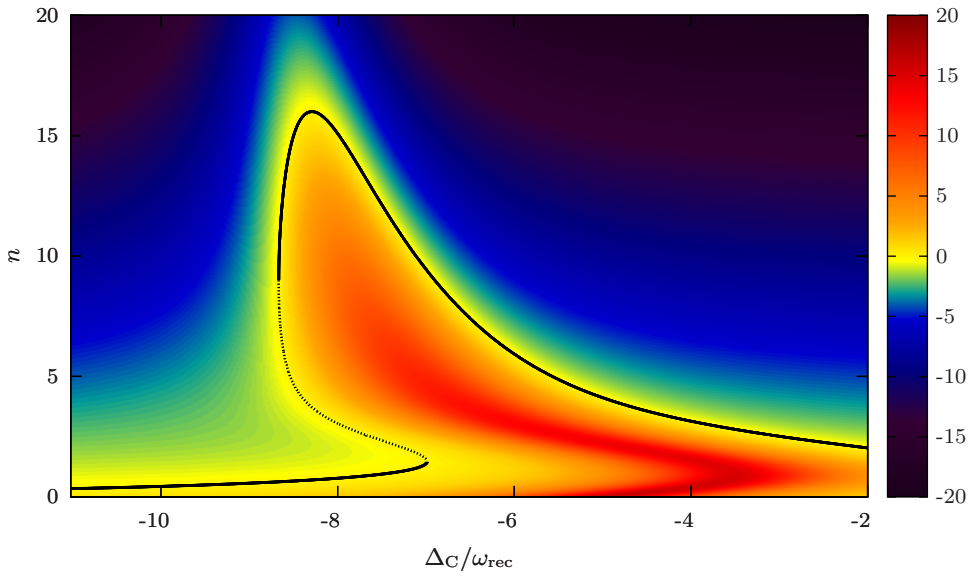

Figure 3.5 Map of the difference function $f(\Delta_C, n)$ as of eq. (3.35) for $\kappa = \omega_{rec}$, $\eta = 4\,\omega_{rec}$, $U_0 = -10\,\omega_{rec}$ and Bloch band index $m = 0$. Positive values suggest that the system tends to evolve to larger photon numbers n than the current value, the opposite holds for negative values. The black line shows $f(\Delta_C, n) = 0$ with the solid part and dashed part being identified as stable and unstable solutions of eq. (3.33), respectively.

4 Numerical Solution of coupled Atom-Field Dynamics

4.1 Computational Basis and Initial Conditions

Before we start numerical computations we have to pick a basis for our quantum system. A natural choice is a direct product of photon Fock states and atomic momentum states. The basis states read

$$|n,\, k\rangle = |n\rangle \otimes |k\rangle \,. \tag{4.1}$$

$|n\rangle$ is a photon Fock state, eqs. (1.11), with n being the number of photons

$$\mathrm{a}^\dagger \mathrm{a}\, |n\rangle = n\, |n\rangle \,. \tag{4.2}$$

$|k\rangle$ is an eigenstate to the atomic momentum operator. In this setup with given cutoffs the Liouvillian can be numerically represented as a sparse matrix and we are able to find its lowest eigenvalues and eigenvectors for Hilbert spaces up to $d \approx 700$. Another option would be to employ the eigenstates of the Hamiltonian as a computational basis for $\mathcal{L}$. In that basis, however, the jump terms of the Liouvillian generate transitions among all basis states and the numerical representation of the Liouvillian would be anything but sparse. In such a setup a direct solution of the master equation would only be feasible for Hilbert spaces up to $d \approx 100$. Similar reasons apply for QMWF (4.3). Quantum jumps among all basis states are just computationally harder than jumps among a few. For that reason it is preferable to remain in the $|n,\, k\rangle$-space, where jump terms only couple neighboring photon number states.

For any practical numerical computation we have to truncate the Hilbert space. Assuming a Poisson-like distribution and considering $\langle n \rangle \leq \frac{\eta^2}{\kappa^2}$ we can safely set the photon number cutoff n_{cut} to $n_{cut} \approx 4\frac{\eta^2}{\kappa^2}$. For the atomic momentum space, however, a rigorously justified cutoff is not so easily found, especially when the effective cavity detuning generates heating in the particle momentum space. Therefore we can only judge a posteriori if the momentum space truncation was chosen sensibly. On the other hand we must not choose the momentum cutoff too high. The Doppler shift changes the detuning Δ_a to $\Delta_a \pm k_{rec}\frac{|p|}{m}$ (the $\pm$ is owing to the standing electromagnetic wave inside the cavity *and* the two possible directions of motion along the cavity axis). For large enough momenta

$$\Delta_a \pm k_{rec}\frac{|p|}{m} \approx \frac{\eta}{\kappa},\, \gamma \tag{4.3}$$

and we would be outside the far-detuned limit, eqs. (2.66). In that regime the adiabatic elimination of section 2.2 cannot be performed and the validity of our model Hamiltonian eq. (2.72) would break down. If the particle had such high momentum, Doppler cooling would stop further heating once it left the far-detuned limit. Since we do not encounter such high momenta in our simulations this is merely a hypothetical remark.

4.1.1 Initial Conditions

We assume that the atom is initially at rest, meaning that its momentum wave function is sharply peaked around $p = 0$, therefore setting $|\Psi_0\rangle = |n_0, 0\rangle$. As mentioned in section (3.2.1) the $\cos^2$ term drives transitions among the states $|q\rangle \leftrightarrow |q \pm 2k_{rec}\rangle$ where we now have $q = 0$. The interaction with the resonator mode then only couples the symmetric superpositions

$$\begin{aligned} &|0\rangle \\ &\frac{1}{\sqrt{2}}\left(|-2k_{rec}\rangle + |2k_{rec}\rangle\right) \\ &\frac{1}{\sqrt{2}}\left(|-4k_{rec}\rangle + |4k_{rec}\rangle\right) \\ &\cdots . \end{aligned} \tag{4.4}$$

Since the states in eq. (4.4) are eigenstates to p^2 we can use them as basis states instead of bare momentum states[1], reducing the size of the Hilbert space by a factor 2. In the following sections we would like to discuss three alternative methods to solve for the equations of motion.

4.2 Direct Solution of the Master Equation

Sometimes the (conceptually) simplest solution is not the best, however it should be mentioned for completeness. The master equation can be implemented as a set of linear differential equations for each element of ρ with the Liouvillian represented by a sparse matrix in the $|n, k\rangle$-basis. If we find the left and right eigenvectors and -values of the Liouville matrix we are done[2]. In a d-dimensional Hilbert space ρ has d^2 elements and the corresponding Liouvillian is $d^2 \times d^2$. The dimension of our Hilbert space is $d = (k_{cut} + 1)(n_{cut} + 1)$, i.e. adding another photon number or momentum state can sensitively increase the numeric size of the master equation. Picking a relatively small Hilbert space with $n_{cut} = 30$ and $k_{cut} = 15$ we already end up diagonalizing a 246016×246016 matrix. The size of the matrix, however, is not

[1] This does not hold for $q \neq 0$ because the p^2 operator would induce transitions between the symmetric and antisymmetric superpositions $\frac{1}{\sqrt{2}}\left(|q - 2k_{rec}\rangle \pm |q + 2k_{rec}\rangle\right)$, $\frac{1}{\sqrt{2}}\left(|q - 4k_{rec}\rangle \pm |q + 4k_{rec}\rangle\right)$ etc.

[2] Though ρ is Hermitian, the Liouville matrix is not and therefore has left and right eigenvectors and -values, see sec.(4.4.1)

the real problem. In solid state physics, for example, much larger sparse matrices are handled using e.g. the Lanczos algorithm [47]. The main difference between the two cases is the form of the matrix. In solid state physics one is looking for the lowest eigenvalues of a specific Hamiltonian[3], whereas the Liouville matrix is non-Hermitian. Numerical experiments in MATLAB with the *eigs* command yield a factor of approximately 1000 in computing time in finding lowest eigenvalues between Hermitian and non-Hermitian matrices of same size and sparsity. A direct solution of the full master equation is thus not feasible for reasonable cutoffs in the physically interesting regime. However, we can obtain the lowest eigenvalues for smaller system sizes in reasonable time. This permits for a study of the long time behavior and, essentially, the steady-state.

4.3 Quantum Monte-Carlo Wave Function Method (QMWF)

The QMWF has already been mentioned in chapter 1. To apply the QMWF we need to transform the master equation to a Quantum Stochastic Schrödinger equation (QSSE) first. This gets us [21]

$$\text{(S)}\quad \partial_t \left|\Psi(t)\right\rangle = \left(-i\mathrm{H}_{sys} + \sqrt{\gamma}\mathrm{b}^\dagger(t)c - \sqrt{\gamma}c^\dagger \mathrm{b}(t)\right)\left|\Psi(t)\right\rangle \tag{4.5}$$

$$\text{(I)}\quad \partial_t \left|\Psi(t)\right\rangle = \left(-i\mathrm{H}_{sys} - \frac{\gamma}{2}\mathrm{c}^\dagger\mathrm{c} + \sqrt{\gamma}\mathrm{b}^\dagger(t)c - \sqrt{\gamma}c^\dagger \mathrm{b}(t)\right)\left|\Psi(t)\right\rangle \tag{4.6}$$

in Stratonovich and Ito differential calculus, respectively. The Stratonovich form mimics the mathematical form of the original, non-stochastic differential equation, such as eq. (4.5) is just the original Schrödinger equation with the bath operators in eq. (1.8) being interpreted as stochastic terms. For practical computational reasons, however, it is advantageous to handle stochastic differential equations in Ito form. The transformation between Ito and Stratonovich form as well as more details on the matter can be found in [38]. We continue in Ito calculus, eq. (4.6) and use $\mathrm{b}^{(\dagger)}$ the same way as in section 1.1. From eq. (4.5) we started the derivation of the master equation. Integrating eq. (4.6) for a small time step Δt and vacuum baths yields

$$\left|\Psi(t+\Delta t)\right\rangle = \left(1 - i\mathrm{H}_{eff}\Delta t + \sqrt{\gamma}\Delta\mathrm{B}^\dagger(t)\right)\left|\Psi(t)\right\rangle, \tag{4.7}$$

where

$$\Delta\mathrm{B}^{(\dagger)}(t) \equiv \int_t^{t+\Delta t} \mathrm{b}^{(\dagger)}(t')\,dt' \tag{4.8}$$

and

$$\mathrm{H}_{eff} = \mathrm{H}_{sys} - i\frac{\gamma}{2}\mathrm{c}^\dagger\mathrm{c}. \tag{4.9}$$

[3] Hamiltonians are Hermitian by definition.

$\Delta \mathrm{B}^{(\dagger)}(t)$ is called an *Ito noise increment*, a stochastic term. How can we interpret eq. (4.7) physically? Let us have the heat bath to be the vacuum modes of the electromagnetic field. Now we build up a perfect photodetector with efficiency 1, i.e. every photon that leaks out of the system in an interval Δt will be detected. Δt has to be chosen such that the probability for two or more photons in Δt is vanishingly small. Now in each interval our wave function will either evolve according to $1 - i\mathrm{H}_{eff}\Delta t$ or perform a *quantum jump*, following $\mathrm{c}\Delta \mathrm{B}^\dagger(t)$. When the system performs a jump, we will detect a photon due to $\Delta \mathrm{B}^\dagger(t)$, if it does not jump, we do not detect a photon. The detection (and non-detection) of the photon represents a measurement process and therefore induces a collapse of the wave function. The collapse destroys the coherence of the wave function, which implies that we can simulate the detection behavior by flipping a coin. All we need to know is the corresponding probabilities. Using that the square of wave function amplitudes give probabilities, we find that the jump probability p_{jump}, which equals the probability for photon detection in a perfect detector, is

$$\begin{aligned} p_{jump}(t) &= \gamma \,\mathrm{Tr}\left\{ \mathrm{c}\Delta \mathrm{B}^\dagger(t)\, |\Psi(t)\rangle\langle\Psi(t)|\, \Delta \mathrm{B}(t)\mathrm{c}^\dagger \right\} \\ &= \gamma \,\langle\Psi(t)|\, \mathrm{c}^\dagger \mathrm{c}\, |\Psi(t)\rangle\, \Delta t \\ &= \gamma \|\mathrm{c}\, |\Psi(t)\rangle\|^2 \Delta t. \end{aligned} \tag{4.10}$$

If we read the detector we always know the state of the system. This goes by *continuous measurement*[4]. If we do not read the detector, however, the state is a classical mixture of a jump part and a coherent part with decay, given by H_{eff}. We start with a pure state and then flip a coin at every time increment whether the wave function evolves according to

$$|\Psi(t_i + \Delta t)\rangle = \frac{(1 - \mathrm{H}_{eff}\Delta t)\, |\Psi(t_i)\rangle}{\|(1 - \mathrm{H}_{eff}\Delta t)\, |\Psi(t_i)\rangle\|} \tag{4.11}$$

with $p = 1 - p_{jump}$ or jumps and becomes

$$|\Psi(t_i + \Delta t)\rangle = \frac{\mathrm{c}\, |\Psi(t_i)\rangle}{\|\mathrm{c}\, |\Psi(t_i)\rangle\|} \tag{4.12}$$

with $p = p_{jump}$. We can continue this procedure until we reach the time t, keeping track of the wave function in each time step, which is called a *quantum trajectory*. We then repeat this Monte-Carlo time evolution many times and merge the single trajectories $|\Psi_j(t)\rangle$ to the density matrix

$$\rho(t) = \lim_{\sharp\text{trajectories}\to\infty} \frac{1}{\sharp\text{trajectories}} \sum_{j=1}^{\sharp\text{trajectories}} |\Psi_j(t)\rangle\langle\Psi_j(t)|. \tag{4.13}$$

Assuming that we do not follow the exact number of counts, simulating and averaging over a large number of trajectories, gives us a numerical approximation to the real

[4] See e.g. [48] for a detailed description of continuous measurement theory.

density matrix [49]. This scheme is known as *Quantum Monte Carlo Wave Function Method (QMWF)*. One advantage of the QMWF is, since we are evolving wave functions only, it is less memory consuming than a direct solution of the master equation and the trajectories can be simulated in parallel. On the other hand, we only get a probabilistic solution, which, however, converges fast enough (in the number of trajectories) to the exact solution. Usually a few hundred trajectories are enough to obtain a valuable solution. Sometimes even a single trajectory can give a good qualitative picture of the underlying dynamics. For a steady-state solution one has to perform time evolution for a very long time, especially if the system has a slowly evolving subspace. A more efficient way to get stationary solutions is to follow a single trajectory for a very long time and replace the ensemble average by a time average [49]. The mathematical setup of QMWF is very intuitive in terms of the measurement process and therefore closely connected to the physical processes occurring in the system under consideration. By that reason, if a property does not occur in QMWF after long time evolution, it will usually not be encountered in experiment either.

4.4 Rate Equations

To avoid a direct solution of the master equation, we have already encountered the QMWF simulation method. Another way to circumvent the large dimensionality of the Liouvillian is to consider the diagonal elements of ρ only. As a first approach we simply neglect the off-diagonal elements of ρ. A thermal state in energy basis, for example, has diagonal elements only and rate equations for diagonal elements have been successfully applied in quantum optics from laser theory up to Sisyphus-cooling [50]. A meaningful application of this approximation, however, requires a sensible choice of basis in our Hilbert space. While picking the eigenstates of H seems natural, the result of this procedure is a bit unsatisfactory:

$$
\begin{aligned}
H\left|E_j\right\rangle &= E_j\left|E_j\right\rangle \\
\rho &= \sum_j \rho_{jj}\left|E_j\right\rangle\!\left\langle E_j\right| \\
\partial_t \rho_{ii} &= \left\langle E_i\right|\partial_t\rho\left|E_i\right\rangle \\
&= \left\langle E_i\right|\sum_j\Big(-i\Big[H,\,\rho_{jj}\left|E_j\right\rangle\!\left\langle E_j\right|\Big] \\
&\quad +\kappa\left(2a\rho_{jj}\left|E_j\right\rangle\!\left\langle E_j\right|a^\dagger - a^\dagger a\rho_{jj}\left|E_j\right\rangle\!\left\langle E_j\right| - \rho_{jj}\left|E_j\right\rangle\!\left\langle E_j\right|a^\dagger a\right)\Big)\left|E_i\right\rangle \\
&= \sum_j\left(-i\left(E_j-E_i\right)\delta_{ij} + \kappa\left(2\left|\left\langle E_i\right|a\left|E_j\right\rangle\right|^2 - \left\langle E_i\right|a^\dagger a\left|E_j\right\rangle\delta_{ij} - \left\langle E_j\right|a^\dagger a\left|E_j\right\rangle\delta_{ij}\right)\right)\rho_{jj} \\
&= 2\kappa\left(-\left\langle E_i\right|a^\dagger a\left|E_i\right\rangle\rho_{ii} + \sum_j\left|\left\langle E_i\right|a\left|E_j\right\rangle\right|^2\rho_{jj}\right). \qquad (4.14)
\end{aligned}
$$

So κ serves as a parameter for setting the time scales, but the steady-state of this equation would be independent of κ as all rates are linear in κ. This is certainly an inappropriate feature if we want to mimic the steady-state of the full master equation. One way to resolve this issue is to employ the eigenstates of the effective Hamiltonian

$$H_{eff} = H - i\kappa a^\dagger a. \tag{4.15}$$

Since H_{eff} is non-Hermitian, it is instructive to examine some general results on non-Hermitian operators first.

4.4.1 Non-Hermitian Operators

$\mathrm{H}\,|E_j\rangle = E_j\,|E_j\rangle$ and its Hermitian adjungate yield $E_j^* = E_j$ and $\langle E_i|E_j\rangle = \delta_{ij}$ if H is Hermitian, i.e. $\mathrm{H}^\dagger = \mathrm{H}$. These relations, however, do not hold for general non-Hermitian operators. A general non-Hermitian operator A has left and right eigenvectors and -values obeying

$$A\,|r_j\rangle = r_j\,|r_j\rangle \tag{4.16}$$
$$A^\dagger\,|l_j\rangle = l_j\,|l_j\rangle \tag{4.17}$$
$$\langle l_i|r_j\rangle = \delta_{ij}. \tag{4.18}$$

Since the indexing in the two sets of eigenvectors is not necessarily in mutual correspondence, the δ_{ij} is merely symbolic.[5] Numerically computed left and right eigenvectors are usually normalized according to

$$\langle \tilde{r}_i|\tilde{r}_i\rangle = 1 = \left\langle \tilde{l}_i\middle|\tilde{l}_i\right\rangle \tag{4.19}$$

This implies that

$$\left\langle \tilde{l}_i\middle|\tilde{r}_j\right\rangle = g_i\delta_{ij} \tag{4.20}$$

with some complex number g_i. In order to get $|r_i\rangle$ and $|l_i\rangle$ of eq. (4.18) one sets

$$|r_i\rangle = \alpha_i\,|\tilde{r}_i\rangle \tag{4.21a}$$
$$|l_i\rangle = \beta_i\left|\tilde{l}_i\right\rangle \tag{4.21b}$$
$$\alpha_i\beta_i = g_i^{-1}. \tag{4.21c}$$

There are infinitely many possibilities of choosing α_i and β_i, but two seem preferable (cf. Fourier transform):

- symmetric: $\alpha_i \equiv \beta_i = \sqrt{g_i^{-1}}$,
- one-sided: either $\alpha_i = 1$ or $\beta_i = 1$.

[5] In actual numerical computations one should not forget about that!

For practical reasons the system operators are usually expressed in the computational basis of section 4.1 and so are $|r_i\rangle$ and $|l_i\rangle$. By changing the norm from eq. (4.20) to eq. (4.18) one has to be aware that this affects the transformation of state vectors from $|r_i\rangle$, $|l_i\rangle$- to $|n,\, k\rangle$-basis too. Let $\{r_i\}_j$ and $\{l_i\}_j$ denote the jth element of the ith right and left eigenvector and Ψ_j^{nk} the jth element of an arbitrary state vector $|\Psi\rangle$ in computational basis. The corresponding coefficients of $|\Psi\rangle$ in the right eigenvector basis, Ψ_i^r, are then

$$\Psi_i^r = \sum_j \{l_i\}_j \, \Psi_j^{nk} g_i \tag{4.22}$$

with g_i as defined in eq. (4.20).

Keeping the scalar product in the form of eq. (4.18) we find

$$\begin{aligned} \langle l_i| \, A \, |r_j\rangle &= \langle l_i| \, r_j \, |r_j\rangle = r_j \delta_{ij} \\ &= \langle l_i| \, l_i^* \, |r_j\rangle = l_i^* \delta_{ij} \\ \rightarrow l_i^* &= r_i. \end{aligned} \tag{4.23}$$

Thus, at first sight, dealing with non-Hermitian operators seems to double the effort in finding eigenvectors for its proper description. This can be circumvented if we exploit symmetry relations between left and right eigenvectors, if there are any. To find such relations, we superimpose transformations on the eigenvalue equations and see to what symmetries the operator A is constrained. Let us assume

$$A^\dagger \, |l_i\rangle = M \, \{A \, |r_i\rangle\} \, , \tag{4.24}$$

where M is arbitrary, but invertible, i.e. $\exists \, M^{-1}$ such that $M^{-1} \, \{M \, \{\cdot\}\} = 1 \cdot$. We get

$$\begin{aligned} A^\dagger \, |l_i\rangle &= M \, \{A \, |r_i\rangle\} \\ &= l_i \, |l_i\rangle \\ &= M \, \{r_i \, |r_i\rangle\} \, . \end{aligned} \tag{4.25}$$

From previous results we know that $l_i = r_i^*$, thus it feels natural to assume

$$M \, \{\cdot\} = \cdot^*, \tag{4.26}$$

which yields

$$A^\dagger \, |l_i\rangle = A^* \, |r_i\rangle^* \, . \tag{4.27}$$

So we arrive at the important result that

$$\text{if} \quad A^\dagger = A^*, \tag{4.28}$$

$$\text{then} \quad |l_i\rangle = |r_i\rangle^* \, . \tag{4.29}$$

Different operations M might then exploit different symmetries of the operator A, which then yield different transformations from right to left eigenvectors. Complex conjugation, however, suffices for our purposes. The reason behind the unitary transformation eq. (2.71) in section 2.2 was to bring our model Hamiltonian in the form of eq. (4.28). We stop our discussion of non-Hermitian operators at this point and continue deriving effective equations for the diagonal elements of ρ.

4.4.2 From the Master Equation to Rate Equations

We return to the master equation and expand ρ in the right eigenstates of the effective Hamiltonian

$$H_{eff} = \frac{p^2}{2m} + \eta\left(a^\dagger + a\right) + \left(-\Delta_C + U_0\cos^2(kx) - i\kappa\right)a^\dagger a \tag{4.30}$$

$$H_{eff}\left|r_j\right\rangle = E_j\left|r_j\right\rangle \tag{4.31}$$

$$H_{eff}^\dagger\left|l_j\right\rangle = E_j^*\left|l_j\right\rangle \tag{4.32}$$

and take into account the diagonal elements only

$$\begin{aligned}\rho &= \sum_j \varrho_{jj}\left|r_j\right\rangle\!\left\langle r_j\right| \\ &= \sum_j \left\langle l_j\right|\rho\left|l_j\right\rangle,\end{aligned} \tag{4.33}$$

keeping in mind that for $\sum_j \varrho_{jj} = 1$, $\operatorname{Tr}\rho = 1$ even if $\langle r_i|r_j\rangle \neq \delta_{ij}$. Rewriting the master equation in terms of H_{eff} we get

$$\begin{aligned}\partial_t\rho &= -i\left[H_{eff}\rho - \rho H_{eff}^\dagger\right] + 2\kappa a\rho a^\dagger \\ &= \sum_j -i\left[H_{eff}\varrho_{jj}\left|r_j\right\rangle\!\left\langle r_j\right| - \varrho_{jj}\left|r_j\right\rangle\!\left\langle r_j\right|H_{eff}^\dagger\right] + 2\kappa\varrho_{jj}a\left|r_j\right\rangle\!\left\langle r_j\right|a^\dagger.\end{aligned} \tag{4.34}$$

Sandwiching with $\langle l_i|\cdot|l_i\rangle$ we arrive at

$$\partial_t\varrho_{ii} = -i\left[E_i - E_i^*\right]\varrho_{ii} + 2\kappa\sum_j\left|\left\langle l_i\right|a\left|r_j\right\rangle\right|^2\varrho_{jj}, \tag{4.35}$$

which is the equation of motion for the diagonal elements ϱ_{ii}, commonly termed *rate equations*. The rate equations completely neglect any coherence between different eigenstates of H_{eff} and may therefore be applied in weakly entangled systems[6] only. A justification for their applicability can rarely be given a priori, since entanglement properties as well as the eigenstates of H_{eff} themselves are highly sensitive to the system parameters manifested in the effective Hamiltonian.

[6] weak or no entanglement between the eigenstates

4.4.3 Perturbative Expansion of Off-Diagonal Elements in the Steady-State

Setting $\partial_t \rho = 0$, the above set of differential equations turns into a set of algebraic equations and their solution are the steady-state values of the diagonal elements of ρ. In this limit, we may perturbatively account for the off-diagonal elements $\varrho_{i\neq j}$, hoping to extend the range of applicability of the rate equations. We assume that the time evolution of the off diagonal elements $\varrho_{i\neq j}$ is dominated by the diagonal elements ϱ_{ii}, but we also take the couplings $\varrho_{i\neq j} \leftrightarrow \varrho_{i\neq j}$ and $\varrho_{i\neq j} \leftrightarrow \varrho_{j\neq i}$ into account. This yields

$$\begin{aligned}\partial_t \varrho_{i\neq j} = &-i\left[E_i - E_j^*\right] + 2\kappa(\langle l_i|\, a\, |r_i\rangle \langle r_j|\, a^\dagger\, |l_j\rangle\, \varrho_{i\neq j} \\ &+ \langle l_i|\, a\, |r_j\rangle \langle r_i|\, a^\dagger\, |l_j\rangle\, \varrho_{j\neq i} + \sum_k \langle l_i|\, a\, |r_k\rangle \langle r_k|\, a^\dagger\, |l_j\rangle\, \varrho_{kk}) \\ \partial_t \varrho_{j\neq i} = &\,\partial_t \varrho_{i\neq j}^*, \end{aligned} \tag{4.36}$$

which is a pair of equations for each $i \neq j$. Solving for the steady-state we may express the solutions in terms of the diagonal elements ϱ_{kk} only:

$$\begin{aligned}\varrho_{i\neq j} = -2\kappa[&-i\left(E_i - E_j^*\right) + 2\kappa \langle l_i|\, a\, |r_i\rangle \langle r_j|\, a^\dagger\, |l_j\rangle \\ &-4\kappa^2 \frac{\left|\langle l_i|\, a\, |r_j\rangle \langle r_i|\, a^\dagger\, |l_j\rangle\right|^2}{i\left(E_i^* - E_j\right) + 2\kappa \langle l_j|\, a\, |r_j\rangle \langle r_i|\, a^\dagger\, |l_i\rangle}]^{-1} \\ &\times \sum_k \left(\langle l_i|\, a\, |r_k\rangle \langle r_k|\, a^\dagger\, |l_j\rangle - 2\kappa \frac{\langle l_i|\, a\, |r_j\rangle \langle r_i|\, a^\dagger\, |l_j\rangle \langle l_j|\, a\, |r_k\rangle \langle r_k|\, a^\dagger\, |l_i\rangle}{i\left(E_i^* - E_j\right) + 2\kappa \langle l_j|\, a\, |r_j\rangle \langle r_i|\, a^\dagger\, |l_i\rangle}\right) \varrho_{kk}. \end{aligned} \tag{4.37}$$

Writing the master equation as

$$\begin{aligned}\partial_t \varrho_{mm} = &-i\left[E_m - E_m^*\right] \varrho_{mm} \\ &+ 2\kappa \sum_k \left|\langle l_m|\, a\, |r_k\rangle\right|^2 \varrho_{kk} + 2\kappa \sum_{i\neq j} \langle l_m|\, a\, |r_i\rangle \langle r_j|\, a^\dagger\, |l_m\rangle\, \varrho_{i\neq j}, \end{aligned} \tag{4.38}$$

and plugging in the approximate steady-state solution for $\varrho_{i\neq j}$, we find

$$\begin{aligned}0 \approx &-i\left[E_m - E_m^*\right] \varrho_{mm} + 2\kappa \sum_k \left|\langle l_m|\, a\, |r_k\rangle\right|^2 \varrho_{kk} - 4\kappa^2 \sum_{i\neq j} \langle l_m|\, a\, |r_i\rangle \langle r_j|\, a^\dagger\, |l_m\rangle \\ &\times [-i\left(E_i - E_j^*\right) + 2\kappa \langle l_i|\, a\, |r_i\rangle \langle r_j|\, a^\dagger\, |l_j\rangle \\ &-4\kappa^2 \frac{\left|\langle l_i|\, a\, |r_j\rangle \langle r_i|\, a^\dagger\, |l_j\rangle\right|^2}{i\left(E_i^* - E_j\right) + 2\kappa \langle l_j|\, a\, |r_j\rangle \langle r_i|\, a^\dagger\, |l_i\rangle}]^{-1} \\ &\times \sum_k \left(\langle l_i|\, a\, |r_k\rangle \langle r_k|\, a^\dagger\, |l_j\rangle - 2\kappa \frac{\langle l_i|\, a\, |r_j\rangle \langle r_i|\, a^\dagger\, |l_j\rangle \langle l_j|\, a\, |r_k\rangle \langle r_k|\, a^\dagger\, |l_i\rangle}{i\left(E_i^* - E_j\right) + 2\kappa \langle l_j|\, a\, |r_j\rangle \langle r_i|\, a^\dagger\, |l_i\rangle}\right) \varrho_{kk} \end{aligned} \tag{4.39}$$

for the steady-state.

To obtain the steady-state solution, one has to find the null space of the right-hand side of eqn. (4.39). Once we have a steady-state solution we may check its faithfulness a posteriori. We calculate the off-diagonal elements explicitly by means of eqn. (4.37) and apply the full $N^2 \times N^2$ Liouville superoperator from the left.

$$\frac{\|L\rho\|_2}{\|\rho\|_2} \ll 1 \tag{4.40}$$

is a necessary, but not sufficient, criterion to claim that our approximation is reasonable.

We could repeat the above procedure to obtain a perturbative expansion of the full density matrix. However, the outlined scheme does not respect Haken's slaving principle (see section 2.2) and thus we cannot expect any faithful physical behavior. Eq. (4.39) remains an intermediate result for further theoretical considerations of the rate equations. We will stick with the original form of the rate equations eq. (4.35) for further numerical experiments.

4.4.4 Numerical Implementation of the Rate Equations

Some properties of ρ are highly sensitive to numerical precision. Therefore, a straightforward implementation of eq. (4.35) can lead to strange or unphysical results. The equation of motion for a density matrix must preserve its trace and its positive definiteness, properties that should be respected by the rate equations as well. Rewriting the rate equations as matrix equation

$$\partial_t \vec{\rho}_{diag} = M \vec{\rho}_{diag}, \tag{4.41}$$

$$\text{with} \quad \vec{\rho}_{diag,\,j} = \varrho_{jj}, \tag{4.42}$$

we find criteria for M. Since we simply drop the off-diagonal terms (eq. (4.34)) we cannot expect that these criteria are met by a direct implementation of eq. (4.35). Obtaining M from eq. (4.35) yields a matrix with negative diagonals and positive off-diagonals. This structure is already sufficient to maintain positive definiteness.[7] Trace preservation implies that the sum of all rows of M is a zero row and guarantees the existence of at least one steady-state. By virtue of eq. (4.34) all transitions between diagonal elements of ρ via off-diagonal elements of ρ are discarded as well. Though the diagonal decay terms in M are accurate, the off diagonal couplings are not and therefore all rows do not sum up to zero unless these elements are renormalized to cancel the diagonal loss terms.

$$M_{ij} \to \tilde{M}_{ij} = \delta_{ij} M_{ij} - (1 - \delta_{ij}) \frac{M_{jj}}{\sum_i M_{ij \neq i}} M_{ij} \tag{4.43}$$

With this modification we are able to find possible steady-states in a weakly interacting regime and may simulate the full system dynamics as well due to the low

[7] if the initial elements were positive

dimensionality of the rate equations. When we use the rate equations to generate the time evolution of a system we have to keep in mind that the representation of the initial density matrix in the right eigenstates of H_{eff} has to follow eq. (4.22).

5 Numerical Solutions to the Master Equation

We would like to compare the different numerical and approximate methods introduced in chapter 4 to each other. For that purpose we choose $\eta = 2\,\omega_{rec}$ and $\kappa = \omega_{rec}$ to allow for low enough Hilbert space cutoffs. For different coupling strengths $U_0 \in \{-0.5, -1.0, -1.5, -2.0\}\ \omega_{rec}$ we calculate the steady-state of the master equation for detunings $\Delta_C \in \{-5.50, -5.25, \ldots, -0.50\}\ \omega_{rec}$. We try to find the null space of the master equation and the stationary limit of the rate equations, respectively. We will refer to these methods as *null-space methods*. In QMWF we cannot find an exact steady-state. However, we can extend time evolution such that $\kappa t \gg 1$. For the same range of parameters we average over 1000 trajectories and evolve up to time $t = 310\omega_{rec}^{-1}$. QMWF is performed in the C++QED framework [51]. For all three methods we compute the photon number expectation value n, its variance $(\Delta n)^2$ and the variance of momentum $(\Delta p)^2$, which indicates the particle's temperature. The results are discussed in the next section and shown in fig. (5.1).

5.1 How Well do the Rate Equations Agree?

QMWF and null-space methods give approximate solutions with their respective limitations and drawbacks mentioned in chapter 4. We are now curios about the quality of the rate equations' results. We picked a few values from the range of parameters in fig. (5.1) and plotted the corresponding photon and momentum distribution on both linear and logarithmic scale. Fig. (5.2) is taken from off-resonant values with low photon numbers. Since the momentum distribution is invariant under $k \to -k$ we may generate distributions function in the basis states of eq. (4.4) that only need positive momentum indices. The value of U_0 is not very large, too, which suggests only perturbative impact from the interaction term on the system properties - good prerequisites for faithful results by the rate equations?

Fig. (5.3) shows another pair of distributions, this time a little closer to resonance. The photon number is larger, but U_0 is smaller than for the previous example of fig. (5.2). According to fig. (5.1) we find excellent agreement of all three methods for the photonic degree of freedom for both examples, but noticeable (fig. (5.2)) and striking (fig. (5.3)) deviations regarding momentum properties (i.e. heating of the atom). The origin of this disagreement is largely indebted to the different solution methods. QMWF evolves in time while the null-space methods balance transition rates. The latter are very sensitive to cutoffs, missing gain/loss channels can

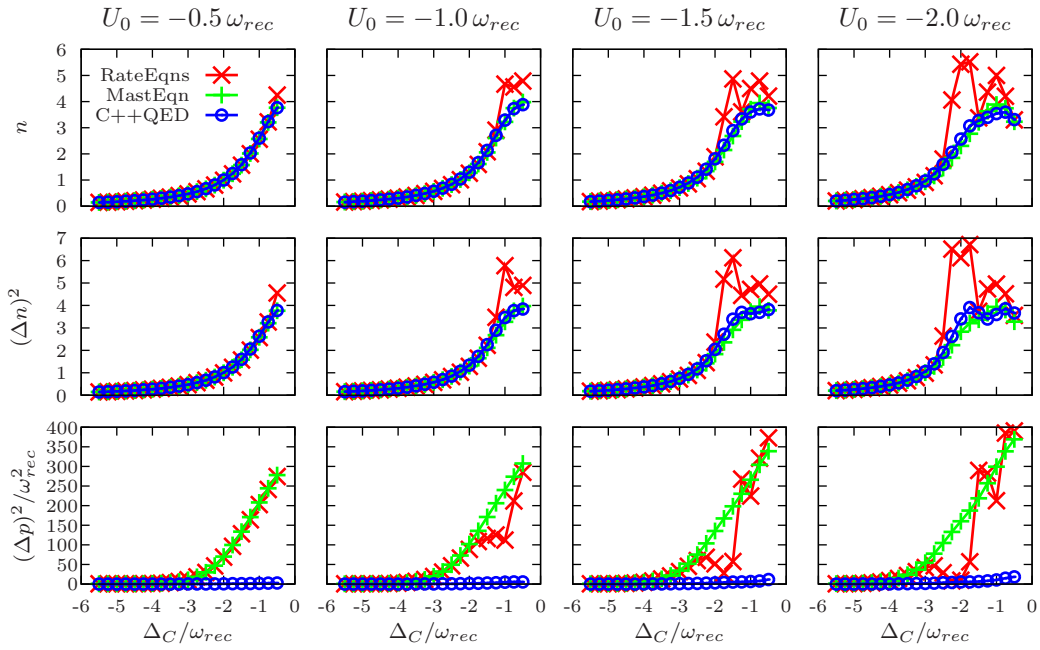

Figure 5.1 n, $(\Delta n)^2$ and $(\Delta p)^2$ provided by the different solution methods: null space of rate equations (red) and master equation (blue), and C++QED (green). The data lines are for $\kappa = \omega_{rec}$ and $\eta = 2\,\omega_{rec}$. The C++QED trajectories have been evolved to $t = 310\,\omega_{rec}^{-1}$

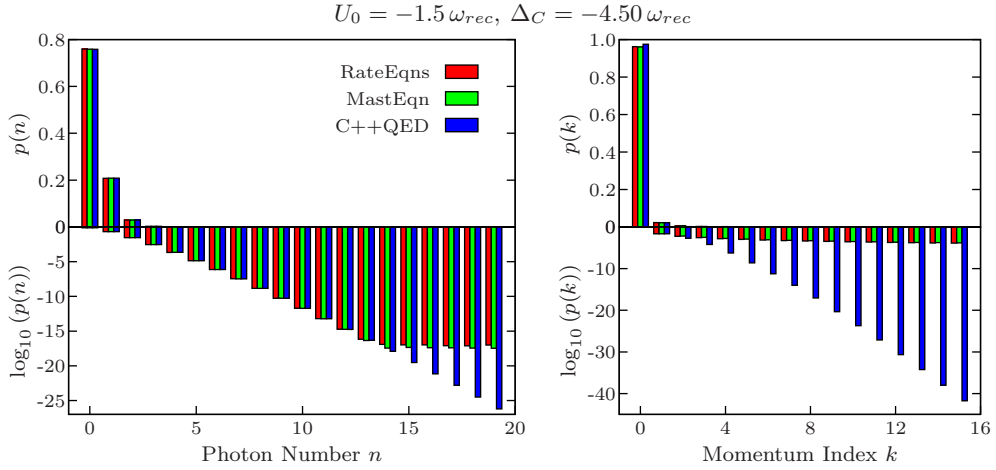

Figure 5.2 $p(n)$ and $p(k)$ provided by the different solution methods: rate equations (red), master equation(blue) and C++QED(green). Parameters are $U_0 = -0.5\,\omega_{rec}$, $\Delta_C = -4.50\,\omega_{rec}$, $\kappa = \omega_{rec}$ and $\eta = 2\,\omega_{rec}$. The C++QED trajectories have been evolved to $t = 310\,\omega_{rec}^{-1}$

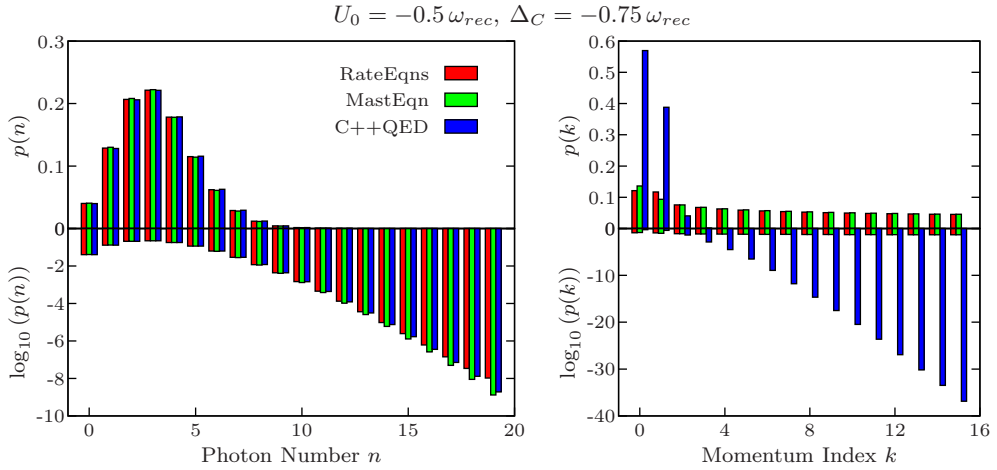

Figure 5.3 $p(n)$ and $p(k)$ provided by the different solution methods: rate equations (red), master equation(gblue) and C++QED(green). Parameters are $U_0 = -0.5\,\omega_{rec}$, $\Delta_C = -0.75\,\omega_{rec}$, $\kappa = \omega_{rec}$ and $\eta = 2\,\omega_{rec}$. The C++QED trajectories have been evolved to $t = 310\,\omega_{rec}^{-1}$

significantly alter the null-space properties, even if their couplings are weak. For that reason the null-space methods produce slowly decreasing momentum distributions.

The rate equations, however, reproduce the results from the full master equation very well. The agreement is excellent on both linear and logarithmic scales.

Figs. (5.4) and (5.5) show two pairs of distributions for parameters close to resonance. Fig. (5.1) suggests that the rate equations yield photon number mean-values and variances similar to QMWF and the master equation, but momentum variances $(\Delta p)^2$ do not fit to the values obtained from either QMWF or the master equation. Fig. (5.5) underlines the rate equations' deviating behavior by revealing momentum distributions $p(k)$ that do not reproduce any of those provided by the other two methods.

The agreement of the photon number distribution $p(n)$ is better but not excellent. Slightly different behavior among the null-space methods is found in the logarithmic plot of $p(n)$. Due to strikingly different properties in momentum space it seems that the rate equations resemble the results of $p(n)$ from the other methods by chance. This coincidental behavior is confirmed by fig. (5.6). $\Delta_C = -1.75\,\omega_{rec}$ is just a little bit off $\Delta_C = -1.50\,\omega_{rec}$ from fig. (5.5), but the rate equations do not resemble any of the other two methods' distributions, not even in photon number space.

We conclude that the rate equations are applicable for sufficiently large detuning Δ_C. Their range of applicability widens as the interaction strength U_0 decreases. Eventually, the empty cavity is solved for all values of Δ_C. Utilization of the rate equations in the empty cavity case, however, does not provide much additional insight due to its analytic solubility, eq. (3.7). For larger U_0 and Δ_C close to resonance, $\Delta_{eff} = 0$ (eq. (3.9)), we have to come back to either the master equation or QMWF.

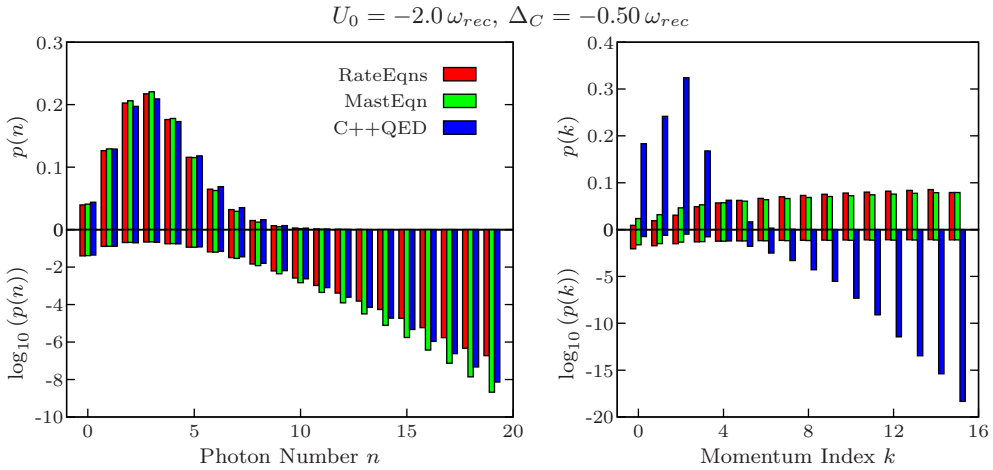

Figure 5.4 $p(n)$ and $p(k)$ provided by the different solution methods: rate equations (red), master equation(gblue) and C++QED(green). Parameters are $U_0 = -2.0\,\omega_{rec}$, $\Delta_C = -0.50\,\omega_{rec}$, $\kappa = \omega_{rec}$ and $\eta = 2\,\omega_{rec}$. The C++QED trajectories have been evolved to $t = 310\,\omega_{rec}^{-1}$

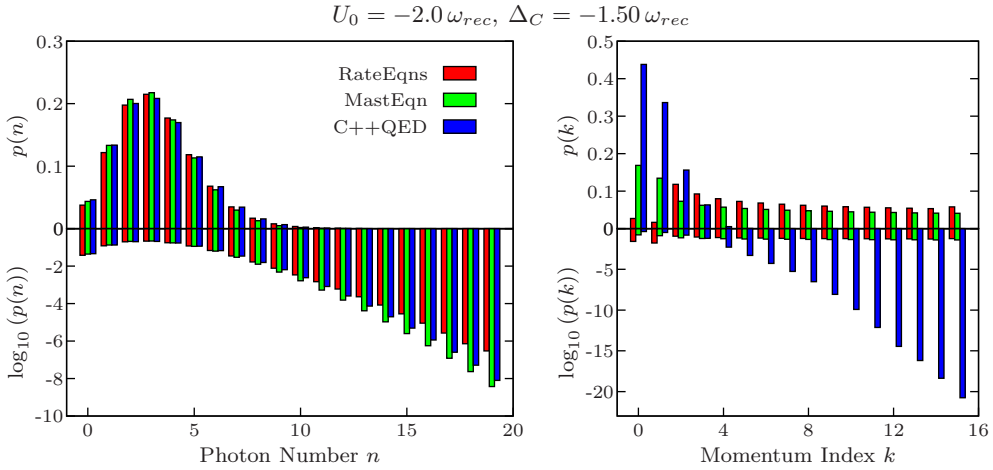

Figure 5.5 $p(n)$ and $p(k)$ provided by the different solution methods: rate equations (red), master equation(gblue) and C++QED(green). Parameters are $U_0 = -2.0\,\omega_{rec}$, $\Delta_C = -1.50\,\omega_{rec}$, $\kappa = \omega_{rec}$ and $\eta = 2\,\omega_{rec}$. The C++QED trajectories have been evolved to $t = 310\,\omega_{rec}^{-1}$

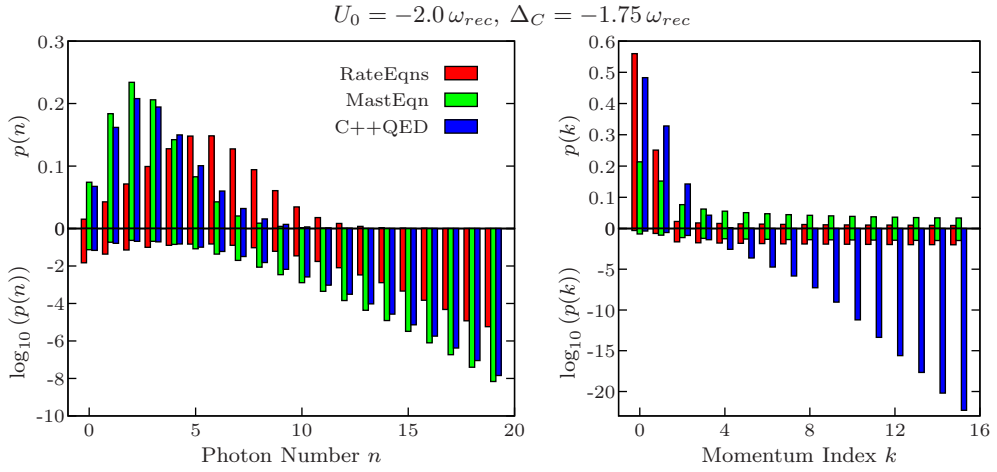

Figure 5.6 $p(n)$ and $p(k)$ provided by the different solution methods: rate equations (red), master equation(gblue) and C++QED(green). Parameters are $U_0 = -2.0\,\omega_{rec}$, $\Delta_C = -1.75\,\omega_{rec}$, $\kappa = \omega_{rec}$ and $\eta = 2\,\omega_{rec}$. The C++QED trajectories have been evolved to $t = 310\,\omega_{rec}^{-1}$

5.2 Time Evolution on Different Scales

In the previous section we found that the null-space methods and QMWF produce significantly different momentum distributions. This was attributed to their different approaches in computing the steady-state. We will try to link these results via the rate equations. The rate equations can be used to predict the time evolution of the system as well. Contrary to solving the full master equation this can be done in reasonably short time with little numerical effort. The rate equations are just a simplified form of the master equation, the QMWF approximates the behavior of the master equation, hence we expect a temporal evolution that is very much alike. We will compare the dynamics of a system subject to the rate equations with that generated by QMWF in C++QED. We hope to resolve the Δp discrepancy between the null-space methods and QMWF that appeared in the previous section by investigating the time scales at which certain subspaces evolve.

For that purpose we choose parameters from the range where the data from fig. (5.1) and the subsequent discussion suggest that the rate equations faithfully reproduce results of more detailed calculations. It is apparent that not all properties of the initial state of C++QED can be captured in formalism of the rate equations. The diagonal elements of ρ do not contain any phase information and therefore multiple states may share the same diagonal elements of ρ. For that reason the initial values for the two methods will deviate slightly, but we expect them to approach each other and the steady-state value in roughly the same period of time.

Fig. (5.7) shows the evolution of n. Though we have evolved the system up to $t = 310\omega_{rec}^{-1}$ we only show the interval $t \in [0,\, 10]\,\omega_{rec}^{-1}$ because the photonic dynamics appear to be fast. The same is true for $(\Delta n)^2$ shown in fig. (5.8). We observe that

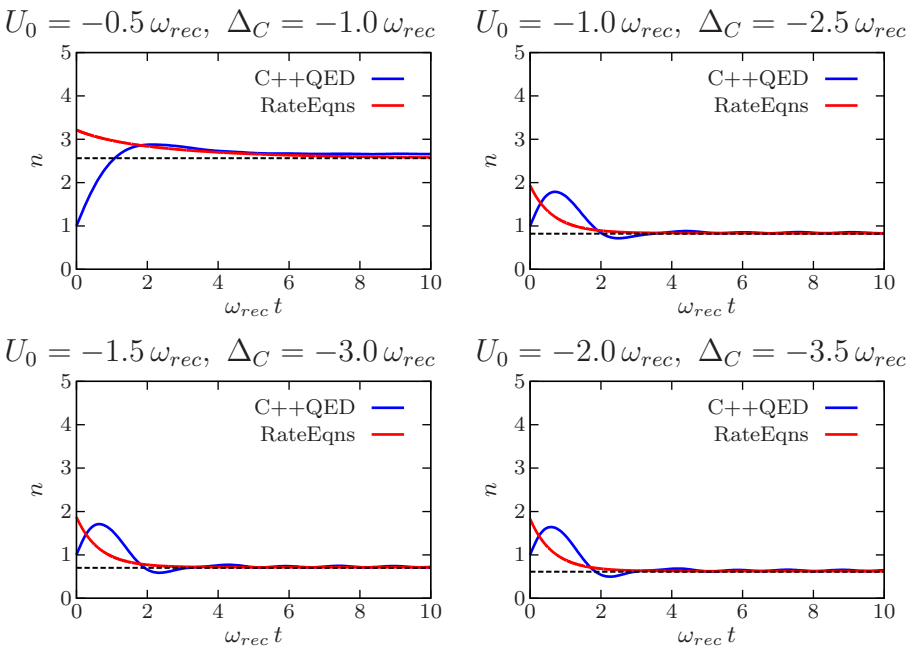

Figure 5.7 Time evolution of n provided by QMWF (C++QED, blue) and the rate equations (red) for $\kappa = \omega_{rec}$ and $\eta = 2\,\omega_{rec}$. The dashed line indicates the steady-state value given by the rate equations.

both methods provide the same time scales for dynamical behavior and approach the same values for long times.

Considering $(\Delta p)^2$ only, the results from the rate equations, in their range of physically valid applicability, agree very well with those obtained from the master equation. The rate equations are just a simplified form of the master equation, hence this does not seem to be a big surprise. But the QMWF just mimics the behavior of the master equation, thus it should also match its results, as it does for the field values n and $(\Delta n)^2$. The gap can be bridged by the rate equations. They can easily be diagonalized due to their lower dimensionality. This means that, besides retrieving the steady-state values, we can also calculate the time evolution of mean values and variances and compare them to the evolution generated in C++QED.

We extend the time range thousandfold and analyze its properties. We observe a continuous growth of $(\Delta p)^2$ throughout the full range of time. It is apparent that the system has not yet reached its steady-state for $t \approx 3 \times 10^5 \omega_{rec}^{-1}$, a time much longer than in any experiment.

For an optical transition in Sodium $3 \times 10^5 \omega_{rec}^{-1}$ corresponds to approximately 20 seconds. For heavier elements or nano-particles the corresponding period of time is even longer. Micro-cavity experiments last up to milliseconds, so we are already exploring a region beyond experimental access.

Cooling processes in longitudinally pumped cavities were predicted to be slower for

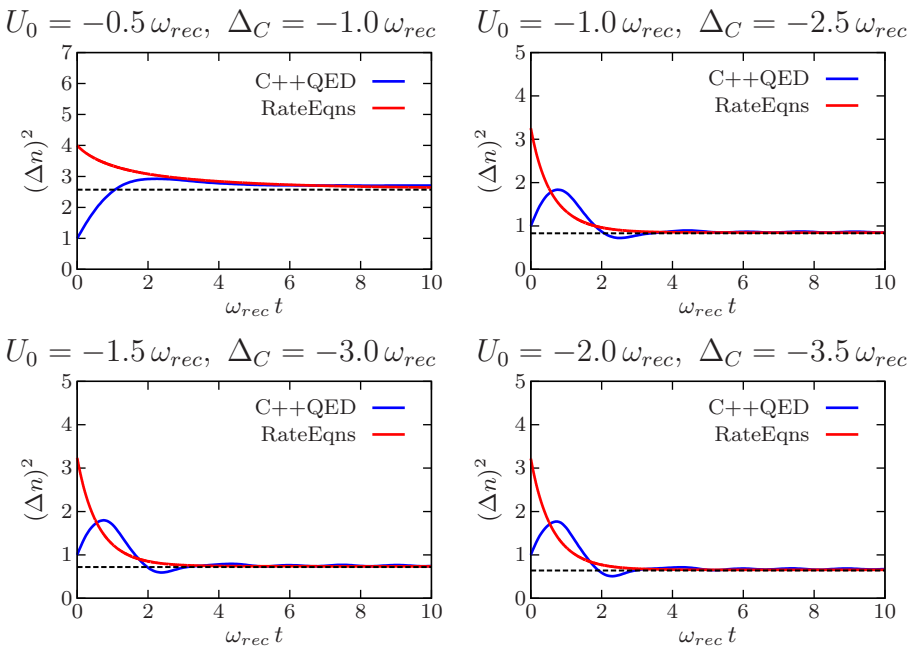

Figure 5.8 Time evolution of $(\Delta n)^2$ provided by QMWF (C++QED, blue) and the rate equations (red) for $\kappa = \omega_{rec}$ and $\eta = 2\,\omega_{rec}$. The dashed line indicates the steady-state value given by the rate equations.

larger number of atoms [19], which may similarly hold for heating processes as well. Since we are only dealing with one particle, larger particle numbers may qualitatively relate to larger absolutes of U_0 in a not necessarily linear manner. Indeed, the curves of fig. (5.9) appear to have larger slope for smaller absolutes of U_0. On the other hand $(\Delta p)^2$ seems to approach its steady-state value faster for larger absolute values of U_0, fig. (5.10). The difference between the steady-state values of $(\Delta p)^2$ in the plots of fig. (5.10), however, is mainly due to different values of Δ_C, see fig. (5.1). At that point it would be interesting whether the momentum relaxation is faster for a transversely pumped configuration.

The rate equations' agreement with the C++QED results is surprisingly good. This suggests that we might exploit the rate equations to study the system's long-term evolution for time scales usually inaccessible to QMWF due to long computation time. The mismatch of momentum variance from different methods in fig. (5.1) has been strapped down to a difference of characteristic time scales. Whereas the photon number and its variance approach their steady-state in a few ω_{rec}^{-1}, the momentum variance will not reach a steady-state in any reasonable period of time. We can therefore conclude that the rate equations and the master equation provide the formally correct numeric steady-state, but the system's evolution into such takes arbitrarily long.

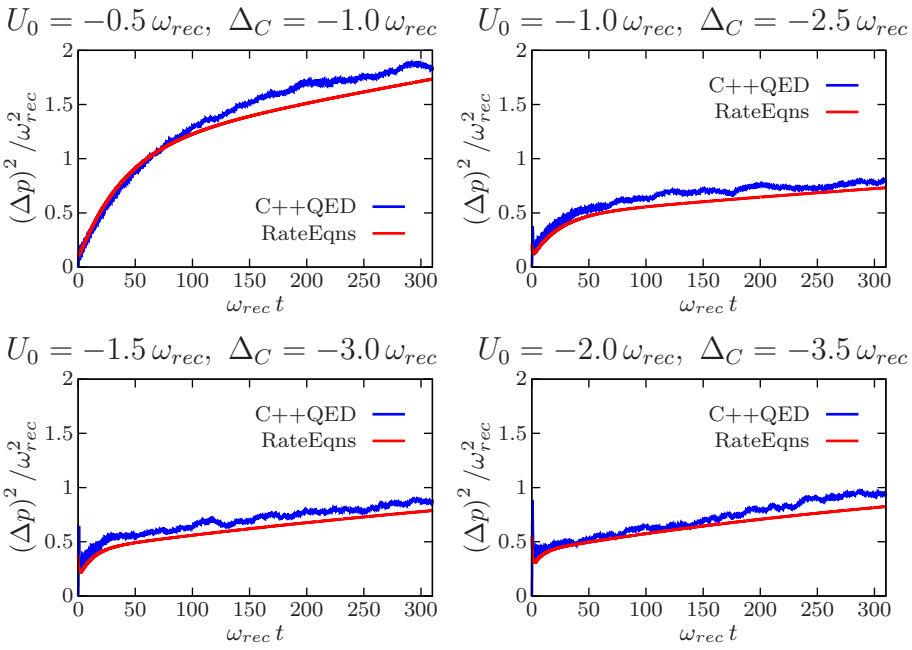

Figure 5.9 Time evolution of $(\Delta p)^2$ provided by QMWF (C++QED, blue) and the rate equations (red) for $\kappa = \omega_{rec}$ and $\eta = 2\,\omega_{rec}$.

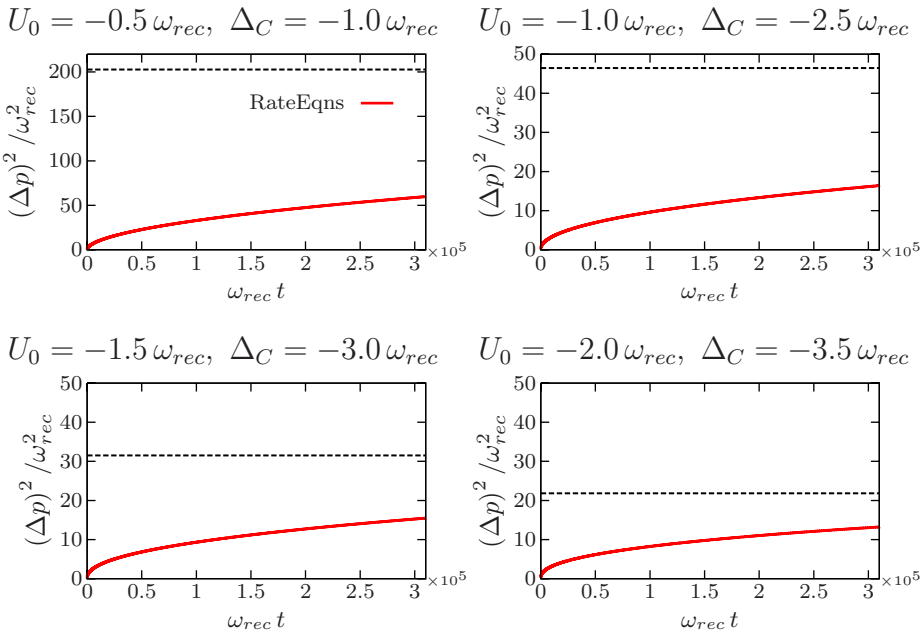

Figure 5.10 Long Time evolution of $(\Delta p)^2$ provided by QMWF (C++QED, blue) for $\kappa = \omega_{rec}$ and $\eta = 2\,\omega_{rec}$.

6 QMWF With C++QED

In the previous chapters we gained some insight into the available solution methods and their applicability in different parameter regimes. It turned out that a direct numerical solution of the full master equation is limited by available memory, which limits the dimensionality of the Hilbert space under consideration as well. Eq. (3.10) would then allow for low pump rates η only. The rate equations do not suffer from that shortcoming, but become invalid close to the system resonance frequency $\Delta_C = U_0 \langle \cos^2(k_{rec}\mathrm{X}_a)\rangle$, which is just the range in which we expect interesting physical effects. Hence QMWF seems preferable for a generic exploration of the long-time behavior of the one particle one mode system in this limit. Larger systems or more accurate results (larger number of trajectories) afflict computation time only, which is an acceptable constraint.

Below we choose a set of parameters that require photon number cutoffs that are too large for a direct solution of the master equation (large η) and for which the rate equations do not provide credible results. We study the variation of the long-time behavior given by the QMWF with changing parameters rather than observing the time evolution for constant parameters.

As before, the QMWF is performed in the C++QED framework [51]. To accelerate dynamics at the beginning the simulation starts with one photon in the cavity. The particle's initial momentum wave function is sharply peaked around $p = 0$. As before, time integration is performed until $t = 310\omega_{rec}^{-1} \equiv 310\kappa^{-1}$. This is long enough to reach an almost stationary state with very weak time-dependence.

6.1 From Single Trajectories to Density Matrices

Fig. (6.1) shows examples of final states of individual trajectories computed by C++QED. The color represents the modulus squared of the wave function amplitudes (in arbitrary units), the diagonal elements of the corresponding density matrix $|\Psi_j\rangle\langle\Psi_j|$ in computational basis (see eqs. (4.13) and (4.1)). C++QED computational basis includes states with momenta that are odd integer multiple of k_{rec} as well. Due to low width in momentum space of the initial wave function and the inversion symmetry preserving character of the Hamiltonian, these states are not populated at all. Therefore the odd momentum states will not be considered in our analysis, fig. (6.1). The total density matrix is now an average over all single trajectory density matrices, eq. (4.13). For practical reasons we plot diagonal elements only, which provides sufficient information for an estimation of many characteristic properties like mean-values and variances.

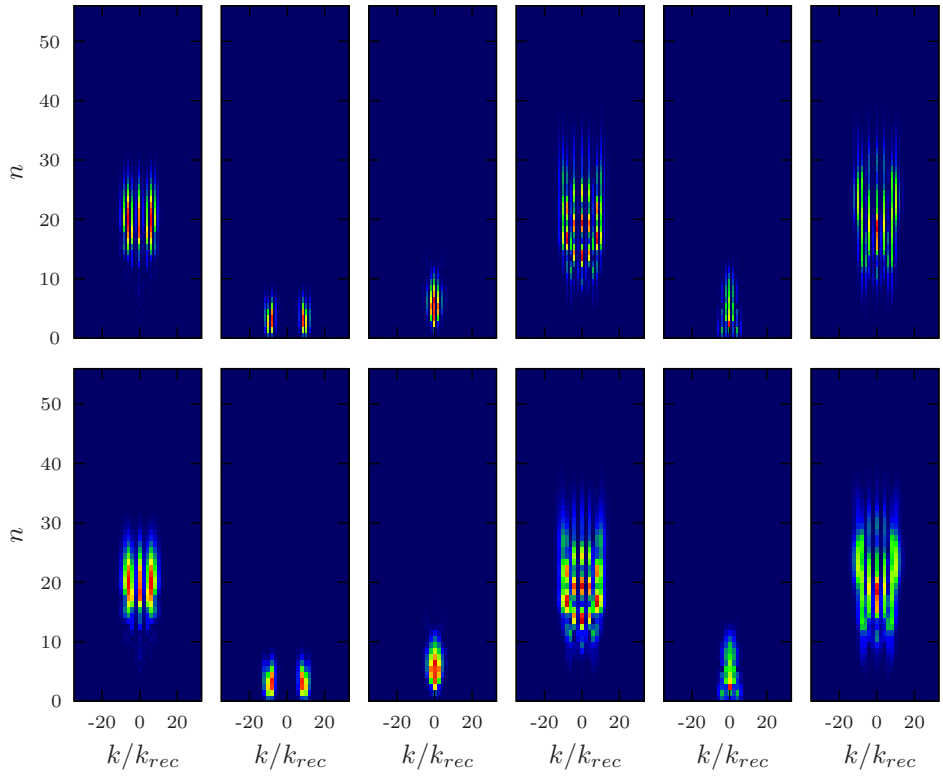

Figure 6.1 A non-representative sample of C++QED quantum trajectories for $\eta = 5\,\omega_{rec}$, $\Delta_C = -7.5\,\omega_{rec}$, $\kappa = \omega_{rec}$ at $t = 310\,\omega_{rec}^{-1}$. The color highlights the modulus squared of the amplitudes in $|n, k\rangle$-basis in arbitrary units with increasing numbers from blue to red (see e.g. fig. (6.2); the scaling, however, is different for every plot). C++QED computes values for the odd momentum states as well (top line), but we will consider even momentum states only (bottom line).

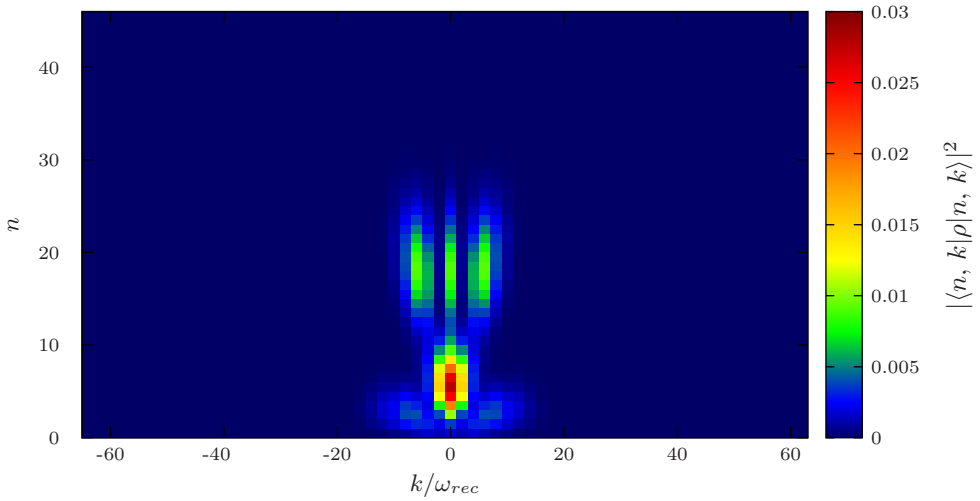

Figure 6.2 The diagonal elements of ρ for $\eta = 5\,\omega_{rec}$, $\Delta_C = -7.5\,\omega_{rec}$, $\kappa = \omega_{rec}$ at $t = 310\,\omega_{rec}^{-1}$. The color highlights the modulus squared of the amplitudes in $|n,\, k\rangle$-basis.

Fig. (6.2) shows the diagonals of the total density matrix ρ for one point in our parameter space. A comparison with fig. (6.1) and a closer inspection of a greater number of single quantum trajectories suggests that peaks at different photon numbers stem from classical mixtures of different trajectories rather than being a manifestation of a larger number of quantum superpositions. We see that the states can be very different and can be well distinguished by e.g. their photon number. This is a strong sign of multistability and large fluctuations. The three leftmost final trajectories in fig. (6.2) appear to form Poissonian like field states around mean photon numbers that seem to be correlated with the shape of momentum distribution. This supports the semi-classical picture of chapter 3 where different Bloch bands ($\leftrightarrow$ different distribution shapes) have different self-consistent mean photon numbers. The three rightmost final trajectories in fig. (6.2) seem to form superpositions of different Bloch bands and corresponding field states. They may give rise to significant particle-field entanglement. Scanning through C++QED final trajectories we observe that final trajectories of the first type (three leftmost) are much more abundant than those of the second type (three rightmost). Since all final trajectories enter the density matrix with equal weights, we expect low particle-field entanglement in our one-particle-one-mode system. Nonetheless we would like to examine the system's entanglement properties a little closer.

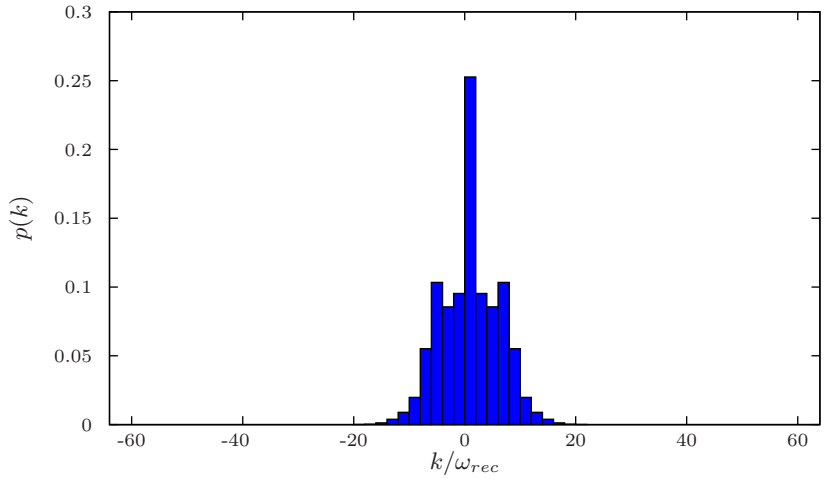

Figure 6.3 The momentum distribution $p(k)$ for the system with the parameters of fig. (6.2). The distribution is symmetric around $k = 0$, i.e. invariant under $k \to -k$.

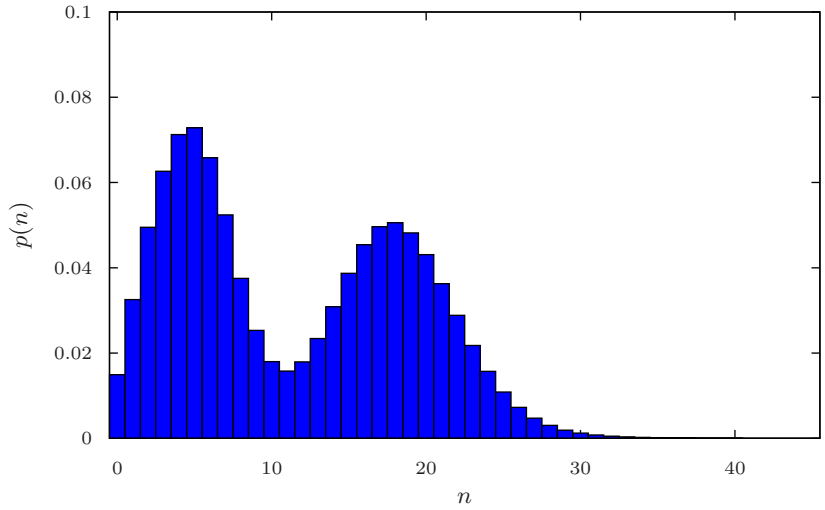

Figure 6.4 The photon number distribution $p(n)$ for the system with the parameters of fig. (6.2) showing two peaks at distinct photon numbers. This bimodal behavior is strong evidence for optical bistability.

6.2 Entanglement Properties of a Bipartite System

Entanglement in quantum systems has first been considered in the famous and controversially discussed paper by Einstein, Podolsky and Rosen [52]. In 1964 Bell's formulation of his well-known inequality [53] has boosted research in quantum information theory. Many papers have been published on the matter since then, both theoretical and experimental. An extensive introduction to quantum information and a comprehensive list of references can be found in [54]. We are looking at the simplest object that can show entanglement: a bipartite quantum system. Bipartite quantum systems, the two-qubit system in particular, have been studied extensively in the past two decades. Various measures for pure state (e.g. *entropy of entanglement* [55]) and mixed state entanglement (e.g. *entanglement of formation* [56]) have been investigated. Entanglement measures do not allow for an effective numerical computation in general. Following [57] (and [58]) we therefore opt for *negativity under partial transposition* $\mathcal{N}(\rho)$. We will briefly introduce the necessary definitions required for its computation.

For a bipartite d^2-dimensional system composed of two d-dimensional subsystems A and B, $\mathcal{H} = \mathcal{H}_A \otimes \mathcal{H}_B$, the basis states may be labeled by two indices $|ij\rangle$ with i running in A and j running in B. Therefore the elements of the density matrix ρ may carry four indices $\rho_{ij,\,i'j'}$.

$$\left(\rho^{T_A}\right)_{ij,\,i'j'} = \rho_{i'j,\,ij'} \tag{6.1}$$

$$\left(\rho^{T_B}\right)_{ij,\,i'j'} = \rho_{ij',\,i'j} \tag{6.2}$$

then defines the *partial transposition* along subsystem A and B, respectively. The *negativity under partial transposition* is then defined as

$$\begin{aligned}\mathcal{N} &= \frac{\left\|\rho^{T_A}\right\|_1 - 1}{2} \\ &= \frac{\left\|\rho^{T_B}\right\|_1 - 1}{2},\end{aligned} \tag{6.3}$$

where $\|\cdot\|_1$ denotes the sum of the absolutes of the eigenvalues. The negativity then corresponds to the absolute value of the sum of all negative eigenvalues of the partially transposed density matrix.

6.2.1 Upper Bound of Negativity under Partial Transposition

Let us consider a maximally entangled state in the Hilbert space $\mathcal{H} = \mathbb{C}^d \otimes \mathbb{C}^d$,

$$|\Psi_{max}\rangle = \frac{1}{\sqrt{d}}\left(|00\rangle + |11\rangle + \cdots + |d-1, d-1\rangle\right). \tag{6.4}$$

Any other maximally entangled state can be generated from $|\Psi_{max}\rangle$ via local unitary transformations (LU), i.e. $U_A \otimes 1_B$ and $1_A \otimes U_B$, respectively. The density matrix of

this state then reads

$$\rho_{max} \equiv |\Psi_{max}\rangle\langle\Psi_{max}| = \begin{pmatrix} \frac{1}{d} & 0 & \cdots & 0 & \frac{1}{d} & 0 & \cdots & \cdots & 0 & \frac{1}{d} \\ 0 & 0 & \cdots & 0 & 0 & 0 & \cdots & \cdots & 0 & 0 \\ \vdots & \vdots & \ddots & \vdots & \vdots & \vdots & \ddots & \ddots & \vdots & \vdots \\ 0 & 0 & \cdots & 0 & 0 & 0 & \cdots & \cdots & 0 & 0 \\ \frac{1}{d} & 0 & \cdots & 0 & \frac{1}{d} & 0 & \cdots & \cdots & 0 & \frac{1}{d} \\ 0 & 0 & \cdots & 0 & 0 & 0 & \cdots & \cdots & 0 & 0 \\ \vdots & \vdots & \ddots & \vdots & \vdots & \vdots & \ddots & \ddots & \vdots & \vdots \\ \vdots & \vdots & \ddots & \vdots & \vdots & \vdots & \ddots & \ddots & \vdots & \vdots \\ 0 & 0 & \cdots & 0 & 0 & 0 & \cdots & \cdots & 0 & 0 \\ \frac{1}{d} & 0 & \cdots & 0 & \frac{1}{d} & 0 & \cdots & \cdots & 0 & \frac{1}{d} \end{pmatrix}. \tag{6.5}$$

So there is a non-zero entry $\frac{1}{d}$ at each index

$$[(m-1)\,d+m,\ (n-1)\,d+n] \mid m,\, n \in \{1,\, 2 \ldots d\}\,.$$

Partial transposition along A or B then gives non-zeros $\frac{1}{d}$ at indices

$$[(n-1)\,d+m,\ (m-1)\,d+n]\,.$$

Since $m,\, n \leq d$, the assignment

$$k = (n-1)\,d+m \mid k \in \left\{1,\, 2,\, \ldots d^2\right\}, \tag{6.6}$$

is unique for a given pair of m and n. The row index and the column index of each non-zero entry in $\rho_{max}^{T_{\{A,\,B\}}}$ are connected via $m \leftrightarrow n$ in eq. (6.6). This means that all off-diagonal non-zero entries of $\rho_{max}^{T_{\{A,\,B\}}}$ form pairwise permutations. The total partially transposed density matrix then decomposes into a direct sum of a d-dimensional identity part 1_{diag} and a direct sum of non-overlapping, pairwise permutations $P_{i\leftrightarrow j}$

$$\begin{aligned} \rho_{max}^{T_A} &= \rho_{max}^{T_B} \\ &= \frac{1}{d}\left(1_{diag} \oplus \bigoplus_{m<n} P_{(n-1)d+m\leftrightarrow(m-1)d+n}\right). \end{aligned} \tag{6.7}$$

The eigenvalues of the total matrix are just the eigenvalues of the individual direct summands. Negative eigenvalues stem from the $\frac{1}{2}\left(d^2-d\right)$ pairwise permutations. The eigenvalues v_i of a permutation cycle of length l are the complex roots of the

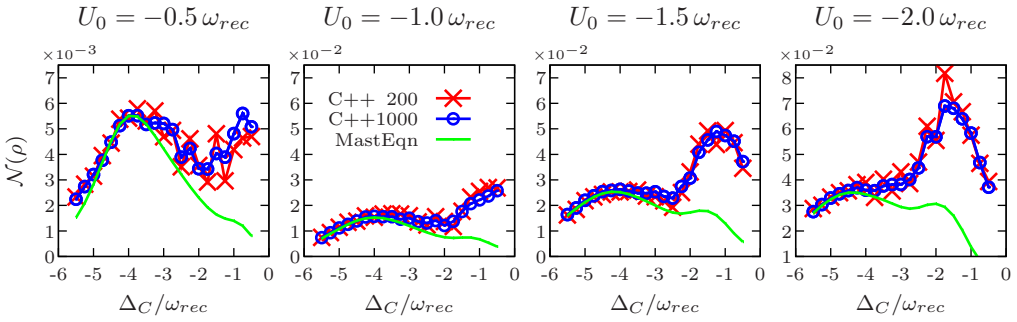

Figure 6.5 Negativity under partial transposition obtained from C++QED with 200 trajectories (C++ 200), 1000 trajectories (C++1000) and from the null space of the Liouvillian (MastEqn): A comparison of the two C++QED data lines suggests that the data for 1000 trajectories has converged well enough. The difference between C++QED and master equation results emerging at higher values of Δ_C do not seem to be of statistical origin.

equation $(v_i)^l = 1$. For $l = 2$ this yields $v_\pm = \pm 1$. So we have everything at hand to straightforwardly compute the sum of the absolutes of the negative eigenvalues:

$$\begin{aligned}\mathcal{N}_{max} &= \frac{1}{2d}\left(d^2 - d\right) \\ &= \frac{1}{2}\left(d - 1\right).\end{aligned} \tag{6.8}$$

For $\mathcal{H} = \mathbb{C}^d \otimes \mathbb{C}^f$, following the arguments of the Schmidt-decomposition [59][60], we get

$$\mathcal{N}_{max} = \frac{1}{2}\Big(\min\left(d,\ f\right) - 1\Big). \tag{6.9}$$

6.2.2 Entanglement in the One-Particle-One-Mode System

Unlike expectation values and variances, entanglement is manifested in the off-diagonal entries of ρ. Therefore only the QMWF or a direct solution of the master equation are able to provide data for entanglement measures. The two subspaces of our system that we hope to find entangled are the photon number space and the particle's momentum space, respectively. We compare the numbers for negativity under partial transposition for density matrices provided by null space of the Liouvillian and the QMWF for the same range of parameters as in chapter 5 (fig. (6.5)). We see that the values from both methods are in the same order of magnitude. Close to resonance, however, we find that the QMWF produces a density matrix that has larger negativity than that obtained from the null space of the Liouvillian. This means that either the number of trajectories was chosen too small or this deviation stems from the slow dynamics encountered in momentum space (sec. 5.2). Comparing QMWF results from C++QED with 200 and 1000 trajectories we see that the number of trajectories

Parameter	Range/Value
η	$\{3, 4, 5, 6\} \times \omega_{rec}$
Δ_C	$\{-11.5, -11, \cdots, -4.5\} \times \omega_{rec}$
κ	$1\,\omega_{rec}$
U_0	$-10\,\omega_{rec}$
t_f	$310\,\omega_{rec}^{-1}$

Table 6.1 Set of parameters used for QMWF in C++QED on a $128 \otimes 96$-dimensional Hilbert space.

has already little effect on the computed values, fig. (6.5). The mismatch might be owing to the slow momentum dynamics already encountered in section 5.2.

We find $\mathcal{N} \ll 1$ throughout the parameter range, which is much smaller than for a fully entangled pair of qubits. In [61] time-dependent entanglement properties in a similar setup is investigated. Decreasing partial transpose negativity $\mathcal{N}$ is found for for particle-field entanglement with increasing time. Entanglement in ring cavities may persist up to $t = 1500\,\omega_{rec}^{-1}$ [62]. The entanglement observed, however, is between two moving particles and not between particle and field. Entanglement in single quantum trajectories can be very high, but entanglement measures for the total density matrix ρ are sensitive to phases between different trajectories. Apparently entanglement in a system is usually much lower than the mean entanglement of QMWF trajectories. The numeric values of $\mathcal{N}(\rho)$ in our computations suggest that entanglement between the field and momentum subspace is almost negligible in the stationary limit. Any observed multistability would be of classical nature.

6.3 QMWF on a Larger Hilbert Space

We have already discussed different solution methods and the QMWF has emerged as the most applicable. Eventually we will investigate a Hilbert space with $n_{cut} = 95$ and $k_{max} = 64$. We choose the following parameters given in tab. (6.1).

As before, each quantum trajectory will be evolved until $t = 310\,\omega_{rec}^{-1}$. Fig. (6.6) shows a plot of the diagonal elements of the obtained density matrices.

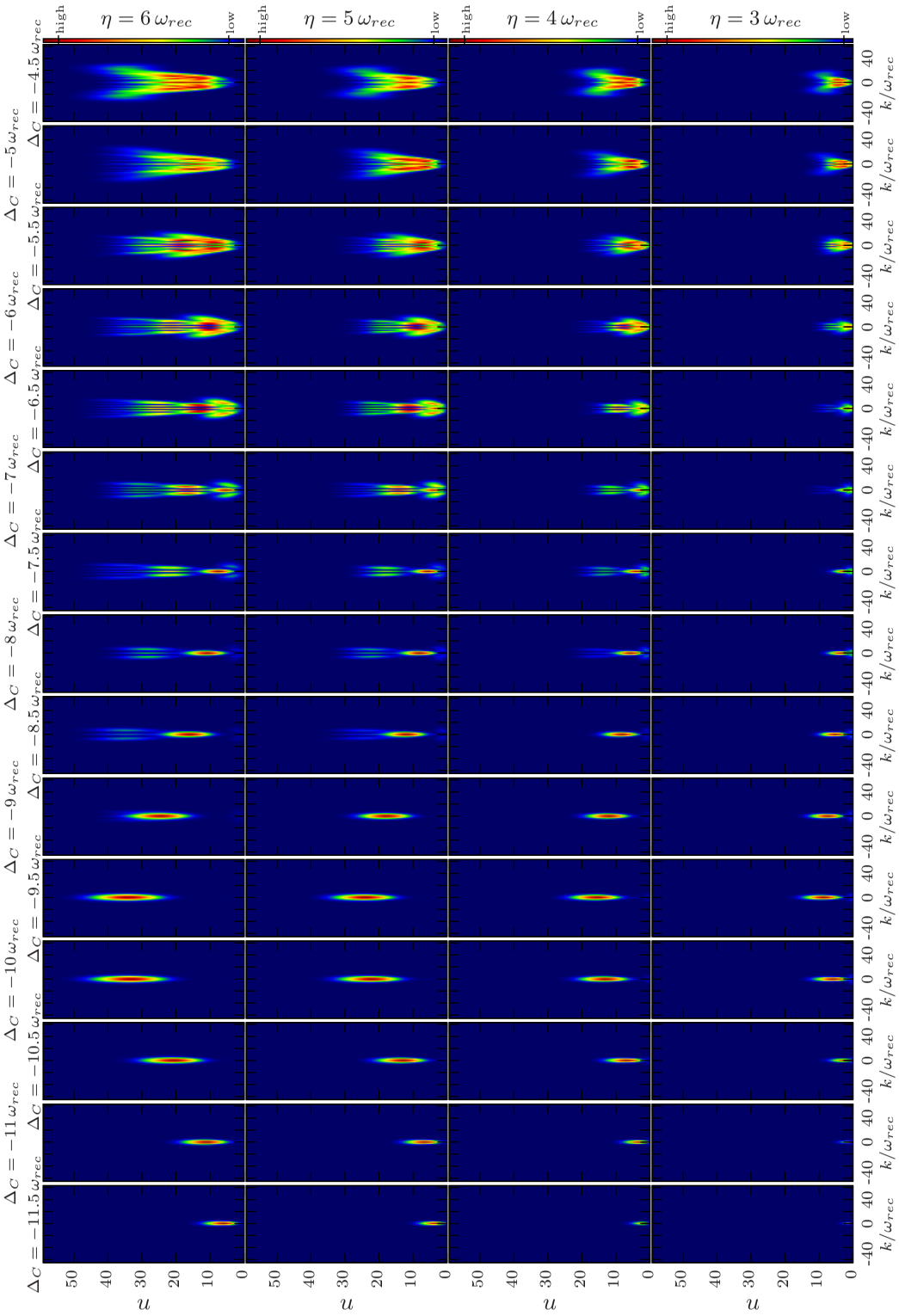

Figure 6.6 Color map of diagonal elements of density matrices in $|n, k\rangle$-basis in arbitrary units for the set of parameters given in tab. (6.1).

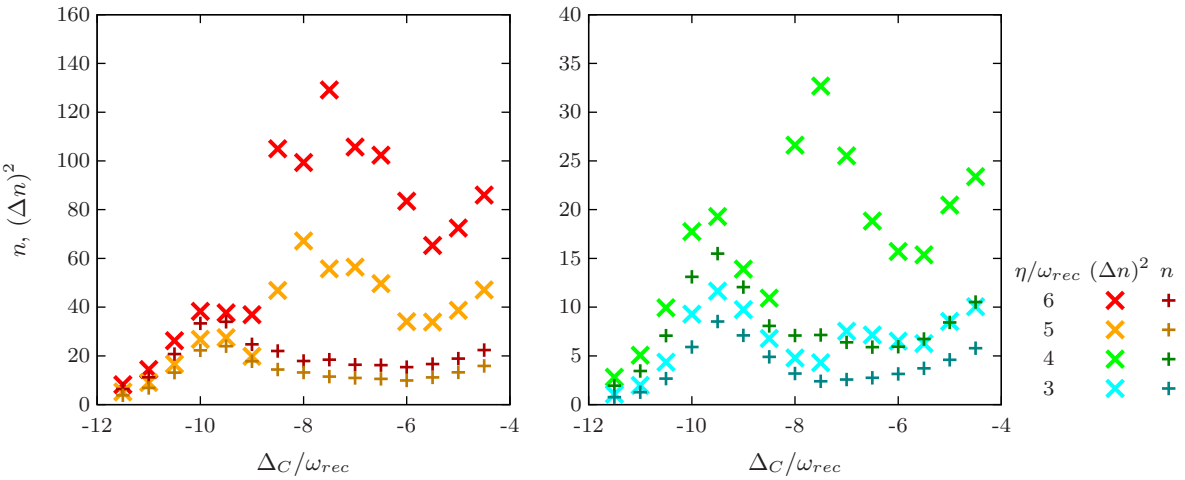

Figure 6.7 Photon number n and variance $(\Delta n)^2$ computed by C++QED for the parameters of tab. (6.1): $(\Delta n)^2 \gg n$ indicates regions of bi- or multimodal photon number distributions.

We can distinguish different momentum modes (Bloch bands) by their number of peaks along the momentum axis k in figs. (6.6) and (6.2). We see that different momentum modes reach their maximum photon number for different detunings Δ_C. This behavior follows our semiclassical considerations of chapter 3. It seems that higher momentum modes only appear if the corresponding self-consistent solutions of eq. (3.33) exist. Low entanglement between photon and momentum space supports the idea of having a classical mixture of different modes rather than a superposition. This might permit for a utilization of eq. (3.33) for the individual momentum modes. The relative weights for each mode are governed by eq. (3.8), which may have multiple solutions as well. As Δ_C approaches 0, higher and higher momentum modes will be populated. At some point our momentum cutoff would become too small and the physical validity of our results would break down.

Fig. (6.7) shows a plot of the photon number, n, and its variance, $(\Delta n)^2$. For $\Delta_C \leq -9\,\omega_{rec}$ we find that $(\Delta n)^2 \approx n$, which is characteristic of (almost) coherent states. Coherent states are solutions to the empty cavity, eq. (3.7), and we can therefore conjecture that the interaction term has little impact on the photon field in that regime. For $\Delta_C > -9\,\omega_{rec}$ the situation is different. Speaking in terms of the semi-classical model we find higher momentum modes (Bloch bands) becoming more highly populated and additional peaks appear in the photon distribution. Therefore the variance $(\Delta n)^2$ is much larger than n in that range and indicates potential multistability.

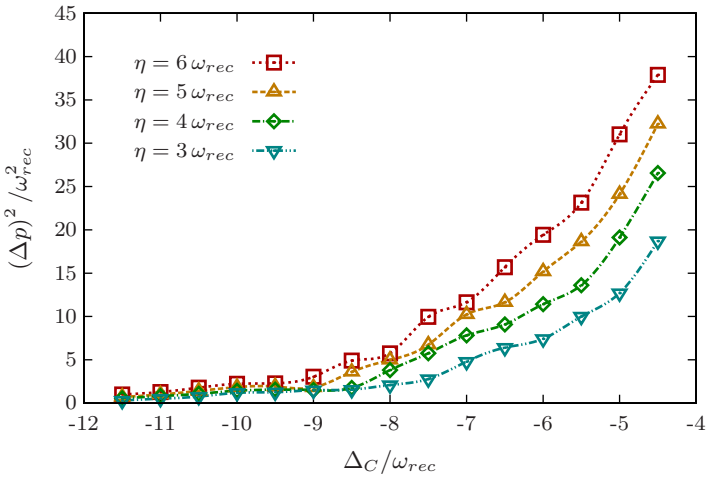

Figure 6.8 Momentum variance $(\Delta p)^2$ computed by C++QED for the parameters of tab. (6.1): Since $\langle \mathrm{p} \rangle = 0$, $(\Delta p)^2$ is proportional to the mean kinetic energy and temperature of the particle.

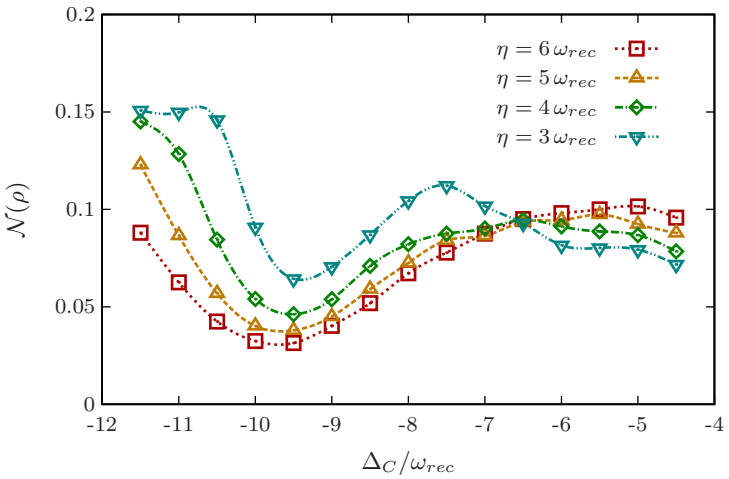

Figure 6.9 Negativity under partial transposition $\mathcal{N}(\rho)$ computed by C++QED for the parameters of tab. (6.1)

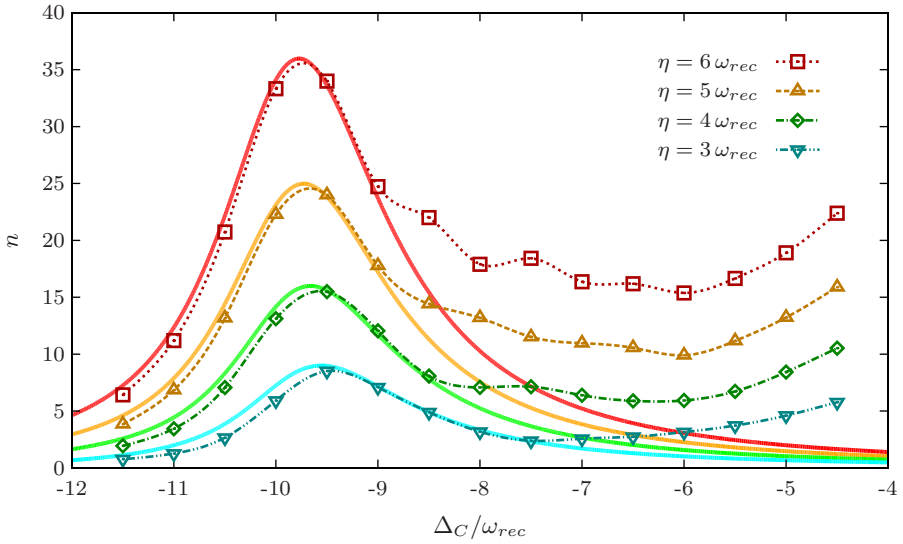

Figure 6.10 Data points for the mean photon number n for the parameters in tab. (6.1) from C++QED. The solid lines are self-consistent contours of eq. (3.33) for the lowest Bloch band $m = 0$ as found in fig. (3.3).

6.4 Comparison to Semi-Classical Computations

Fig. (6.10) shows the QMWF results from C++QED for the mean photon numbers n in comparison to the self-consistent contour of eq. (3.33) for the lowest Bloch band $m = 0$ (solid lines). For $\Delta_C \leq -9\,\omega_{rec}$ the QMWF data fits to the semiclassical results. Though self-consistent solutions of eq. (3.33) exist in that range for higher bands, $m > 0$, as well, they are not populated. These solutions are stable according to the stability analysis conducted in section 3.2.2, but a look at fig. (3.3) reveals that these states are not bound for large negative values of Δ_C. But this is not the essential point here. Looking at larger values of Δ_C we find free states at small photon numbers. They key process in this situation is *cavity mediated (laser) cooling*. Whenever the effective detuning Δ_{eff} (eq. (3.9)) is lower than zero, the atomic motion is cooled, i.e. its width in momentum space Δ_p decreases in time through the loss of cavity photons [17]. It is very easy to graphically determine the sign of $\Delta_{eff,m}$ for each band m for a given Δ_C. For $\Delta_{eff} = 0$ the mean photon number reaches its maximum value on the self-consistent contours of figs. (3.3) and (6.10). Δ_{eff} is positive for all Δ_C to the right of the maximum photon number along the self-consistent contour and negative to the left, respectively. The dynamics of the system is an interplay between heating an cooling of different bands. For a given value of Δ_C some bands are heated while others are cooled, depending on the value $\Delta_{eff,m}$, where m is the band index, as usual. The sign of $\Delta_{eff,m}$ indicates whether it is heated (+) or cooled (-). Since we consider individual bands and not the total system, heating and cooling of individual bands is understood as whether transitions

to higher and lower bands are preferred, respectively.

The picture of different eigenstates forming along the self-consistent contours of eq. (3.8) is very tempting but not necessarily complete. It would require that the relaxation time to self-consistency is much faster than typical transition times between two bands (Haken's slaving principle, see sec. 2.2). But transitions between different bands in our description are basically driven by photon dynamics and overlaps of Wannier states for different photon numbers/potential depths. Relaxation to self-consistency (along constant values of Δ_C) is also a photonic process, therefore it is very unlikely that both processes occur at largely different time scales. Consequently one should consider the value of $\Delta_{eff,m}$ across the whole Δ_C-$n-$plane. With this little extension our previous considerations remain valid. We would like to conclude our comparison of QMWF and our semi-classical approach of section 3.2 with this qualitative analysis of dynamic processes. It is remarkable that our simple, stationary approach qualitatively resembles results from a fully quantum mechanical simulation for long times. For a quantitative comparison we would have to extend the semi-classical model of section 3.2 to a time-dependent version that provides transition rates.

7 Conclusion and Outlook

The semi-classical treatment of the one particle - one mode system developed in this thesis appears to capture many features of fully quantum mechanical solution methods such as QMWF. Moreover, it permits for a simple interpretation of the raveled, non-linear dynamics in terms of Bloch states in a periodic potential. With that simple picture at hand a time-dependent semi-classical model may be developed whose stationary solution may provide the relative weights of the individual Bloch bands in the steady state. Due to low particle-field entanglement found in the one particle - one mode system, the results of such a model could qualitatively compete with QMWF.

Both the semi-classical modeling and the QMWF revealed optical bi- and multistability for a certain range of parameters. In the semi-classical picture of bands of localized Wannier states even single bands show regions that permit for two stable, self-consistent solutions. Looking at final states of single quantum trajectories we found that the system evolves into both stable states separately, superpositions are rare.

In search of other possibilities of approximate numerical solutions we have encountered the rate equations, a concept familiar from laser theory. Their formulation for a generic dissipative quantum system has been given in terms of left and right eigenstates of a non-hermitian effective Hamiltonian. An ansatz for a possible extension that permits for a perturbative expansion of off-diagonal elements of the density matrix has been provided. A refinement of this ansatz with respect to Haken's slaving principle might yield interesting results.

The model of the rate equations developed in this thesis was sufficient to link the results of QMWF and the steady state of the master equation. It revealed that evolution in momentum space is very slow compared to field dynamics and that the formally correct steady state is only reached after very long time.

Bibliography

[1] WH Eccles and FW Jordan. A trigger relay utilizing three-electrode thermionic vacuum tubes. *Radio Review*, 1(3):143, 1919.

[2] Henri Poincaré. Sur le probleme des trois corps et les équations de la dynamique. *Acta mathematica*, 13(1):A3–A270, 1890.

[3] Georg Duffing. *Erzwungene Schwingungen bei veränderlicher Eigenfrequenz und ihre technische Bedeutung*. Number 41-42. R, Vieweg & Sohn, 1918.

[4] Balthasar Van der Pol. A theory of the amplitude of free and forced triode vibrations. *Radio Review*, 1(1920):701–710, 1920.

[5] Balthasar Van der Pol. The nonlinear theory of electric oscillations. *Radio Engineers, Proceedings of the Institute of*, 22(9):1051–1086, 1934.

[6] Willis E. Lamb. Theory of an optical maser. *Phys. Rev.*, 134:A1429–A1450, Jun 1964.

[7] A. Szöke, V. Daneu, J. Goldhar, and N. A. Kurnit. Bistable optical element and its applications. *Applied Physics Letters*, 15(11):376–379, 1969.

[8] H. M. Gibbs, S. L. McCall, and T. N. C. Venkatesan. Differential gain and bistability using a sodium-filled fabry-perot interferometer. *Phys. Rev. Lett.*, 36:1135–1138, May 1976.

[9] Hyatt Gibbs. *Optical bistability: controlling light with light*. Elsevier, 1985.

[10] P D Drummond and D F Walls. Quantum theory of optical bistability. i. nonlinear polarisability model. *Journal of Physics A: Mathematical and General*, 13(2):725, 1980.

[11] G. Rempe, R. J. Thompson, R. J. Brecha, W. D. Lee, and H. J. Kimble. Optical bistability and photon statistics in cavity quantum electrodynamics. *Phys. Rev. Lett.*, 67:1727–1730, Sep 1991.

[12] D. Jaksch, C. Bruder, J. I. Cirac, C. W. Gardiner, and P. Zoller. Cold bosonic atoms in optical lattices. *Phys. Rev. Lett.*, 81:3108–3111, Oct 1998.

[13] RichardP. Feynman. Simulating physics with computers. *International Journal of Theoretical Physics*, 21(6-7):467–488, 1982.

[14] L. Tagliacozzo, A. Celi, A. Zamora, and M. Lewenstein. Optical abelian lattice gauge theories. *Annals of Physics*, 330(0):160 – 191, 2013.

[15] L. Tagliacozzo, A. Celi, P. Orland, M. W. Mitchell, and M. Lewenstein. Simulation of non-abelian gauge theories with optical lattices. *Nat Commun*, 4, Oct 2013.

[16] Peter Domokos and Helmut Ritsch. Collective cooling and self-organization of atoms in a cavity. *Phys. Rev. Lett.*, 89:253003, Dec 2002.

[17] Peter Horak, Gerald Hechenblaikner, Klaus M. Gheri, Herwig Stecher, and Helmut Ritsch. Cavity-induced atom cooling in the strong coupling regime. *Phys. Rev. Lett.*, 79:4974–4977, Dec 1997.

[18] Peter Domokos and Helmut Ritsch. Mechanical effects of light in optical resonators. *J. Opt. Soc. Am. B*, 20(5):1098–1130, May 2003.

[19] J. K. Asbóth, P. Domokos, H. Ritsch, and A. Vukics. Self-organization of atoms in a cavity field: Threshold, bistability, and scaling laws. *Phys. Rev. A*, 72:053417, Nov 2005.

[20] Helmut Ritsch, Peter Domokos, Ferdinand Brennecke, and Tilman Esslinger. Cold atoms in cavity-generated dynamical optical potentials. *Rev. Mod. Phys.*, 85:553–601, Apr 2013.

[21] Crispin W. Gardiner and Peter Zoller. *Quantum Noise*. Springer-Verlag Berlin Heidelberg New York, 2nd edition, 2000.

[22] D. F. Walls and G. J. Milburn. *Quantum Optics*. Springer-Verlag Berlin Heidelberg New York, 1st edition, 1995.

[23] Miguel Orszag. *Quantum Optics*. Springer-Verlag Berlin Heidelberg New York, 2nd edition, 2008.

[24] V. Weisskopf and E. Wigner. Berechnung der natürlichen linienbreite auf grund der diracschen lichttheorie. *Zeitschrift für Physik*, 63(1-2):54–73, 1930.

[25] G. Lindblad. On the generators of quantum dynamical semigroups. *Communications in Mathematical Physics*, 48(2):119–130, 1976.

[26] C. W. Gardiner and M. J. Collett. Input and output in damped quantum systems: Quantum stochastic differential equations and the master equation. *Phys. Rev. A*, 31:3761–3774, Jun. 1985.

[27] M. J. Collett and C. W. Gardiner. Squeezing of intracavity and traveling-wave light fields produced in parametric amplification. *Phys. Rev. A*, 30:1386–1391, Sep. 1984.

[28] Claude Cohen-Tannoudji, Jacques Dupont-Roc, and Gilbert Grynberg. *Photons & Atoms*. Wiley-VCH Verlag GmbH & Co KGaA, Weinheim, 1st edition, 2004.

[29] Joan Solà. Cosmological constant and vacuum energy: old and new ideas. *Journal of Physics: Conference Series*, 453(1):012015, 2013.

[30] G. C. Wick. The evaluation of the collision matrix. *Phys. Rev.*, 80:268–272, Oct 1950.

[31] Michael E Peskin and Daniel V Schroeder. *An Introduction to Quantum Field Theory*. Westview, 1995.

[32] G.D. Boyd and J. P. Gordon. Confocal multimode resonator for millimeter through optical wavelength masers. *Bell Sys. Tech. J.*, 40:489–508, Mar. 1961.

[33] Claude Cohen-Tannoudji, Bernard Diu, and Frank Laloe. *Quantenmechanik Band 2*. Walter de Gruyter Berlin New York, 3rd edition, 2008.

[34] E.T. Jaynes and F.W. Cummings. Comparison of quantum and semiclassical radiation theories with application to the beam maser. *Proceedings of the IEEE*, 51:89–109, Jan. 1963.

[35] H. Haken. Generalized ginzburg-landau equations for phase transition-like phenomena in lasers, nonlinear optics, hydrodynamics and chemical reactions. *Zeitschrift für Physik B Condensed Matter*, 21(1):105–114, 1975.

[36] Hermann Haken. *Synergetik: eine Einführung; Nicht-Gleichgewichts-Phasnübergänge und Selbstorganisation in der Physik, Chemie und Biologie*. Springer-Verlag Berlin Heidelberg New York, 3 edition, 1990.

[37] Hermann Haken. *Advanced Synergetics*. Springer-Verlag Berlin Heidelberg New York Tokyo, 1 edition, 1983.

[38] Crispin W. Gardiner. *Stochastic Methods - A Handbook for the Natural and Social Sciences*. Springer-Verlag Berlin Heidelberg, 4 edition, 2009.

[39] M. Diver, G. R. M. Robb, and G.-L. Oppo. Nonlinear and chaotic dynamics of a bose-einstein condensate in an optical cavity. *Phys. Rev. A*, 89:033602, Mar 2014.

[40] Katharina Renz. Two interacting atoms in a quantum potential. Master's thesis, Universität Innsbruck, Dec 2005.

[41] Christoph Maschler. *Ultracold Atoms in Resonator-Generated Optical Lattices*. PhD thesis, Universität Innsbruck, Oct 2007.

[42] Gerd Czycholl. *Theoretische Festkörperphysik*. Springer-Verlag Berlin Heidelberg, 3rd edition, 2008.

[43] Felix Bloch. Über die quantenmechanik der elektronen in kristallgittern. *Zeitschrift für Physik*, 52(7-8):555–600, 1929.

[44] Gregory H. Wannier. The structure of electronic excitation levels in insulating crystals. *Phys. Rev.*, 52:191–197, Aug 1937.

[45] W. Kohn. Analytic properties of bloch waves and wannier functions. *Phys. Rev.*, 115:809–821, Aug 1959.

[46] Tobias Grießer and Helmut Ritsch. Nonlinear atom-field dynamics in high-q cavities: from a bec to a thermal gas. *Opt. Express*, 19(12):11242–11255, Jun 2011.

[47] Cornelius Lanczos. *An iteration method for the solution of the eigenvalue problem of linear differential and integral operators*. United States Governm. Press Office, 1950.

[48] A. Barchielli, L. Lanz, and G.M. Prosperi. A model for the macroscopic description and continual observations in quantum mechanics. *Il Nuovo Cimento B*, 72(1):79–121, 1982.

[49] R. Dum, P. Zoller, and H. Ritsch. Monte carlo simulation of the atomic master equation for spontaneous emission. *Phys. Rev. A*, 45:4879–4887, Apr 1992.

[50] Y. Castin and J. Dalibard. Quantization of atomic motion in optical molasses. *EPL (Europhysics Letters)*, 14(8):761, 1991.

[51] A. Vukics and H. Ritsch. C++qed: an object-oriented framework for wavefunction simulations of cavity qed systems. *The European Physical Journal D*, 44(3):585–599, 2007.

[52] A. Einstein, B. Podolsky, and N. Rosen. Can quantum-mechanical description of physical reality be considered complete? *Phys. Rev.*, 47:777–780, May 1935.

[53] John S Bell et al. On the einstein-podolsky-rosen paradox. *Physics*, 1(3):195–200, 1964.

[54] M.A. Nielsen and I.L. Chuang. *Quantum Computation and Quantum Information: 10th Anniversary Edition*. Cambridge University Press, 2010.

[55] Sandu Popescu and Daniel Rohrlich. Thermodynamics and the measure of entanglement. *Phys. Rev. A*, 56:R3319–R3321, Nov 1997.

[56] Charles H. Bennett, David P. DiVincenzo, John A. Smolin, and William K. Wootters. Mixed-state entanglement and quantum error correction. *Phys. Rev. A*, 54:3824–3851, Nov 1996.

[57] G. Vidal and R. F. Werner. Computable measure of entanglement. *Phys. Rev. A*, 65:032314, Feb 2002.

[58] Karol Życzkowski, Paweł Horodecki, Anna Sanpera, and Maciej Lewenstein. Volume of the set of separable states. *Phys. Rev. A*, 58:883–892, Aug 1998.

[59] Erhard Schmidt. Zur theorie der linearen und nichtlinearen integralgleichungen. *Mathematische Annalen*, 63(4):433–476, 1907.

[60] Artur Ekert and Peter L. Knight. Entangled quantum systems and the schmidt decomposition. *American Journal of Physics*, 63(5):415–423, 1995.

[61] András Vukics, Wolfgang Niedenzu, and Helmut Ritsch. Cavity nonlinear optics with few photons and ultracold quantum particles. *Phys. Rev. A*, 79:013828, Jan 2009.

[62] Wolfgang Niedenzu, Raimar M Sandner, Claudiu Genes, and Helmut Ritsch. Quantum-correlated motion and heralded entanglement of distant optomechanically coupled objects. *Journal of Physics B: Atomic, Molecular and Optical Physics*, 45(24):245501, 2012.

A Mean Value Equations of Motion for an Approximate One Particle - One Mode Hamiltonian

We expand the $\cos^2$-term of the one particle - one mode Hamiltonian (eq. (2.72))

$$\mathrm{H}_{1p1m} = \frac{\mathrm{p}^2}{2m} + \eta\left(\mathrm{a}^\dagger + \mathrm{a}\right) + \left(-\Delta_C + U_0\cos^2(k_{rec}\mathrm{x})\right)\mathrm{a}^\dagger\mathrm{a} \tag{A.1}$$

to fourth order

$$\cos^2(k_{rec}\mathrm{x}) = \frac{1+\cos(2k_{rec}\mathrm{x})}{2} \approx 1 - k_{rec}^2\mathrm{x}^2 + \frac{k_{rec}^4\mathrm{x}^4}{3} \tag{A.2}$$

for small fluctuations of x around an antinode, $k_{rec}\langle \mathrm{x}\rangle = m\pi \mid m \in \mathbb{N}$. This yields the approximate Hamiltonian

$$\tilde{\mathrm{H}}_{1p1m} = \frac{\mathrm{p}^2}{2m} + \eta\left(\mathrm{a}^\dagger + \mathrm{a}\right) + \left(-\Delta_C + U_0\frac{1+\cos(2k_{rec}\mathrm{x})}{2} \approx 1 - k_{rec}^2\mathrm{x}^2 + \frac{k_{rec}^4\mathrm{x}^4}{3}\right)\mathrm{a}^\dagger\mathrm{a}. \tag{A.3}$$

Via the master equation

$$\begin{aligned}\partial_t\tilde{\rho} &= \tilde{\mathcal{L}}\tilde{\rho}\\ &\equiv -i\left[\tilde{\mathrm{H}},\,\tilde{\rho}\right] + \kappa\left(2\mathrm{a}\tilde{\rho}\mathrm{a}^\dagger - \mathrm{a}^\dagger\mathrm{a}\tilde{\rho} - \tilde{\rho}\mathrm{a}^\dagger\mathrm{a}\right)\end{aligned} \tag{A.4}$$

we may calculate the mean value equations of motion for time independent Schrödinger operators by virtue of (see also eq. (2.56))

$$\begin{aligned}\partial_t\langle\,\cdot\,\rangle &= \mathrm{Tr}\left\{\,\cdot\,\partial_t\tilde{\rho}\right\}\\ &= \mathrm{Tr}\left\{\,\cdot\,\tilde{\mathcal{L}}\tilde{\rho}\right\}.\end{aligned} \tag{A.5}$$

We derive the mean value equations of motion for $\mathrm{a}^{(\dagger)}$, $\mathrm{a}^\dagger\mathrm{a}$ and hermitian combin-

ations of x and p up to fourth order under the Hamiltonian $\tilde{\mathrm{H}}_{1p1m}$ as in eq. (A.3):

$$\partial_t \langle \mathrm{a} \rangle = \left(-i\Delta_C + iU_0 \left(1 - k_{rec}^2 \left\langle \mathrm{x}^2 \right\rangle + \frac{k_{rec}^4}{3} \left\langle \mathrm{x}^4 \right\rangle \right) - \kappa \right) \langle \mathrm{a} \rangle + i\eta \tag{A.6a}$$

$$\begin{aligned} \partial_t \left\langle \mathrm{a}^\dagger \right\rangle &= \partial_t \langle \mathrm{a} \rangle^* \\ &= \left(i\Delta_C - iU_0 \left(1 - k_{rec}^2 \left\langle \mathrm{x}^2 \right\rangle + \frac{k_{rec}^4}{3} \left\langle \mathrm{x}^4 \right\rangle \right) - \kappa \right) \left\langle \mathrm{a}^\dagger \right\rangle - i\eta \end{aligned} \tag{A.6b}$$

$$\partial_t \left\langle \mathrm{a}^\dagger \mathrm{a} \right\rangle = \eta \left(-i \left\langle \mathrm{a}^\dagger \right\rangle + i \langle \mathrm{a} \rangle \right) - 2\kappa \left\langle \mathrm{a}^\dagger \mathrm{a} \right\rangle \tag{A.6c}$$

$$\partial_t \left\langle \mathrm{x}^2 \right\rangle = \frac{1}{m} \left(\langle \mathrm{px} \rangle + \langle \mathrm{xp} \rangle \right) \tag{A.6d}$$

$$\partial_t \left(\langle \mathrm{xp} \rangle + \langle \mathrm{px} \rangle \right) = \frac{2}{m} \left\langle \mathrm{p}^2 \right\rangle + 4U_0 \left(k_{rec}^2 \left\langle \mathrm{x}^2 \right\rangle - \frac{2}{3} k_{rec}^4 \left\langle \mathrm{x}^4 \right\rangle \right) \left\langle \mathrm{a}^\dagger \mathrm{a} \right\rangle \tag{A.6e}$$

$$\partial_t \left\langle \mathrm{x}^4 \right\rangle = -\frac{2}{m} \left(\left\langle \mathrm{px}^3 \right\rangle + \left\langle \mathrm{x}^3 \mathrm{p} \right\rangle \right) \tag{A.6f}$$

$$\begin{aligned} \partial_t \left\langle \mathrm{p}^2 \right\rangle = 4U_0 \Bigg(& \frac{1}{2} k_{rec}^2 \left(\langle \mathrm{xp} \rangle + \langle \mathrm{px} \rangle \right) \\ & - \frac{1}{3} k_{rec}^4 \left(\left\langle \mathrm{x}^3 \mathrm{p} \right\rangle + \left\langle \mathrm{px}^3 \right\rangle \right) \Bigg) \left\langle \mathrm{a}^\dagger \mathrm{a} \right\rangle \end{aligned} \tag{A.6g}$$

$$\begin{aligned} \partial_t \left(\left\langle \mathrm{x}^3 \mathrm{p} \right\rangle + \left\langle \mathrm{px}^3 \right\rangle \right) = & \frac{1}{m} \left(\left\langle \mathrm{x}^2 \mathrm{p}^2 \right\rangle + \langle \mathrm{xpxp} \rangle + 2 \left\langle \mathrm{px}^2 \mathrm{p} \right\rangle + \langle \mathrm{pxpx} \rangle + \left\langle \mathrm{p}^2 \mathrm{x}^2 \right\rangle \right) \\ & + 4U_0 \left(k_{rec}^2 \left\langle \mathrm{x}^4 \right\rangle + \frac{2}{3} k_{rec}^4 \left\langle \mathrm{x}^6 \right\rangle \right) \left\langle \mathrm{a}^\dagger \mathrm{a} \right\rangle \end{aligned} \tag{A.6h}$$

$$\begin{aligned} \partial_t \left(\left\langle \mathrm{x}^2 \mathrm{px} \right\rangle + \left\langle \mathrm{xpx}^2 \right\rangle \right) = & \frac{1}{m} \left(\left\langle \mathrm{x}^2 \mathrm{p}^2 \right\rangle + \langle \mathrm{xpxp} \rangle + 2 \left\langle \mathrm{xp}^2 \mathrm{x} \right\rangle + \langle \mathrm{pxpx} \rangle + \left\langle \mathrm{p}^2 \mathrm{x}^2 \right\rangle \right) \\ & + 4U_0 \left(k_{rec}^2 \left\langle \mathrm{x}^4 \right\rangle + \frac{2}{3} k_{rec}^4 \left\langle \mathrm{x}^6 \right\rangle \right) \left\langle \mathrm{a}^\dagger \mathrm{a} \right\rangle \end{aligned} \tag{A.6i}$$

$$\begin{aligned} \partial_t \left(\left\langle \mathrm{x}^2 \mathrm{p}^2 \right\rangle + \left\langle \mathrm{p}^2 \mathrm{x}^2 \right\rangle \right) = & \frac{1}{m} \left(\left\langle \mathrm{xp}^3 \right\rangle + \left\langle \mathrm{pxp}^2 \right\rangle + \left\langle \mathrm{p}^2 \mathrm{xp} \right\rangle + \left\langle \mathrm{p}^3 \mathrm{x} \right\rangle \right) \\ & + 4U_0 \Bigg(\frac{1}{2} k_{rec}^2 \left(\left\langle \mathrm{x}^3 \mathrm{p} \right\rangle + \left\langle \mathrm{x}^2 \mathrm{px} \right\rangle + \left\langle \mathrm{xpx}^2 \right\rangle + \left\langle \mathrm{px}^3 \right\rangle \right) \\ & - \frac{1}{3} k_{rec}^4 \left(\left\langle \mathrm{x}^5 \mathrm{p} \right\rangle + \left\langle \mathrm{x}^3 \mathrm{px}^2 \right\rangle + \left\langle \mathrm{x}^2 \mathrm{px}^3 \right\rangle + \left\langle \mathrm{px}^5 \right\rangle \right) \Bigg) \left\langle \mathrm{a}^\dagger \mathrm{a} \right\rangle \end{aligned} \tag{A.6j}$$

$$\partial_t \left(\langle \mathrm{xpxp}\rangle + \langle \mathrm{pxpx}\rangle\right) = \frac{1}{m}\left(\left\langle \mathrm{xp^3}\right\rangle + \left\langle \mathrm{pxp^2}\right\rangle + \left\langle \mathrm{p^2xp}\right\rangle + \left\langle \mathrm{p^3x}\right\rangle\right) + 4U_0\left(\frac{1}{2}k_{rec}^2\left(\left\langle \mathrm{x^3p}\right\rangle + \left\langle \mathrm{x^2px}\right\rangle + \left\langle \mathrm{xpx^2}\right\rangle + \left\langle \mathrm{px^3}\right\rangle\right) - \frac{1}{3}k_{rec}^4\left(\left\langle \mathrm{x^5p}\right\rangle + \left\langle \mathrm{x^4px}\right\rangle + \left\langle \mathrm{xpx^4}\right\rangle + \left\langle \mathrm{px^5}\right\rangle\right)\right)\left\langle \mathrm{a^\dagger a}\right\rangle \tag{A.6k}$$

$$\partial_t \left\langle \mathrm{xp^2x}\right\rangle = \frac{1}{m}\left(\left\langle \mathrm{xp^3}\right\rangle + \left\langle \mathrm{p^3x}\right\rangle\right) + 4U_0\left(\frac{1}{2}k_{rec}^2\left(\left\langle \mathrm{x^2px}\right\rangle + \left\langle \mathrm{xpx^2}\right\rangle\right) - \frac{1}{3}k_{rec}^4\left(\left\langle \mathrm{x^4px}\right\rangle + \left\langle \mathrm{xpx^4}\right\rangle\right)\right)\left\langle \mathrm{a^\dagger a}\right\rangle \tag{A.6l}$$

$$\partial_t \left\langle \mathrm{px^2p}\right\rangle = \frac{1}{m}\left(\left\langle \mathrm{pxp^2}\right\rangle + \left\langle \mathrm{p^2xp}\right\rangle\right) + 4U_0\left(\frac{1}{2}k_{rec}^2\left(\left\langle \mathrm{x^3p}\right\rangle + \left\langle \mathrm{px^3}\right\rangle\right) - \frac{1}{3}k_{rec}^4\left(\left\langle \mathrm{x^5p}\right\rangle + \left\langle \mathrm{px^5}\right\rangle\right)\right)\left\langle \mathrm{a^\dagger a}\right\rangle \tag{A.6m}$$

$$\partial_t \left(\left\langle \mathrm{xp^3}\right\rangle + \left\langle \mathrm{p^3x}\right\rangle\right) = \frac{2}{m}\left\langle \mathrm{p^4}\right\rangle + 4U_0\left(\frac{1}{2}k_{rec}^2\left(\left\langle \mathrm{x^2p^2}\right\rangle + \langle \mathrm{xpxp}\rangle + 2\left\langle \mathrm{xp^2x}\right\rangle + \langle \mathrm{pxpx}\rangle + \left\langle \mathrm{p^2x^2}\right\rangle\right) - \frac{1}{3}k_{rec}^4\left(\left\langle \mathrm{x^4p^2}\right\rangle + \left\langle \mathrm{x^3p^2x}\right\rangle + \left\langle \mathrm{xpx^3p}\right\rangle + \left\langle \mathrm{xp^2x^3}\right\rangle + \left\langle \mathrm{px^3px}\right\rangle + \left\langle \mathrm{p^2x^4}\right\rangle\right)\right)\left\langle \mathrm{a^\dagger a}\right\rangle \tag{A.6n}$$

$$\partial_t \left(\left\langle \mathrm{pxp^2}\right\rangle + \left\langle \mathrm{p^2xp}\right\rangle\right) = \frac{2}{m}\left\langle \mathrm{p^4}\right\rangle + 4U_0\left(\frac{1}{2}k_{rec}^2\left(\left\langle \mathrm{x^2p^2}\right\rangle + \langle \mathrm{xpxp}\rangle + 2\left\langle \mathrm{px^2p}\right\rangle + \langle \mathrm{pxpx}\rangle + \left\langle \mathrm{p^2x^2}\right\rangle\right) - \frac{1}{3}k_{rec}^4\left(\left\langle \mathrm{x^4p^2}\right\rangle + \left\langle \mathrm{x^3pxp}\right\rangle + 2\left\langle \mathrm{px^4p}\right\rangle + \left\langle \mathrm{pxpx^3}\right\rangle + \left\langle \mathrm{p^2x^4}\right\rangle\right)\right)\left\langle \mathrm{a^\dagger a}\right\rangle \tag{A.6o}$$

$$\partial_t \left\langle \mathrm{p^4}\right\rangle = 2U_0\left[k_{rec}^2\left(\left\langle \mathrm{xp^3}\right\rangle + \left\langle \mathrm{pxp^2}\right\rangle + \left\langle \mathrm{p^2xp}\right\rangle + \left\langle \mathrm{p^3x}\right\rangle\right) - \frac{1}{3}k_{rec}^4\left(\left\langle \mathrm{x^3p^3}\right\rangle + \left\langle \mathrm{x^2pxp^2}\right\rangle + \left\langle \mathrm{x^2p^2xp}\right\rangle + \left\langle \mathrm{x^2p^3x}\right\rangle + \left\langle \mathrm{xp^3x^2}\right\rangle + \left\langle \mathrm{pxp^2x^2}\right\rangle + \left\langle \mathrm{p^2xpx^2}\right\rangle + \left\langle \mathrm{p^3x^3}\right\rangle\right)\right]\left\langle \mathrm{a^\dagger a}\right\rangle . \tag{A.6p}$$

Eidesstattliche Erklärung

Ich erkläre hiermit an Eides statt durch meine eigenhändige Unterschrift, dass ich die vorliegende Arbeit selbständig verfasst und keine anderen als die angegebenen Quellen und Hilfsmittel verwendet habe. Alle Stellen, die wörtlich oder inhaltlich den angegebenen Quellen entnommen wurden, sind als solche kenntlich gemacht.

Die vorliegende Arbeit wurde bisher in gleicher oder ähnlicher Form noch nicht als Magister-/Master-/Diplomarbeit/Dissertation eingereicht.

Datum	Unterschrift